2010

Role of extrinsic factors in utilizing the Giant Magnetocaloric Effect on materials: Frequency and time dependence

Sesha Chalapathi Madireddi
Iowa State University

Role of extrinsic factors in utilizing the Giant Magnetocaloric Effect on materials: Frequency and time dependence

by

Sesha Madireddi

A dissertation submitted to the graduate faculty

in partial fulfillment of the requirements for the degree of

DOCTOR OF PHILOSOPHY

Major: Materials Science and Engineering

Program of Study Committee:
Vitalij K. Pecharsky, Co-major professor
Karl A. Gschneidner, Co-major professor
Rohit K. Trivedi
Scott Chumbley
Ruslan Prozorov

Iowa State University

Ames, Iowa

2010

TABLE OF CONTENTS

LIST OF FIGURES

LIST OF TABLES

ABSTRACT

Magnetic refrigeration (MR) is potentially a high efficiency, low cost, and greenhouse gas-free refrigeration technology, and with the looming phase out of HCFC and HFC fluorocarbons refrigerants is drawing more attention as an alternative to the existing vapor compression refrigeration. MR is based on the magnetocaloric effect (MCE), which occurs due to the coupling of a magnetic sublattice with an external magnetic field. With the magnetic spin system aligned by magnetic field, the magnetic entropy changes by ΔS_M as a result of isothermal magnetization of a material. On the other hand, the sum of the lattice and electronic entropies of a solid must be changed by $-\Delta S_M$ as a result of adiabatically magnetizing the material, thus resulting in an increase of the lattice vibrations and the adiabatic temperature change, $\Delta T_{ad.}$ Both the isothermal entropy change ΔS_M and adiabatic temperature change ΔT_{ad} are important parameters in quantifying the MCE and performance of magnetocaloric materials (MCM). In general, ΔS_M and ΔT_{ad} are obtained using magnetization and heat capacity data and the Maxwell equations. Although Maxwell equations can be used to calculate MCE for first order magnetic transition (FOMT) materials due to the fact that the transition is not truly discontinuous, there can be some errors depending on the numerical integration method used. Thus, direct measurements of ΔT_{ad} are both useful and required to better understand the nature of the giant magnetocaloric effect (GMCE). Moreover, the direct measurements of ΔT_{ad} allow investigation of dynamic performance of FOMT materials experiencing repeated magnetization/demagnetization cycles. This research utilized a special test facility to directly measure MCE of $Gd_5Si_2Ge_{2,}$ $Gd_5Si_{2.7}Ge_{1.3,}$ MnFePAs, LaFeSiH , $Ni_{55.2}M_{18.6}Ga_{26.2,}$ Dy, Tb, $DyCo_2$, $(Hf_{0.83}\,Ta_{0.17})Fe_{1.98,}$

$GdAl_2$ and Nd_2Fe_{17}, MCMs, both FOMT and second order magnetic transition (SOMT) materials, at different magnetizing speeds, and the resulting data will be compared to indirect MCE data. The study can help understand the difference between direct and indirect measurement of MCE, as well as time dependence of MCE for FOMT materials.

CHAPTER 1. LITERATURE REVIEW AND PRELIMINARY RESULTS

1.1 Introduction

Magnetic refrigeration (MR) is potentially a high efficiency, low cost, and greenhouse gas-free refrigeration technology, and, with the looming phase-out of HCFC and HFC fluorocarbon refrigerants, is drawing more attention as an alternative to the existing vapor compression refrigeration. MR is based on the magnetocaloric effect (MCE), which occurs due to the coupling of a magnetic sublattice with an external magnetic field. The magnetocaloric effect is defined as the temperature change produced by the adiabatic application of a magnetic field, or the magnetic entropy change produced by the isothermal application of a magnetic field, to a magnetic material. This phenomenon was first discovered by Warburg [1] in 1881, in pure iron metal (where the cooling effect varied from 0.5 to 2.0 K/T [2]). Since then, many materials with large MCEs have been discovered, providing a much clearer understanding of this phenomenon.

In a magnetic material one finds, in addition to the lattice entropy related to phonons, a magnetic contribution related to magnons. Upon an adiabatic application of a magnetic field, the entropy in the spin system will change. As a consequence, the lattice entropy should change in order to keep the total entropy of the system constant. Thus, the system either heats up or cools down depending on the sign of the magnetic entropy change triggered by the magnetic field. The normal (conventional) MCE occurs when the temperature increases upon application of a magnetic field, and the inverse MCE results in a decrease of temperature upon the application of a magnetic field.

Magnetic refrigeration utilizes the magnetocaloric effect for cooling applications. In 1926, Debye [3] and in 1927, Giauque [4] independently suggested that the effect could be used to reach temperatures below 1 K. In 1933, Giauque and MacDougall demonstrated the first operating adiabatic demagnetization refrigerator that reached 0.25K [5]. They used $Gd_2(SO_4)_3 \cdot 8H_2O$ as a magnetic coolant and a magnetic field of 0.8 T to reach 0.53 K, 0.34 K, and 0.25 K starting at 3.4 K, 2.0 K, and 1.5 K, respectively. Between 1933 and 1997, a number of advances in the utilization of the MCE for cooling have been reported [6-9].

The discovery of the giant MCE in $Gd_5(Si,Ge)_4$ compounds has triggered vast interest in magnetic cooling. In addition, in 1997 the first near room-temperature magnetic refrigerator was demonstrated by Zimm et al. at the Astronautics Corporation of America [10]. These two events attracted interest from both scientists and companies who started developing new kinds of room-temperature materials and magnetic-refrigerator designs. Figure1.1 shows the number of publications on magnetic cooling since 1992, and Figure 1.2 presents the number of magnetic refrigerators developed per year since 1970. By using solid magnetic materials as coolants instead of conventional gases, magnetic refrigeration avoids all harmful gases including ozone-depleting gases, global warming greenhouse-effect gases, and other hazardous gaseous refrigerants. A solid coolant can easily be recycled. Furthermore, it has been demonstrated that magnetic cooling is energetically more energy-efficient than conventional gas-compression cooling. This is of particular interest in view of the global energy problems [8]. In addition, magnetic refrigerators make very little noise and may be built very compact. Therefore, magnetic refrigeration has attracted attention in recent years as a promising environmentally-friendly alternative to conventional gas-compression cooling.

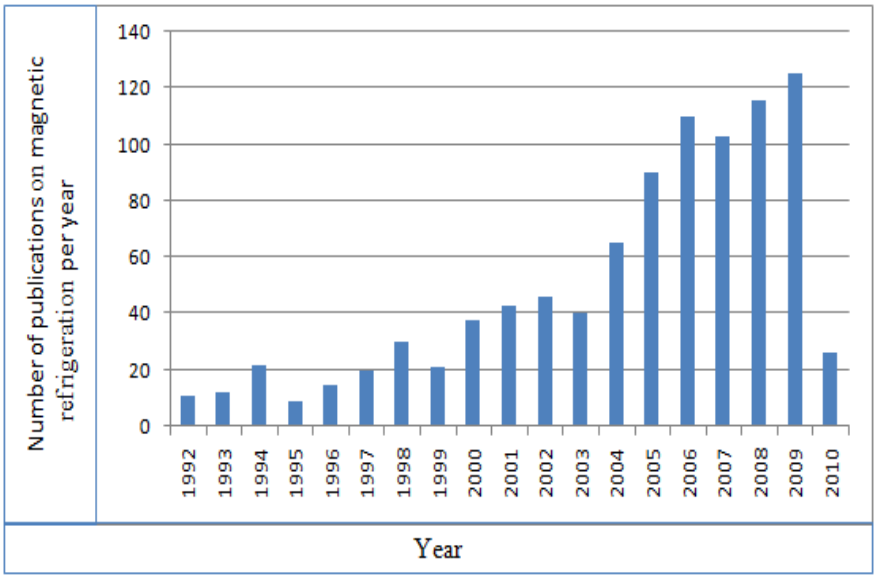

Figure 1.1. Publications on magnetic refrigeration since 1992 (Source: ISI web, *Science*, May 5, 2010)

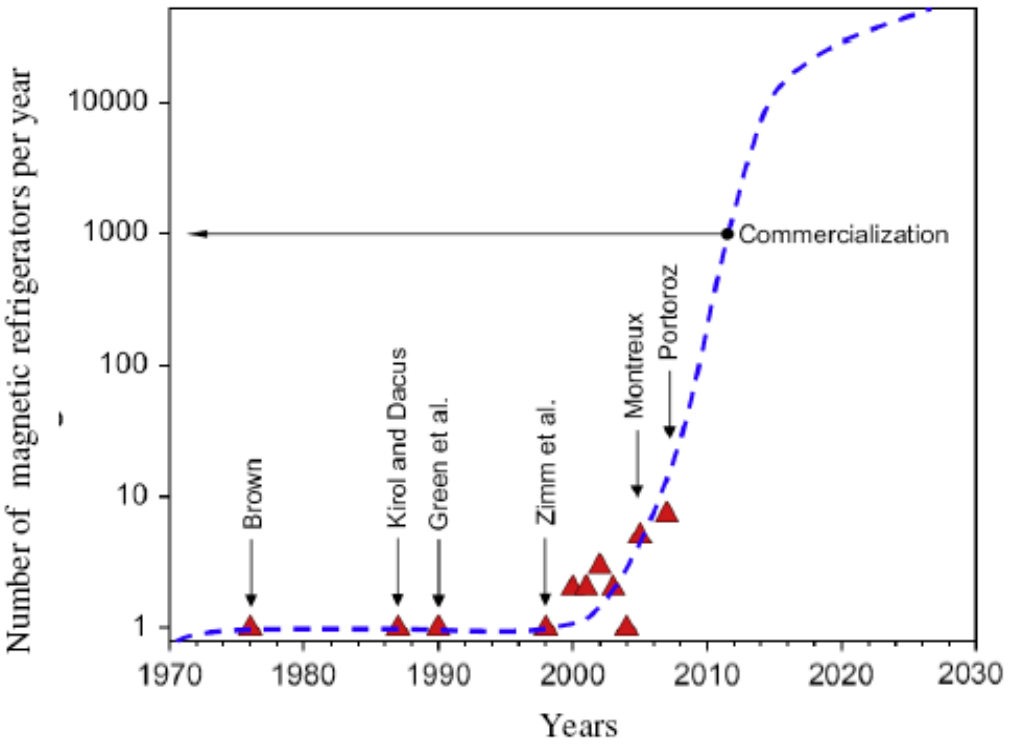

Figure 1.2. Number of magnetic refrigerators developed per year [31].

In the magnetic-refrigeration cycle depicted in Figure1.3, initially randomly (or nearly randomly)-oriented magnetic moments are aligned by a magnetic field, resulting in heating of the magnetic material. This implies a reduction of the entropy of the spin system. The entropy is transferred via the spin-lattice coupling to the lattice, resulting in heating of the magnetic material. The heat is removed from the material to the ambient environment by heat transfer fluid. In a conventional vapor refrigeration system, the gas medium is compressed, thereby increasing its pressure and temperature, followed by a condensation process to transfer the heat to ambient environment. Upon the removal of the field as shown in step 3 of Fig 1.3, the magnetic moments randomize, which leads via spin-lattice coupling to cooling of the material below ambient temperature. Heat from the system to be cooled can then be extracted using a heat transfer medium. In a conventional refrigeration system, high-pressure liquid expands and absorbs heat from the space to be cooled. When the magnetic field is generated by superconducting solenoids or permanent magnets, a high-energy efficiency can be achieved as entropy is transferred to and from the quantum-physical spin system.

Entropy is a property which describes the amount of disorder, or chaos of a system. In a system of spins, for example, a ferromagnetic or a paramagnetic material, the entropy can be changed by variation of the magnetic field, temperature, or other thermodynamic parameters. The total entropy of a metallic magnetic material at constant pressure is represented by:

$$S_t(B,T) = S_m(B,T) + S_l(B,T) + S_e(B,T)$$

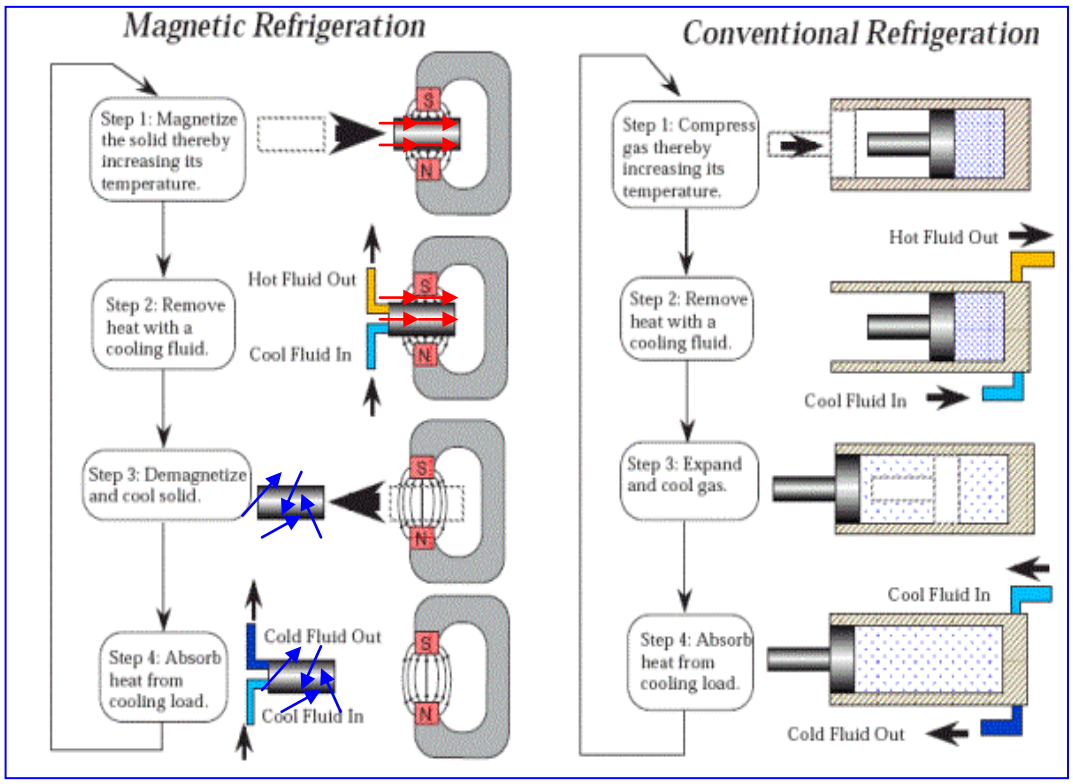

Figure 1.3. Magnetic refrigeration process and its analogy to conventional refrigeration.

Where S_m is the magnetic entropy, S_l and S_e are the lattice and electronic contributions to the total entropy, respectively, B is magnetic induction, and T is temperature.

In general, these three contributions depend on magnetic field and temperature, and it is difficult to clearly separate them. However, in this thesis, the focus is on magnetocaloric materials near room temperatures where the contribution of electrons to the total entropy can be neglected.

The change in magnetic entropy upon an application/removal of magnetic field can be obtained fromisothermal magnetization measurements as shown in Figure1.4.

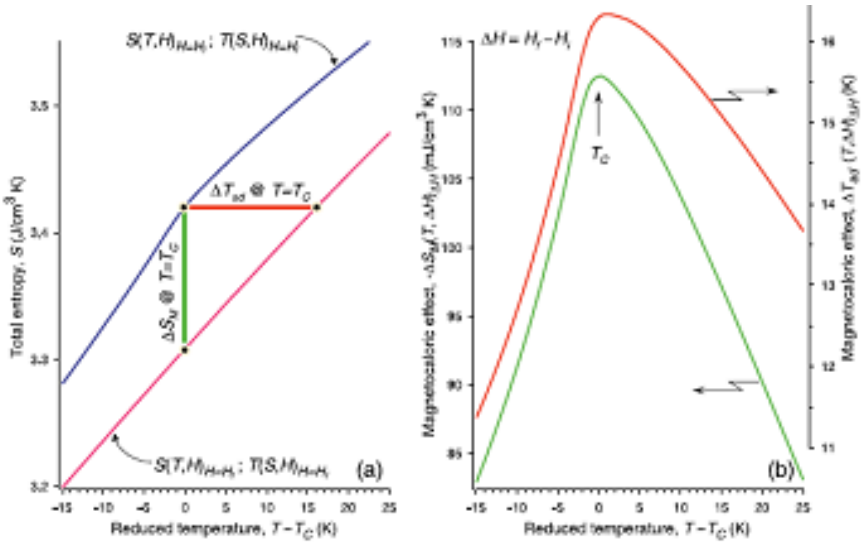

Figure 1.4**.** The total entropies in the initial *(H*i*)* zero and final *H*f) magnetic fields (*a*), and the MCE (*b*) in the vicinity of the Curie temperature of gadolinium, a ferromagnet with nearly zero coercively and remanence plotted as functions of reduced temperature (Gschneidner et al., 2005) [12].

1.2 Theoretical Aspects

The MCE of a magnetic material is associated with the magnetic-entropy of the material. The theoretical aspects of MCE have been discussed in Refs.27 and 28. According to thermodynamic principles, the MCE is proportional to $\frac{\partial M}{\partial T}$ at constant field (M = magnetization), and inversely proportional to the field dependence of the heat capacity Cp (T, B). In the temperature region of a magnetic phase transition, the magnetization changes rapidly and, therefore, a large MCE is expected in this region [29, 30]. However, the critical behavior of the physical quantities in the phase- transition region is so complicated that there is no unified theory. The theoretical description of MCE is still far from complete. Therefore, the adiabatic temperature change ΔT_{ad} of a given material can only be determined by using experimental methods.

1.2.1 Gibbs free energy

The thermodynamic properties of a system are fully determined by the Gibbs free energy or free enthalpy of the system. The system considered here consists of a magnetic material in a magnetic field B at a temperature T under a pressure p. The Gibbs free energy G of the system is given by

$$G = U - TS + pV - MB \tag{2.1}$$

where U is the internal energy of the system, S is the entropy of the system, and M is the magnetization of the magnetic material. The volume, V, magnetization, M, and entropy, S, of the material are given by the first derivatives of the Gibbs free energy as follows:

$$\begin{aligned} V(T,B,p) &= -\left[\frac{\partial G)}{\partial p}\right]_{T,B} \\ M(T,B,p) &= -\left[\frac{\partial G)}{\partial B}\right]_{T,p} \\ S(T,B,p) &= -\left[\frac{\partial G)}{\partial T}\right]_{B,p} \end{aligned} \tag{2.2}$$

The specific heat of the material is given by the second derivative of the Gibbs free energy with respect to temperature:

$$Cp(T,B) = -T\left[\frac{\partial^2 G)}{\partial T^2}\right]_{p,B} \tag{2.3}$$

By definition, if the first derivative of the Gibbs free energy is discontinuous at the phase transition, then the phase transition is of first-order. Therefore, the volume, magnetization, and entropy of the magnetic material are discontinuous at a first-order phase transition. If the first derivative of the Gibbs free energy is continuous at the phase transition, but the second derivative is discontinuous, then the phase transition is of second-order.

1.2.2 Magnetic entropy

The total entropy of a magnetic material in which the magnetism is due to localized magnetic moments, as for instance in lanthanide-based materials, is presented by:

$$S(T, B, p) = S_l(T, B, p) + S_e(T, B, p) + S_m(T, B, p) \qquad (2.4)$$

Where S_l represents the entropy of the lattice subsystem, S_e the entropy of conduction-electron subsystem and S_m the magnetic entropy, i.e., the entropy of the subsystem of the magneticspins. In magnetic solids exhibiting itinerant-electron magnetism, separation of these three contributions to the total entropy is, in general, not straightforward because the 3d electrons give rise to the itinerant-electron magnetism but also participate in conduction. Separation of the lattice entropy is possible only if electron-phonon interaction is not taken into account.

Since the entropy is a state function, the full differential of the total entropy of a closed system is given by:

$$dS = \left[\frac{\partial S}{\partial T}\right]_{P,B} dT + \left[\frac{\partial S)}{\partial P}\right]_{T,B} dP + \left[\frac{\partial S)}{\partial B}\right]_{T,P} dB \qquad (2.5)$$

Among these three contributions, the magnetic entropy is strongly field dependent, and the electronic and lattice entropies are much less field dependent. Therefore, for an isobaric-isothermal ($dP = 0$; $dT = 0$) process, the differential of the total entropy can be represented by:

$$dS = \left[\frac{\partial S_m)}{\partial B}\right]_{T,p} dB \qquad (2.6)$$

For a field change from the initial field B_i to the final field B_f, integration of Eq. (2.6) yields the total entropy change:

$$\Delta S(T, \Delta B) = \left[S(T, B_f) - S(T, B_i) \right] = \Delta S_m(T, \Delta B) \qquad (2.7)$$

Where $\Delta B = B_f - B_i$. This means that the isothermal-isobaric total entropy change of a magnetic material in response to a field change, ΔB, is also presented by the isothermal-isobaric magnetic-entropy change.

The magnetic-entropy change is related to the bulk magnetization, the magnetic field, and the temperature through the Maxwell relation:

$$\left[\frac{\partial S_m(T, B)}{\partial B} \right]_{T,p} = \left[\frac{\partial M(T, B)}{\partial T} \right]_{B,p} dB \qquad (2.8)$$

Integration yields:

$$\Delta S_M(T, \Delta B) = \int_{B_i}^{B_f} \left(\frac{\partial M(T, B)}{\partial T} \right)_{B,p} dB \qquad (2.9)$$

On the other hand, according to the second law of thermodynamics:

$$\left[\frac{\partial S}{\partial T} \right] B, p = \frac{Cp(T, B)}{T} \qquad (2.10)$$

Integration yields:

$$S(T, B) = S_0 + \int_0^T \left(\frac{C_p(T, B)}{T} dT \right) \qquad (2.11)$$

In the absence of configurational entropy, the entropy will be zero at T = 0 K, so that the value of S_o is usually chosen to be zero. Therefore, the entropy change in response to a field change, ΔB, is given by:

$$\Delta S(T,\Delta B) = \int_0^T \frac{C_p(T`,B_f) - C_p(T`,B_i)}{T`} dT` \qquad (2.12)$$

Where $C_p(T`,B_f)$ and $C_p(T`,B_i)$ represent the specific heat at constant pressure, *p*, in the magnetic fields, B_f and $B_{i,}$ respectively.

When an external magnetic field is applied to a ferromagnetic or paramagnetic MCM, the magnetic part of the total entropy of the solid is suppressed by ΔS_M. With the magnetic spin system aligned, the sum of the lattice and electronic entropies of the solid must change by $-\Delta S_M$ as a result of adiabatically magnetizing the material, thus causing an increase of the lattice vibrations and an adiabatic temperature change, $\Delta T_{ad.}$ Both the isothermal entropy and adiabatic temperature changes are important parameters in quantifying the MCE and performance of MCMs. In general, ΔS_M and ΔT_{ad} are obtained using magnetization and heat capacity data and the following Maxwell's equations:

$$\Delta S_M = \mu_o \int_{H_i}^{H_f} \left(\frac{\partial M(T,H)}{\partial T} \right)_H dH \qquad (2.13)$$

$$\Delta T_{ad} = -\mu_o \int_{H_i}^{H_f} \left(\frac{T}{C(T,H)} \times \frac{\partial M(T,H)}{\partial T} \right)_H dH \qquad (2.14)$$

Here, μ_0 is vacuum magnetic permeability, H_f is the final magnetic field, H_i is the initial magnetic field, *C* is heat capacity, *M* is magnetization, and *T* is temperature. Equations (2.13) and (2.14), therefore, represent what is known as the indirect method of evaluating MCE.

Obviously, the MCM is the key to the success of MR technology. A good MR device will depend on an MCM material with high MCE, low cost, easy fabrication, and good anti-

corrosion performance. Currently, most baseline MCMs are second-order magnetic phase transition materials (SOMT), such as Gadolinium (Gd). Gd is an MCM with high $\Delta T_{ad,}$ reasonable ΔS_M, and ease of processing. However, for commercial use of an MR technology, one needs to explore the first-order magnetic phase transition materials (FOMT) that have much higher MCE and possibly a lower cost. Since 1997, when Pecharsky and Gschneidner discovered the giant magnetocaloric effect (GMCE) in the FOMT material $Gd_5Si_2Ge_2$ (see section 1.3), significant progress in this field has been made. Although equations (2.13) and (2.14) can be used to calculate MCE for FOMT materials due to the fact that the transition is not truly discontinuous, there can be some error depending on the numerical integration method used. Thus, direct measurement of ΔT_{ad} is both useful and required to better understand the nature of the GMCE. Moreover, the direct measurement of ΔT_{ad} allows investigation of dynamic performance of FOMT materials experiencing repeated magnetization/demagnetization cycles.

This research utilized a special test facility to directly measure MCE for various MCMs, both FOMT and SOFT materials, at different magnetizing speeds (see "Experimental Method" section for details), and the resulting data were compared to the indirect MCE data. This can help in understanding the difference between direct and indirect measurement of MCE and time-dependence of MCE for FOMT materials. In addition, the equipment had the capability to test multiple cycles of magnetization/demagnetization, which can help in the understanding of dynamic performance of MCMs and simulate real-life conditions in which an MCM is set in a magnetic refrigerator.

1.3 Giant Magnetocaloric Effect

The discovery of the GMCE in $Gd_5Si_2Ge_2$ [6] and the pioneering work by Ames Laboratory/Astronautics Corporation of America on a near room temperature reciprocating MR [10] in 1997 stimulated intensive research work in MR machines and MCMs [12], especially those using FOMT materials with GMCE. As a result, a number of other intermetallics such as MnAs and $MnFeP_{1-x}As_x$-based [11, 13], $La(Fe_{1-x}Si_x)_{13}$ and its hydrides [14, 15], and Heusler-based Ni-Mn-Z (Z=Ga, In, Sn) ferromagnetic shape memory alloys [16, 17, 18] have been reported to display attractive magnetocaloric properties. Presently, it is generally acknowledged that the GMCE observed in these materials is due to a contribution from the elastic subsystem. For FOMT material investigation, most researchers employ the indirect methods defined by Maxwell's equations (2.8) and (2.10) to obtain ΔS_M and ΔT_{ad}. A major problem may occur when applying Maxwell's equations (2.13) and (2.14) at the FOMT, especially if it is a sharp first-order transition. In practice, for the majority of materials, the transitions are not ideal (i.e., not truly discontinuous) and thus, one can calculate the derivative, ∂ M(T ,H)/ ∂ T, making it possible to use Maxwell's equations.

Some work has been carried out to directly measure the ΔT_{ad} for $Gd_5Si_2Ge_2$ [8, 19], and $La(Fe_{1-x}Si_x)_{13}H_y$ [20, 21]. For $Gd_5Si_2Ge_2$, the normal procedure leads to a value that is ~ 50% too small for ΔT_{ad} (8.5 K) compared with the indirect value obtained from heat capacity measurements (16.5 K), while the ΔT_{ad} value determined by slowly ramping the field up or down agrees with the indirect value to within ±5% [22]. For $La(Fe_{1-x}Si_x)_{13}$ materials, the direct and indirect ΔT_{ad} values are available for two different alloy compositions. The direct

ΔT_{ad} value of 5.7 K for $La(Fe_{11.7}Si_{1.3})$ is ~30% smaller than the indirect value of 8.1 K, and for $La(Fe_{11.44}Si_{1.56})$, the direct ΔT_{ad} value of 6 K is ~20% smaller than the indirect value of 7.6 K. The discrepancy between the direct ΔT_{ad} measurements and the ΔT_{ad} values determined from heat capacity measurements was not found for the SOMT material Gd [23, 24]. Based on these results, Gschneidner et al. [12] suggested that there may be a time dependence of the ΔT_{ad} measurement for an FOMT, which probably varies from one material to another. They attributed the time dependence to the slow kinetics of the first-order transformation. Gschneidner et al. [12] also noted that these values are based on static and semi-static measurements, but in most magnetic refrigerators, the magnetization and demagnetization steps are dynamic, and in some cases may become non-equilibrium processes, i.e., the devices run at frequency from 0.1 to 4 Hz and, thus, the direct measurements of ΔT_{ad} may better approximate the actual conditions experienced in a magnetic refrigerator than the static values of ΔT_{ad} determined from heat capacity measurements.

Spichkin et al. [25] reported their work on dynamic magnetocaloric and magnetic properties of $La(Fe_{1-x}Si_x)_{12}$ alloy and its hydride. In their investigation, the temperature and magnetic field dependence of the adiabatic temperature change, $\Delta T_{ad,}$ were measured by a direct method with two magnetic field change rates: 0.5 and 0.05 T/s ($\Delta B \sim 1.1$ T). Essential magnetic field hysteresis of ΔT_{ad} was revealed at the magnetic change field rate of 0.5 T/s, but for the slower rate, 0.05 T/s, the hysteresis was observed only for LaFeSi, but not for LaFeSiH. The magnetocaloric effect is maximized near the Curie points with the following

relative ΔT_{ad} and ΔS_M change values (for ΔH = 1 T): ~3.4 K/T and ~11 J/kg K T for $La_{1.091}Fe_{11.31}Si_{1.56}Al_{0.039}$ and ~2.5 K/T and ~14.5 J/kg K T for its hydrogenated alloy.

Khovaylo et al. [26] recently conducted a study of the adiabatic temperature change, ΔTad, in the vicinity of a first-order magnetostructural phase transition on a $Ni_{2.19}Mn_{0.81}Ga$ Heusler alloy. With an electromagnet of 1.85 T, they directly measured adiabatic temperature change, ΔT_{ad}, at different operating temperature, and carried out dynamic magnetization/demagnetization step test (multiple cycles). It was found that the directly measured ΔT_{ad} ~1 K is one order of magnitude smaller than that expected from isothermal magnetic entropy change and specific heat data reported in the literature. The new feature of the adiabatic temperature change in materials with GMCE, specifically an irreversible characteristic of ΔT_{ad} when the sample is subjected to repeatable action of a magnetic field at a constant temperature, was observed. This effect was attributed to the irreversible magnetic field-induced structural transformation. It was shown that the small value of ΔT_{ad} in $Ni_{2.19}Mn_{0.81}Ga$ is not due to the kinetics of the transformation, but originates from other factors that are intrinsic to FOMT. Relevance of these factors to other GMCE was outlined. They compared ΔT_{ad} vs. time curves for different magnetic field sweeping rates (0.12 T/s, 0.4 T/s, and 3 T/s) and found these temperature curves can be extrapolated by the same function, and, based on this, they concluded the sweeping rate has no influence on adiabatic temperature change.

McKenna et al. [27] reported their work on Tb and Dy. These a.c. specific heat experiments have shown that there is temperature hysteresis in the first-order transitions for terbium and dysprosium, thus verifying their first-order nature. The behaviors of the deduced values of the specific heats in the vicinities of the Nėel temperatures were as expected for

these higher-order transitions. It was shown that a.c. specific heat measurements performed as a function of the modulation amplitude, ΔT may be used to test for first-order behavior through the association with temperature hysteresis in the transition. The technique is applicable even when the inhomogeneous broadening is much greater than the temperature hysteresis width. Tb has a first-order transition at ~220K, but the transition is weak and sometimes it is not seen.

1.4 Experimental Methods

This research collaborated with the AMT&C Corporation in Moscow, Russia to develop a Magnetocaloric Measuring Setup (MMS) test facility. The MMS allows direct measurement of MCE magnetic field dependences ($\Delta T(H)$) at different temperatures (from 100 to 370 K) and magnetic field sweeping rates (from 0.05 to 6 T/s) in both automatic and manual modes. A photo of the MMS and controller is given in Figure 1.5. The schematic diagram of the MMS is shown in Figure 1.6. It consists of the following main parts:

1. Computer-controlled Halbach-type magnetic field permanent magnet source (the magnetic field range is from 0.02 Tesla to 1.78 Tesla);
2. Measuring insert with support;
3. Liquid nitrogen shank end Dewar; and
4. Data acquisition, processing and control unit and software, including: magnetic field measuring and control system, temperature measuring and control system, ΔT measuring system, and control computer.

Figure 1.5. Photo of MMS and controller.

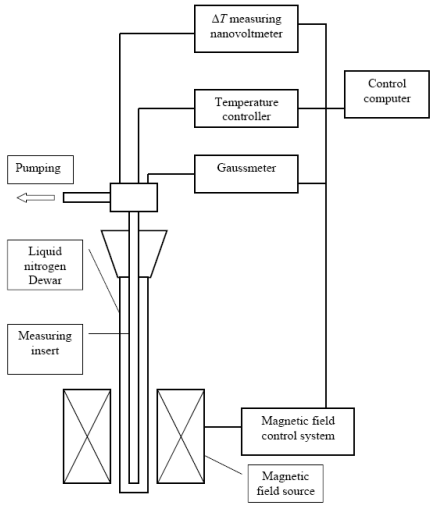

Figure 1.6. Schematic diagram of MMS.

The computer-controlled Halbach-type magnetic field permanent magnet source creates a variable magnetic field acting on the sample, placed in an evacuated measuring insert, which causes a change of the sample temperature, the MCE. The Halbach-type magnet has a double ring structure, the inside ring is rotated with a step motor to change the magnetic field in the central workspace around the sample. When the inside ring is rotated a full cycle (9600 steps), the field changes from 0 to 1.78 Tesla (maximum field), then back to 0, then to 1.78 Tesla again in opposite polar mode, and then back to 0. The Hall sensor near the sample and magnetic field measuring system based on the Lake Shore 475 DPS Gaussmeter gives the value of the magnetic field. The magnet source is guided by a National Instruments (NI) Two Axis PCI 7340 Motion Controller and a magnet power supply module. It allows setting of the required magnetic field sweep rate.

The evacuated measuring insert is placed inside the liquid nitrogen shank end Dewar (cryostat) and contains a sample holder with resistive heater, resistive temperature sensor, Hall sensor and thermocouple for MCE measurement. The sample consists of two flat pieces

measuring (1-2) × (2-5) × (8-10) mm each. The resistive thermometer is on the holder, and thermocouple has the reference junction near the resistive thermometer. The measuring junction is sandwiched between the two sample pieces. Thus, the initial work temperature can be determined by the output of both the resistive thermometer and thermocouple, and the MCE is measured by the thermocouple with a nanovoltmeter (Agilent 34420A). The temperature measuring and control system is based on a Lake Shore Model 331 Temperature Controller and allows for stabilizing and maintaining initial temperature of measurement (measurement temperature) set by the operator or a program of measurements. The nanovoltmeter, gaussmeter, and temperature controller of the data acquisition system are connected to the control computer via a GPIB interface. The process of measurement is controlled by software developed on LabView8.0. The control computer acquires the values of ΔT and H change during the measurement process. On the basis of these values, the computer program plots $\Delta T(H)$ dependence.

A close-up of the measuring insert is shown in Figure 1.7. Initial testing showed inconsistent MCE and unacceptable temperature difference between the test sample and the holder (ΔT = 5 ~ 10 K). It was decided that significant radiation heat transfer existed between the sample and the inside wall of the measuring insert tube which is immersed in liquid nitrogen. To significantly reduce the radiation heat loss, a thin aluminum foil was wrapped around the sample (see Figure 1.8). The foil had to be handled very carefully to make sure it was within the plastic spacer so the foil did not touch the wall of the measuring insert tube that has very low temperature. After the change, the temperature difference between the

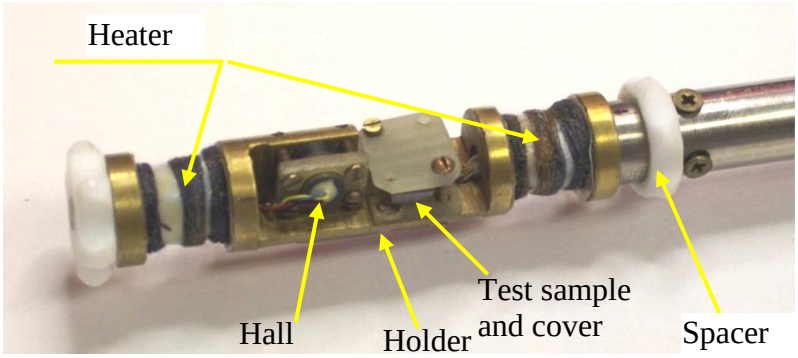

Figure 1.7. Close-up of measuring insert.

Figure 1.8. Measuring insert covered with aluminum foil.

sample and holder was lowered to 0.3 ~ 3 K , depending on the sample tested, and MCE testing results were much more consistent. All results discussed in the latter section were tested with the aluminum foil acting as an isothermal heat shield.

Based on our knowledge, this MMS device is the first one that can directly measure adiabatic temperature change, ΔT_{ad}, at a wide temperature range (100K to 370K), wide magnetic field sweeping rate (0.05 to 6 T/s), and at a maximum field of 1.78 T, and can, therefore, carry out study of dynamic performance for continuous magnetization/demagnetization steps.

1.5 Gadolinium – Prototype MCM

A pure Gadolinium sample was tested with the MMS to confirm the MMS worked correctly. Figure 1.9 shows the MCE curve for 1.78 Tesla, and Figure 1.10 shows

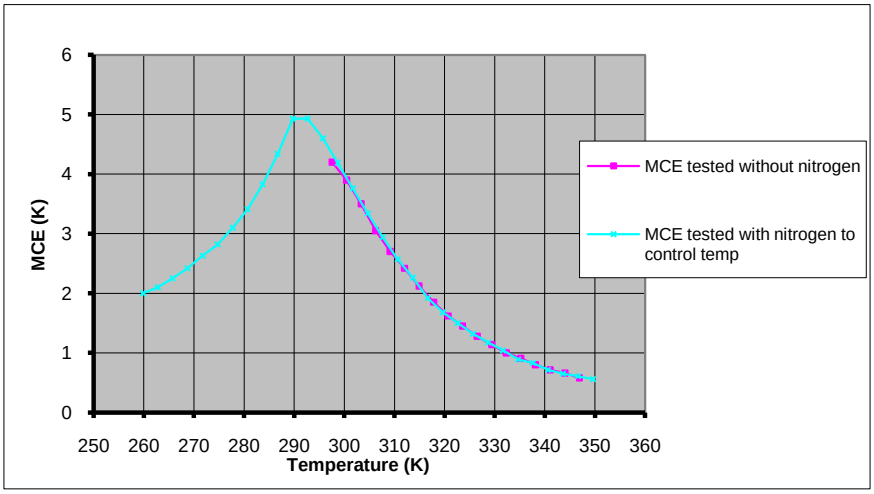

Figure 1.9. MCE of Gadolinium at 1.78 T.

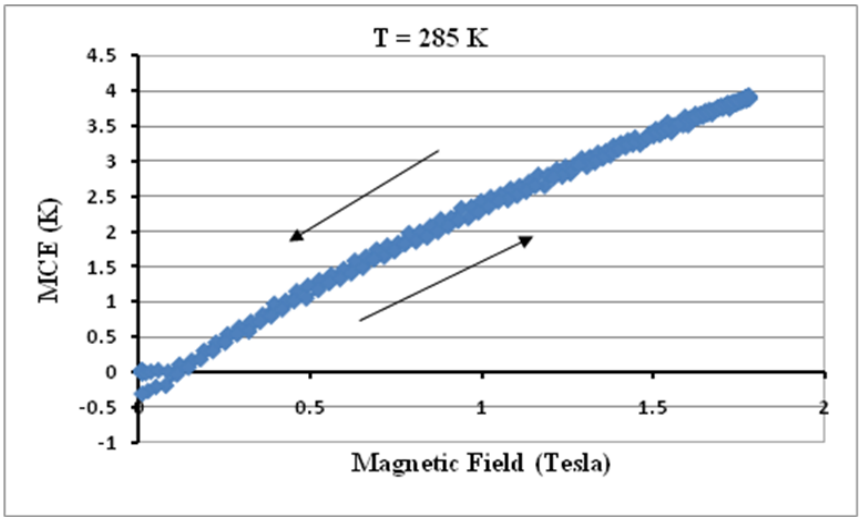

Figure 1.10. Adiabatic temperature change vs. field for Gadolinium at 285 K and 1 T/s.

temperature vs. field curve at 285K and 1 T/s. These results are consistent with results published in the literature. The test shown in Figure 1.10 for a half cycle rotation field climbs to 1.78 Tesla, and then goes back to 0 at a rate of 1 T/s. Note the magnetizing and demagnetizing curve are almost overlapping indicating that the heat loss to the environment can be neglected. Thus, all the tests with sweeping rate of 1 T/s or higher can be treated as "adiabatic". However, when the field change rate is less than 1 T/s, the demagnetizing curve is significantly below the magnetizing curve for Gadolinium due to heat loss. Several methods were tried to reduce the loss, such as using thread instead of the plastic cover to fix the sample, or using Teflon tape to simply fix the sample. None of these trials proved to be a good solution. Based on the best results Gadolinium test data, the MCE (the peak point of the temperature curve) is lower than correct value by 0.15 K, 0.35 K, and 1.2 K is at sweeping rates of 0.5 T/s, 0.25 T/s, and 0.05 T/s, respectively. Further, the maximum gap between the magnetizing and demagnetizing curve is 0.5 K, 1.0 K, and 2.1 K is at 0.5 T/s, 0.25 T/s, and 0.05 T/s, respectively.

1.6 Near Room Temperature Prototype Magnetic Refrigerators

Interest in magnetic refrigeration as a new solid state cooling technology competitive with vapor compression has grown considerably over the past 10 years coinciding with rising international concerns about global warming due to an ever increasing energy consumption [32]. Number of prototype models were built and tested as shown in the following sections.

1.6.1 Brown's (1976) magnetic heat pump

Brown [33] showed that a continuously operating device working near room temperature could achieve much larger temperature spans than the maximum observed magnetocaloric effect (MCE, or the adiabatic temperature change, ΔT_{ad}). Brown's near room temperature reciprocating magnetic refrigerator used one mole of 1 mm thick Gd plates separated by a wire screen (Curie temperature, T_C = 294 K) and an 80% water 20% ethyl alcohol solution as a regenerator in an alternating 7.0 T field produced by a superconducting magnet (see Fig. 1.11). A maximum temperature span of 47 K was attained after 50 cycles (T_{hot} = 319 K and T_{cold} = 272 K where T_{hot} is the hot end temperature and T_{cold} is the cold end temperature). This temperature span is more than three times larger than the MCE of Gd metal between 272 K (ΔT_{ad} = 11 K) and 319 K (ΔT_{ad} = 13 K); Gd has a maximum ΔT_{ad} value of 16 K at its Curie temperature T_C = 294 K. Subsequently, Brown [34] was able to attain a temperature span of 80 K (from 248 to 328 K) using the same apparatus.

1.6.2 Near room temperature reciprocating proof-of-principle magnetic refrigerator

The Astronautics Corporation of America (ACA), who was a subcontractor to the Ames Lab (AL), designed, built and tested the demonstration unit (see Fig 1.12) under the supervision of C.B. Zimm. A successful operating proof-of-principle demonstration unit, showing that magnetic refrigeration is a feasible and competitive technology for large scale building air conditioning, and for refrigeration and freezing units in supermarkets and food processing plants, was developed. This device operated in magnetic fields up to 5.0 T using a superconducting magnet, and it achieved a cooling power of 600Wwith a COP (coefficient of

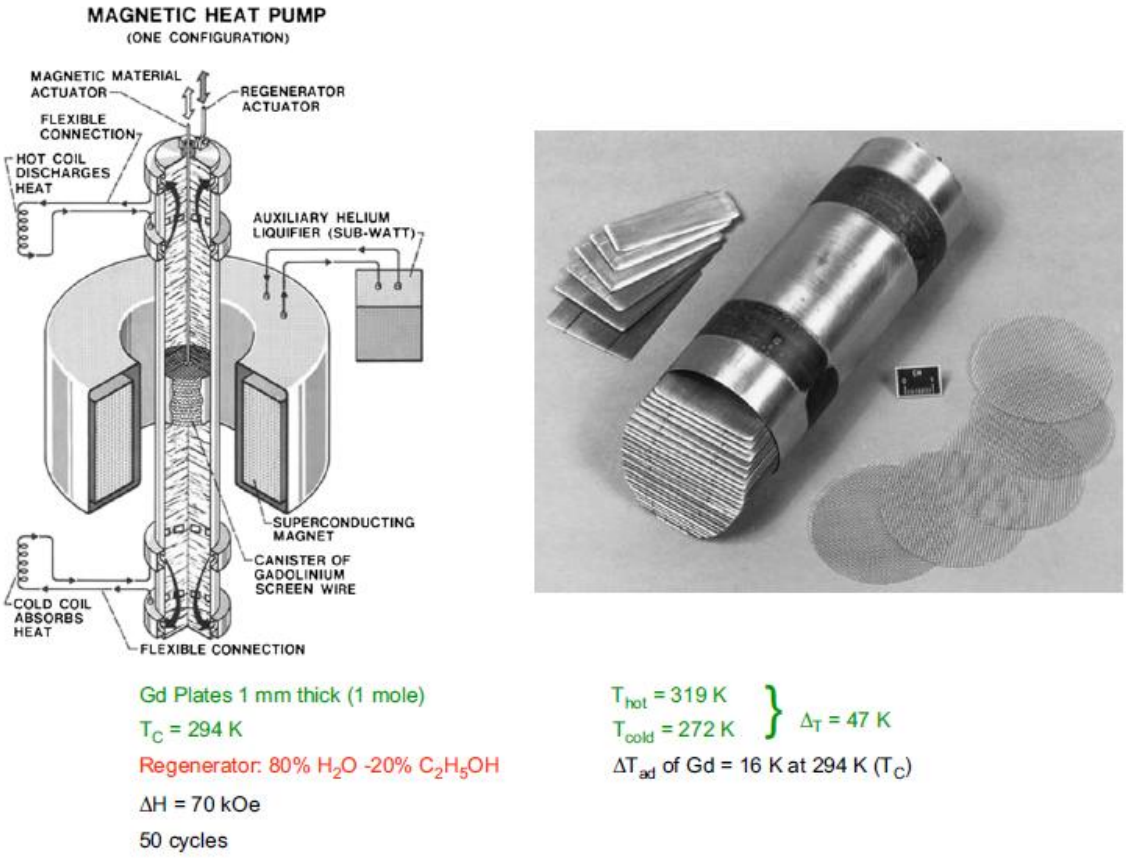

Figure 1.11. Brown's magnetic heat pump [34].

performance) approaching 10, a maximum of 60% of Carnot efficiency with a 10 K temperature span (between 281 K and 291 K) in magnetic fields of 5T [10,34].

1.6.3 The second generation magnetic refrigerator

Following the success of the proof-of-principle magnetic refrigerator the Astronautics Corporation of America (ACA) scientists and engineers evaluated its performance and concluded that the cycle time of 6 s (operating frequency of 0.16 Hz) for this reciprocating machine was too slow to be practical. An analysis indicated that for high frequencies, >1 Hz, a rotary device would be better than a reciprocating machine. Furthermore, a decision was

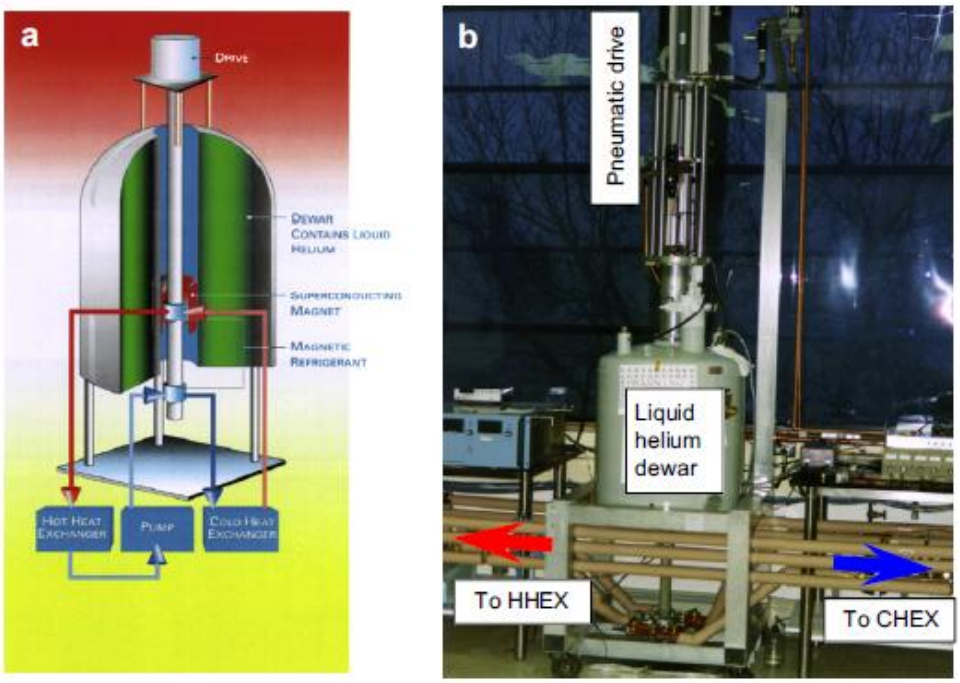

Figure 1.12. Ames Laboratory/Astronautics Corporation of America's reciprocating proof-of-principle magnetic refrigerator: (a) schematic and (b) photograph [10].

made to build a small cooling machine using a permanent magnet as the field source rather than build a large size magnetic refrigerator using a superconducting magnet as the magnetic field source [36, 37].

Work on the second generation magnetic cooling device – a rotary, room temperature, permanent magnet, magnetic refrigerator (now called the Rotating Bed Magnetic Refrigerator–RBMR)–began in 1998 at ACA. In the meanwhile AL entered into a three-year CRADA (1999–2001) with ACA to assist ACA to bring this apparatus, called a laboratory demonstration magnetic refrigerator (see Fig. 1.13), to an operational status, which was

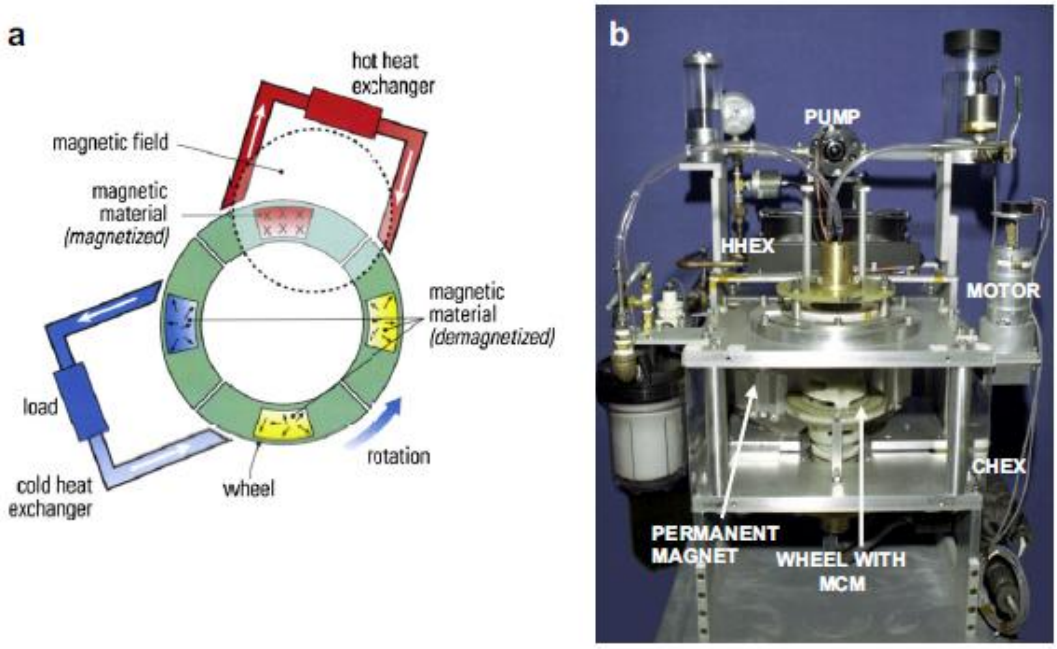

Figure 1.13. Astronautics Corporation of America laboratory prototype permanent magnet, rotating bed magnetic refrigerator (RBMR): (a) schematic and (b) photograph [36–39].

achieved on September 18, 2001. In this refrigerator the porous beds of the magnetocaloric material, 160 g (initially spheres of Gd and later both Gd and a 94%Gd–4%Er alloy in a layered bed), are rotated through a magnetic field of 1.5 T produced by a $Nd_2Fe_{14}B$ permanent magnet with steel flux concentration poles. Water is used as the heat exchange fluid. The design of this laboratory demonstration unit easily allows it to operate over a range of frequencies from 0.5 to 4 Hz and at various fluid flows to achieve a range of cooling powers. The maximum temperature span was 25 K under a no load condition, and the maximum cooling power of 50W was realized at 0 K temperature span.

1.6.4 The third generation magnetic refrigerator

The third generation magnetic refrigerator (the Rotating Magnet Magnetic Refrigerator–RMMR) by ACA consists of two 1.5 T modified Halbach magnets which rotate while 12 magnetocaloric beds remain fixed (see Fig. 1.14) [39]. The two rotating permanent magnets are arranged so that the moment of inertia of the magnet is minimized and the inertial forces are balanced. The main advantage of the fixed beds is that the valving and timing of the fluid flows through the beds and heat exchangers are simpler than that for the second generation machine (RBMR) in which the beds rotate through a gap in the magnet (see Fig. 1.13). The magnetic refrigerant used in the initial tests was Gd foils. The performance at the time of the Thermag II conference in Portoroz, Slovenia (April 11–13, 2007) had not reached the expected theoretical cooling power, e.g. 140W actual vs. 190W calculated for a 4 K temperature span at a flow rate of 3 l/min, i.e. ~ 75% of theoretical. However, since this machine is in the early stages of testing, these results are not unexpected.

1.6.5 Other magnetic refrigerators

Blumenfeld et al. designed [40], built and tested a magnetic refrigerator which uses charging/discharging of a superconducting coil to generate the changing magnetic field. The significant feature is that there are no moving parts (i.e., both the magnet and the magnetocaloric beds are stationary), which makes the engineering of heat transfer system much simpler, see Fig. 1.15. The main penalty is the slow cycle time, which is 30 s. However, on the other hand, the giant magnetocaloric effect materials may be utilized to their maximum potential, which may not be true for most machines built to date because they

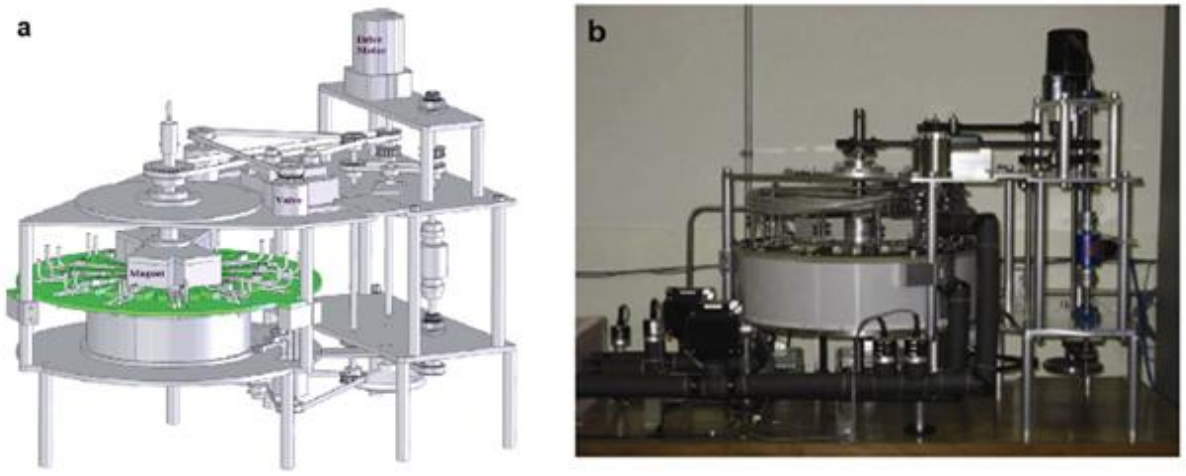

Figure 1.14. Astronautics Corporation of America's rotating magnet magnetic refrigerator (RMMR): (a) schematic and (b) photograph [39].

generally operate between 0.1 and 4 Hz. This novel refrigerator achieved 3W of cooling power at a 15 K temperature span for a 17 kOe field change.

The magnetic refrigerator built in Nanjing, China, see Fig. 1.16, was the first reciprocating apparatus using two 1.4 T Halbach permanent magnets (the previous reciprocating machines used a superconducting magnet) [41,42]. The authors were able to obtain a cooling power of 40W at a 5 K temperature span using ~1 kg of the magnetic refrigerant material. At a zero heat load, a temperature span of ~25 K was reached in about20 min of running time using either Gd powders or $Gd_5(Si_{1.895}Ge_{1.895}Ga_{0.03})$ powders. Wu (2003) [42] and Lu et al. (2005) [41] were the first to use a giant magnetocaloric effect material in a magnetic refrigerator, however, the performance of the latter was marginally better than that when Gd metal was used in the magnetocaloric beds, i.e., the temperature span was only 1 K greater. The operating frequency of the reciprocating machine was not given.

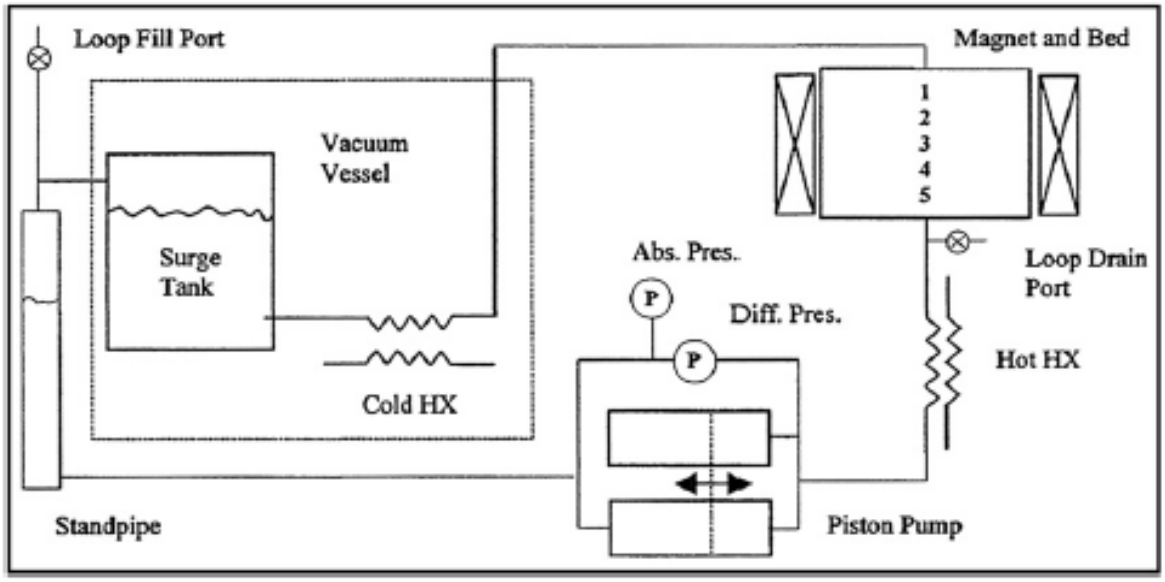

Figure 1.15. Schematic of Los Alamos National Laboratory's superconducting magnetic refrigerator [40] (by permission of the American Institute of Physics).

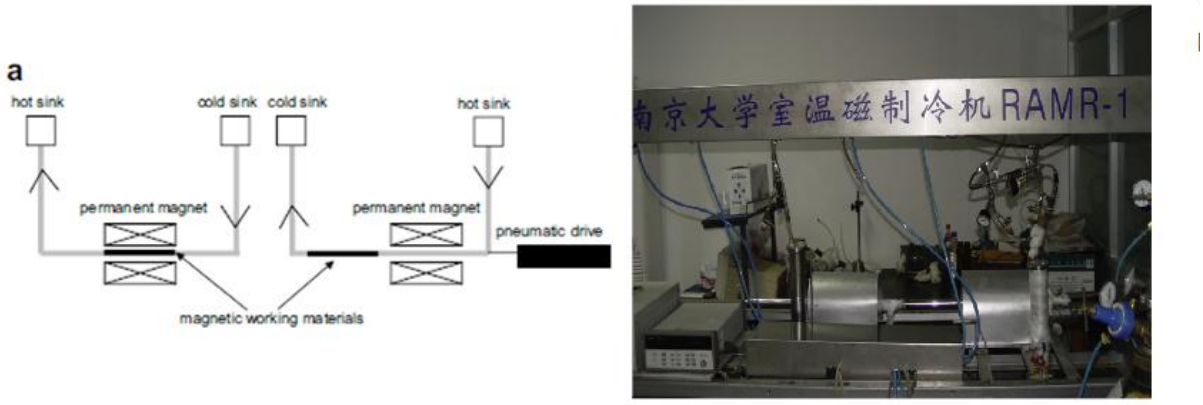

Figure 1.16. Nanjing reciprocating dual permanent magnet magnetic refrigerator: (a) schematic and (b) photograph (by permission of [42] (Sichuan Institute of Technology, Chengdu, Sichuan, PR China, and Lu et al. Nanjing University, Nanjing, PR China [41]).

A compact rotary permanent magnet magnetic refrigerator was described by Tura and Rowe [43] at Thermag II. This apparatus utilized two pairs of concentric Halbach arrays which are synchronized such that one magnetocaloric bed is being demagnetized while the second one is being magnetized, see Fig. 1.17. The maximum field inside the concentric Halbach magnet array was 1.4 T, and the inner cylinder could be rotated to operate at a frequency as high as 5 Hz. Since the magnetocaloric beds are stationary the valving and timing of the fluid flows are simpler than in machines in which the beds are rotated. Preliminary results showed that a maximum temperature span of 15 K could be reached under no load conditions.

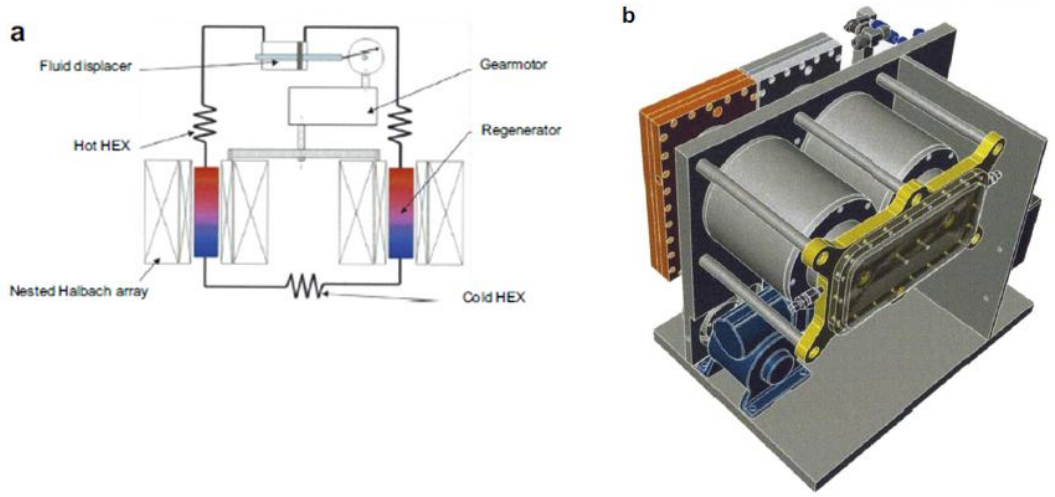

Figure 1.17. University of Victoria's compact permanent magnet magnetic refrigerator: (a) schematic and (b) artist's rendition (by permission of Tura and Rowe [43]).

Okamura et al. [44] reported at Thermag II on their improvements of a rotating permanent magnet magnetic refrigerator first described at Thermag I in September 2005 (Okamura et al. [45]. In the Tokyo Institute of Technology (TIT) device a permanent magnet

rotates inside a four segmented magnetocaloric ring (the four ‘‘AMR ducts’’ shown in Fig. 1.18a) which is surrounded by an iron yoke (Fig. 1.18b). The magnetic field in the AMR ducts when the poles of the inner permanent magnet are next to the duct is 1.1 T. The authors tested four different Gd- based alloys as the magnetic refrigerant, each weighing 4 kg. They realized a cooling power of 540 W, and a COP of 1.8 when the hot end of the AMR duct was 21˚C with a 0.2 K temperature span and the water flow rate was 13.3 l/min. The cycle time is 2.4s. The major disadvantage is that the rotation is not continuous, i.e. magnet stops after each quarter turn next to the AMR duct for 0.7 s before the next quarter turn, which takes 0.5s.

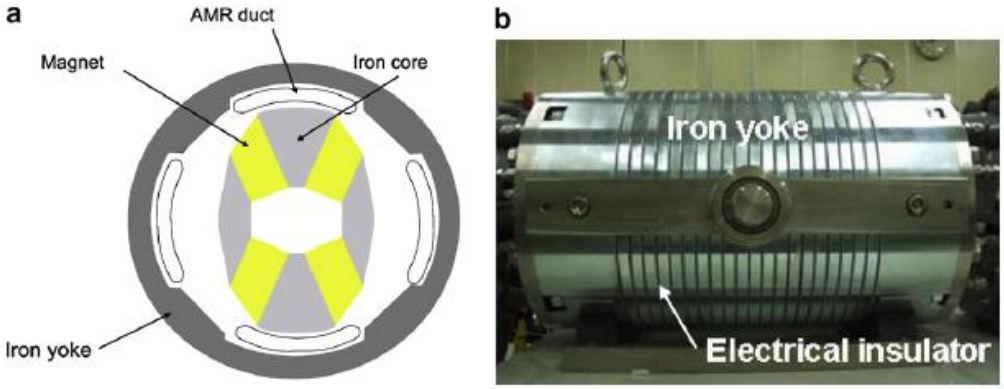

Figure 1.18. Tokyo Institute of Technology’s rotating magnet magnetic refrigerator: (a) schematic and (b) photograph (by permission of Okamura et al. [45]).

1.7 References

[1] E. Warburg, *Ann. Phys. Chem.* **13** (1881) 141.

[2] http://en.wikipedia.org/wiki/Magnetic_refrigeration#History.

[3] P. Debye, *Ann. Physik.* **81** (1926) 1154.

[4] W.F. Giauque, *J. Amer. Chem. Soc*. **49** (1927) 1864.

[5] W.F. Giauque and D.P. MacDougall *Phys. Rev.* **43** (1933) 768.

[6] K.A. Gschneidner, Jr. and V.K. Pecharsky, *Rare Earths: Science,Technology and Applications III,* Ed. R.G. Bautista et al. Warrendale, PA: The Minerals, Metals and Materials Society (1997) p 209.

[7] V.K. Pecharsky and K.A. Gschneidner, Jr., *J. Magn. Magn. Mater.* **200** (1999) 44.

[8] K.A. Gschneidner, Jr. and V.K. Pecharsky, *Annu. Rev. Mater. Sci.* **30** (2000) 387.

[9] K.A. Gschneidner, Jr. and V.K. Pecharsky, *Fundamentals of Advanced Materials for Energy Conversion,* Ed. D. Chandra and R.G. Bautista, Warrendale, PA: The Minerals, Metals and Materials Society (2002) p 9.

[10] C.B. Zimm, A. Jastrab, A. Sternberg, V. Pecharsky, K. Gschneidner, Jr., M. Osborne, and I. Anderson, *Adv. Cryog. Eng.* **43** (1998) 1759.

[11] O. Tegus, E. Brück, K.H.J. Buschow, and F.R. de Boer, *Nature* **415** (2002) 150.

[12] K A. Gschneidner Jr, V K Pecharsky, and A O Tsokol, *Rep. Prog. Phys*. **68 (**2005) 1479-1539.

[13] H. Wada and Y. Tanabe, *Appl. Phys. Lett*. **79** (2001) 3302.

[14] F. Hu, B. Shen, J. Sun, Z. Cheng, G. Rao, and X. Zhang, *Appl. Phys. Lett*. **78**, (2001) 3675.

[15] A. Fujita, S. Fujieda, Y. Hasegawa, and K. Fukamichi, *Phys. Rev. Lett*. **78**, (2003) 3675.

[16] T. Krenke, E. Duman, M. Acet, E.F. Wassermann, A. Moya, L. Monosa, and A. Planes, *Nat. Mater* **4** (2005) 450.

[17] Z.D. Han, D.H. Wang, C.L. Zhang, S.L. Tang, B.X. Gu, and Y.W. Du, *Appl. Phys. Lett*. **89** (2006) 182-507.

[18] S. Stadler, M. Khan, J. Mitchell, N. Ali, A.M. Gomes, I. Dubenko, A.Y. Takeuchi, and A.P. Duimaraes, *Appl. Phys. Lett* **88** (2006) 192-511.

[19] A. Giguere, M. Foldeaki, B.R. Gopal, R. Chahine, T.K. Bose, Frydman, and J.A. Barclay, *Phys. Rev. Lett*. **83** (1999) 2262.

[20] F.X. Fu, M. Ilyn, A.M. Tishin, J.R. Sun, G.J. Wang, Y.F. Chen, F. Wang, Z.H. Cheng, and B.J. Shen, *J. Appl. Phys*. **93**, (2003) 5503.

[21] S. Fujieda, Y. Hasegawa, A. Fujita, and K. Fukamichi, *J. Magn. Mater*. 272-276 (2004) 2365.

[22] K. A. Gschneidner, Jr., V. K. Pecharsky, E. Brück, H. G. M. Duijn, and E. M. Levin, *Phys. Rev. Lett*. **85**, (2000) 4190.

[23] S. Y. Dan'kov, A.M. Tishin, V.K. Pecharsky, and K.A. Schneidner Jr, *Phys. Rev.* **B 57** (1998) 3478.

[24] S. Y. Dan'kov, A.M. Tishin, V.K. Pecharsky, and K.A. Schneidner Jr, *Rev. Sci. Instrum*. **68** (1997) 2432.

[25] Y.I. Spichkin,C.B. Zimm, and A.M. Tishin, Proc. *2nd Int. Conf. Magnetic Ref. at Room Temp*. **135–143** (2007).

[26] K.P. Khovaylo, V.V. Skokov,Y.S. Koshkid'ko, V.V. Koledov, V.G. Shavrov, V.D. Buchelnikov, S.V. Taskaev, H. Miki, T. Takag, and A.N. Vasiliev, *Phy. Rev*. B **78** (2008) 060403.

[27] T.J. McKenna, S.J. Campbell, D.H. Chaplin and G.V.H. Wilson

Solid State Comm. **40**, (1981) 177-181.

[28] M.D. Kuz`min and A.M. Tishin, Cryogenics **32** (1992) 545.

[29] M.D. Kuz`min and A.M. Tishin, Cryogenics **33** (1993) 868.

[30] K.A.Gschneidner Jr. and V.K. Pecharsky, Mater. Sci.Eng.A **287** (2000) 301.

[31] O. Tegus, E. Bruck, L. Zhang, K.H.J. Dagula, J. Buschow, and F.R. deBoer,Physica B **319** (2002) 174.

[32] K.A. Gschneidner Jr., and V.K. Pecharsky, Int. J. Refrig. **31** (2008) 945–961

[33] G.V. Brown, *J. Appl. Phys.* **47** (1976) 3673–3680.

[34] G. V. Brown, Practical and efficient magnetic heat pump. *NASA Tech. Brief* **3** (1978) 190–191.

[35] M.L. Lawton Jr., C.B. Zimm, and A.G. Jastrab, Reciprocating active magnetic regenerator refrigeration apparatus (1999) U.S. Patent 5,934,078.

[36] C. Zimm, Paper No. K7. 003, presented at the American Physical Society Meeting (2003, March 4) Austin, TX, http://www.aps.org/meet/MAR03/bapstocK.html

[37] C.B. Zimm, A. Sternberg, A.G. Jastrab, A. M. Boeder, L.M. Lawton, and J.J. Chell, Rotating bed magnetic refrigeration apparatus (2003) U.S. Patent 6,526,759.

[38] C. Zimm, A. Boeder, A., J. Chell, A. Sternberg, A. Fujita, S. Fujieda, and K. Fukamichi, Design and performance of a permanent magnet rotary refrigerator. *Int. J. Refrigeration* **29** (2006) 1302–1306.

[39] C. Zimm, J. Auringer, A. Boeder, J. Chells, S. Russek, and A. Sternberg, In: Poredos, A., Sarlah, A. (Eds.), Proceedings of the Second International Conference on Magnetic Refrigeration at Room Temperature Portoroz, Slovenia. International Institute of Refrigeration, Paris (2007, April 11–13) pp. 341–347

[40] P.E. Blumenfeld, F.C. Prenger, A. Sternberg, and C.B. Zimm, Adv. Cryog. Eng. **47** (2002) 1019–1026.

[41] D.W. Lu, X.N. Xu, H.B. Wu, and X. Jin, In: Egolf, P.W. (Ed.), Proceedings of the First International Conference on Magnetic Refrigeration at Room Temperature, Montreux, Switzerland. International Institute of Refrigeration, Paris, (2005, September 27-30) pp. 291–296.

[42] W. Wu, Development of a magnetic refrigeration prototype for operation at ambient temperature. Paper No. K7.004, presented at the American Physical Society Meeting, Austin, TX (2003, March 4) http://www.aps.org/meet/MAR03/baps/tocK.html

[43] A. Tura and A. Rowe, Design and testing of a permanent magnet magnetic refrigerator. In: Poredos, A., Sarlah, A. (Eds.), Proceedings of the Second International Conference on Magnetic Refrigeration at Room Temperature,, Portoroz, Slovenia. International Institute of Refrigeration, Paris, (2007 April 11–13) pp. 363–370.

[44] T. Okamura, K. Yamada, N. Hirano, and N. Nagay, Performance of a room-temperature rotary magnetic refrigerator. *Int. J. Refrigeration* **29** (2006) 1327–1331.

[45] T. Okamura, R. Rachi, N. Hirano, and S. Nagaya, Improvement of 100W class room temperature magnetic refrigerator. In: Poredos, A., Sarlah, A. (Eds.), Proceedings of the Second International Conference on Magnetic Refrigeration at Room Temperature (2007 April 11–13) Portoroz, Slovenia.

CHAPTER 2. MCE of $Gd_5Si_2Ge_2$ AND $Gd_5Si_{2.7}Ge_{1.3}$

Sesha Madireddi

A paper to be submitted to *The Journal of Applied Physics*

2.1 Introduction

Two Gd-Si-Ge series materials were prepared by the Ames Laboratory of the Iowa State University. One sample was $Gd_5Si_{2.7}Ge_{1.3}$ with the Curie temperature of 315 K, and the other $Gd_5Si_2Ge_2$ with the Curie temperature of 268 K. These samples were prepared by arc melting, and heat-treated as described by Percharsky et al. [1–3].

These two samples were tested using the AMT&C MMS to measure adiabatic temperature change at various magnetizing speeds from 0.25 T/s to 6 T/s. The two materials were very brittle, and it was hard to cut them to the correct size and shape. Figure 2.1 shows the photo of the tested $Gd_5Si_{2.7}Ge_{1.3}$ sample. They were not perfect, but could fit into the holder of the MMS machine.

Figure 2.1. Photo of the $Gd_5Si_{2.7}Ge_{1.3}$ sample.

2.2 Results and Discussion for $Gd_5Si_2Ge_2$

An elemental gadolinium sample was tested with the MMS to confirm it was operating correctly. Figure 2.2 shows the MCE (adiabatic temperature change ΔT_{ad}) curve for

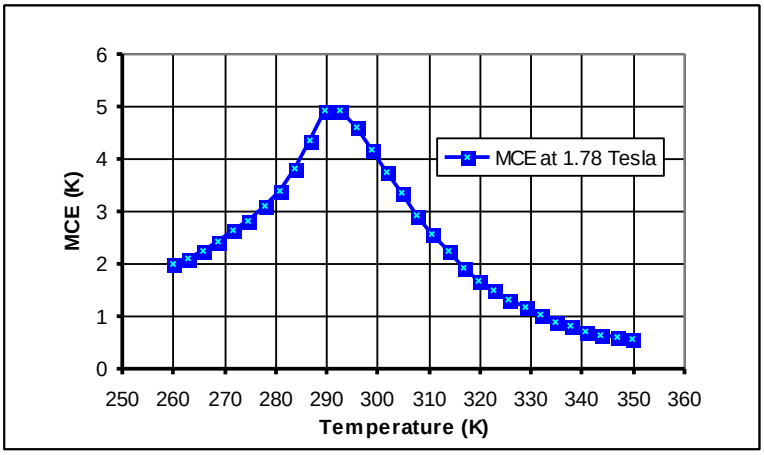

Figure 2.2. Adiabatic temperature change of gadolinium measured for the magnetic field change of 1.78 T as a function of temperature.

1.78 Tesla, and Figure 2.3 shows dynamic temperature vs. field curve at 295 K and 1 T/s. The peak MCE near the Curie temperature of 293K is 4.92K at 1.78 Tesla (2.76K/T) which is consistent with numerous publications [4 and references therein]. The data shown in Figure 2.2 are for a half-cycle rotation – the field climbs to 1.78 Tesla, and then

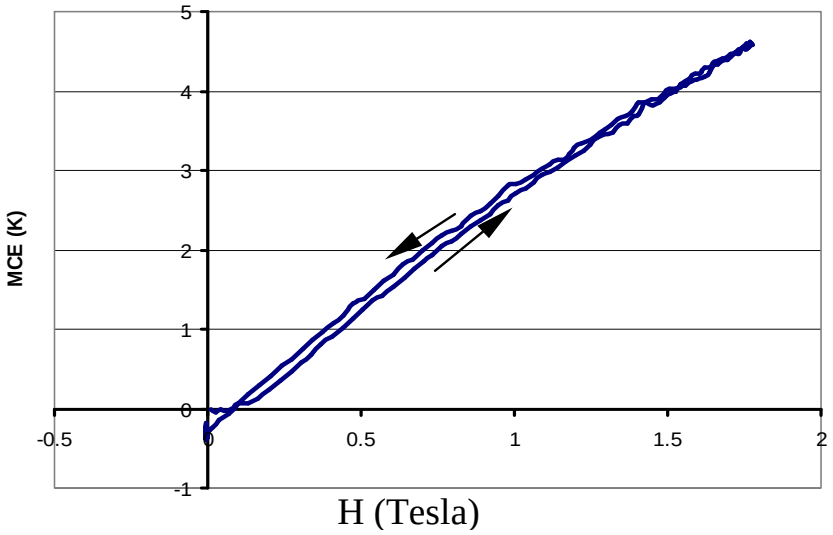

Figure 2.3. Adiabatic temperature change vs. field for gadolinium at T = 295 K and field change rate 1 T/s.

drops back to zero at a rate of 1 T/s. Note that the magnetizing and demagnetizing curve are almost overlapping. This indicates that gadolinium exhibits little, if any, thermal hysteresis.

Figure 2.4 shows magnetic field dependence of the adiabatic temperature changes for $Gd_5Si_2Ge_2$ at 1T/s and several different initial temperatures (265K, 268.5K, and 272K). Based on magnetization data, the Curie temperature of this specimen is about 268 K, thus the 265K, 268.5K, and 272K represent temperatures below, near, and above the first-order magnetostructural transition temperature, respectively. Similar to that shown in Figure 2.3, these tests were also half cycle rotations, and the arrows in Figure 2.4 show the direction of the field or temperature change. Unlike elemental gadolinium, $Gd_5Si_2Ge_2$ is a first-order material which has dynamic hysteresis, thus the demagnetizing curve is above the magnetizing curve, and the gap between the curves is an indication of the hysteresis magnitude. In this study, hysteresis is defined as the maximum gap. In general, the maximum hysteresis of the $Ge_5Si_2Ge_2$ material is high, but the hysteresis near the zero-field, which has

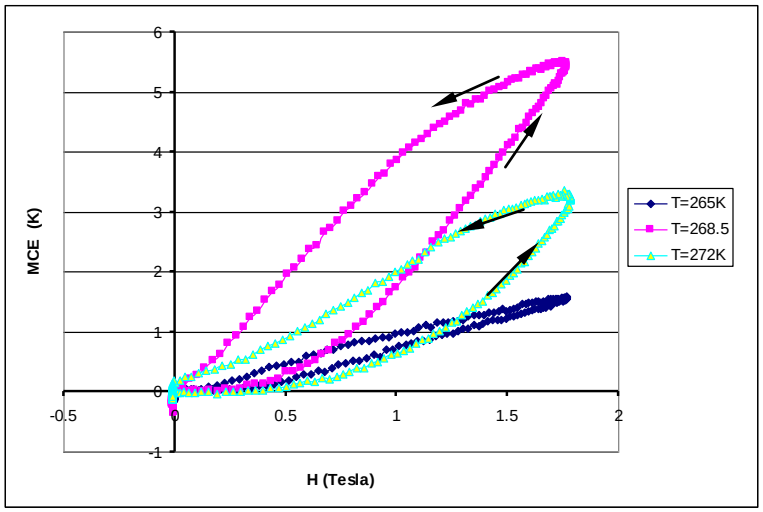

Figure 2.4. Typical testing curves of MCE vs. magnetic field for $Gd_5Si_2Ge_2$ measured in the heating mode. The difference between the up field and down field values is defined as the dynamic hysteresis.

the most influence on the magnetic refrigeration cycle, is quite low. Figure 2.4 also reflects the presence of a temperature dependent critical field (H_{cr}), above which the MCE rises significantly. For the initial temperature of 268.5K, H_{cr} is about 0.5 Tesla. This value is in agreement with the H_{cr} observed in the isothermal magnetization measurements [5, 6].

Figure 2.5 shows temperature dependence of MCE and dynamic hysteresis at 1.78 maximum field strength and 1 T/s sweeping rate for both heating and cooling modes. In the heating mode, the sample is cooled to temperature below the temperature of the measurement, and then the temperature of the first measurement is approached by heating the sample. For subsequent measurements, sample temperature progressively increases. In the cooling regime, the sample is heated to temperature exceeding the highest temperature of the measurement. The sample is then cooled to the first measurement temperature and for each subsequent measurement sample temperature progressively decreases. The results for the heating mode are the same as for the cooling mode for all sample temperatures exceeding the Curie temperature, but the peak MCE of the cooling curve is by 1.3 K higher than that of the heating curve. Further, as shown in Figure 2.5, the cooling curve is located above the heating curve for certain temperatures below the Curie temperature. Notice also that the peak point of the cooling curve shifts to the left by about 2.5 K – from 268.5K to 266K, compared to the heating curve.

The phenomenon is similar to that observed for $Ni_{2.19}Mn_{0.81}Ga$ by Khovaylo et al. [7]. When explaining this phenomenon for $Ni_{2.19}Mn_{0.81}Ga$, Khovaylo et al. stated that upon heating at a temperature in the phase transition region, contribution of the structural subsystem to the adiabatic temperature change is unlikely to occur due to a low sensitivity of

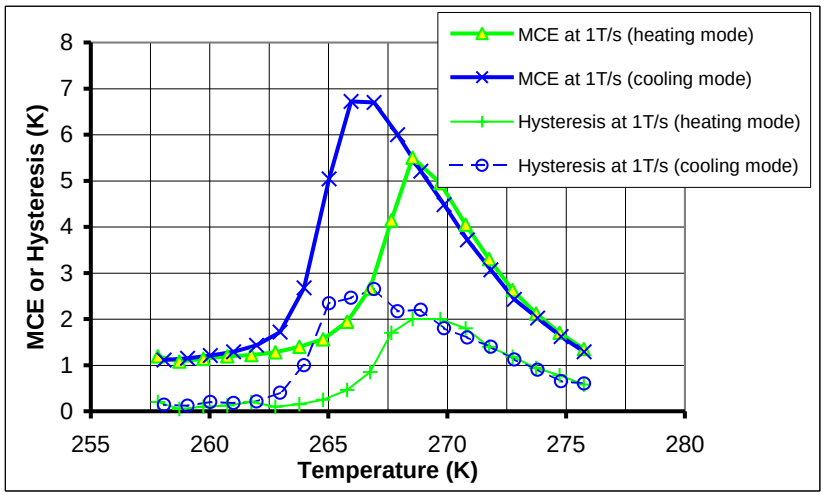

Figure 2.5. MCE and dynamic hysteresis of $Gd_5Si_2Ge_2$ at 1 T/s.

the phase transition temperature to the magnetic field, while for cooling mode, there are contributions to ΔT_{ad} from both magnetic and elastic subsystems. However, this explanation does not hold for $Gd_5Si_2Ge_2$. The structural transition in $Gd_5Si_2Ge_2$ occurs regardless of whether temperature increases or decreases. Actually, the first-order magneto-structural change process, and associated magnetic-field-induced entropy change process, is generally different for the heating and cooling modes, as follows from the phase diagram in the temperature-magnetic field coordinates of the material [8]. In fact, from the phase diagram in Figure 2.6 [8] one can see the 1.78 T magnetic field is sufficient to complete the phase transformation on cooling but is insufficient to complete the phase transformation on heating.

Fig. 2.6 shows that at low temperatures and high magnetic fields the compound is ferromagnetically ordered and all slabs are interconnected as shown in the icon. At high temperatures and low magnetic fields the compound is magnetically disordered (paramagnetic) and only 1/2 of the slabs are interconnected as also shown in the icon. The red area is the region where the paramagnetic/monoclinic phase transforms into the

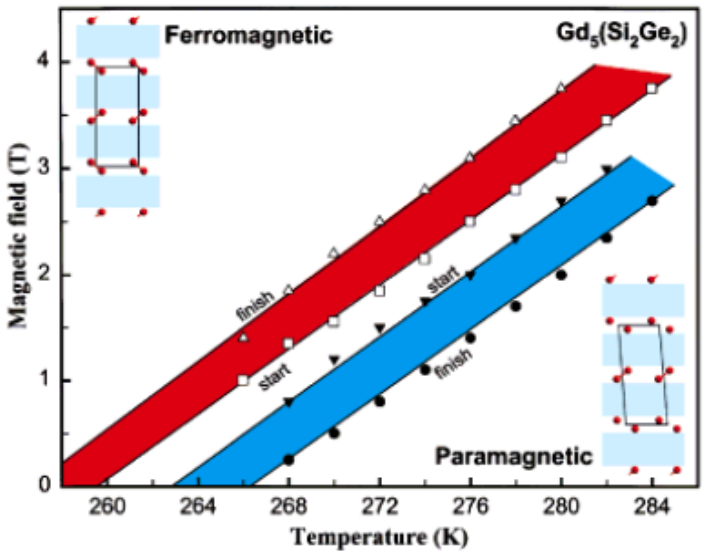

Figure 2.6. Phase diagram for $Gd_5(Si2Ge_2)$.

ferromagnetic/orthorhombic phase during magnetic field increase and/or temperature reduction. The blue area is the region where the ferromagnetic/orthorhombic phase transforms into the paramagnetic/monoclinic phase during magnetic field reduction and/or temperature increase. Both the red and the blue areas indicate the two regions where the $Gd_5(Si_2Ge_2)$ system is both structurally and magnetically inhomogeneous, i.e., it consists of the two phases, ferromagnetic/orthorhombic and paramagnetic/monoclinic [8].

It is worthy to note that the maximum MCE near the temperature of the first-order transition shown in Figure 2.5 is 5.5K or 3.1 K/T (for heating mode) and 6.7K or 3.8 K/T (for cooling mode), which are 12% and 36% higher than the baseline gadolinium material, respectively. This difference is close to that based on the reported indirect measurement, and much higher than that based on the stepping direct measurement reported by Giguere et al. [9].

Figure 2.7 shows a comparison of results for various magnetic field sweep rates. Although the peak MCEs at 2 T/s and 6 T/s are slightly lower than that at 1 T/s, the behavior of the MCE and the dynamic hysteresis curves for different sweeping rates are nearly the same. Thus, the time-dependence of the MCE for this material is not evident, at least over this range of magnetic field sweep rates. Figure 2.8 represents the multiple cycle measurement for the 6 T/s testing at 272 K. Based on this figure, it appears that the kinetics of the magnetostructural structural change and the associated MCE are fast enough to respond to the magnetic field change rate of up to 6 T/s. Khovaylo et al. [7] also reported no time dependence of MCE in their work on $Ni_{2.19}Mn_{0.81}Ga$. Although Spichkin et al. [10] showed some time dependence of MCE for $La(Fe_{1-x}Si_x)_{12}$ materials based on their 0.05 T/s and 0.5 T/s data, one cannot exclude the possibility that the heat losses, which disrupt the adiabatic condition, and not another physical reason, cause the difference in 0.05 T/s and 0.5 T/s data of Ref. 10.

Adiabatic temperature change, $\Delta T_{ad,}$ from the direct measurement at field change of 0 to 1.78T (Figure 2.6) is in agreement with the indirect measurements of Pecharsky et al. 1997 [3] for magnetic field change of 0 to 2T (Figure 2.9).

2.3 Conclusions

The MCE characteristics of the first-order material $Gd_2Si_2Ge_2$ were measured under different operating conditions. The absolute value of the directly measured MCE is close to that obtained from indirect measurement. Significant differences in the heating mode and cooling mode were observed. The kinetic response of the magneto-structural change in

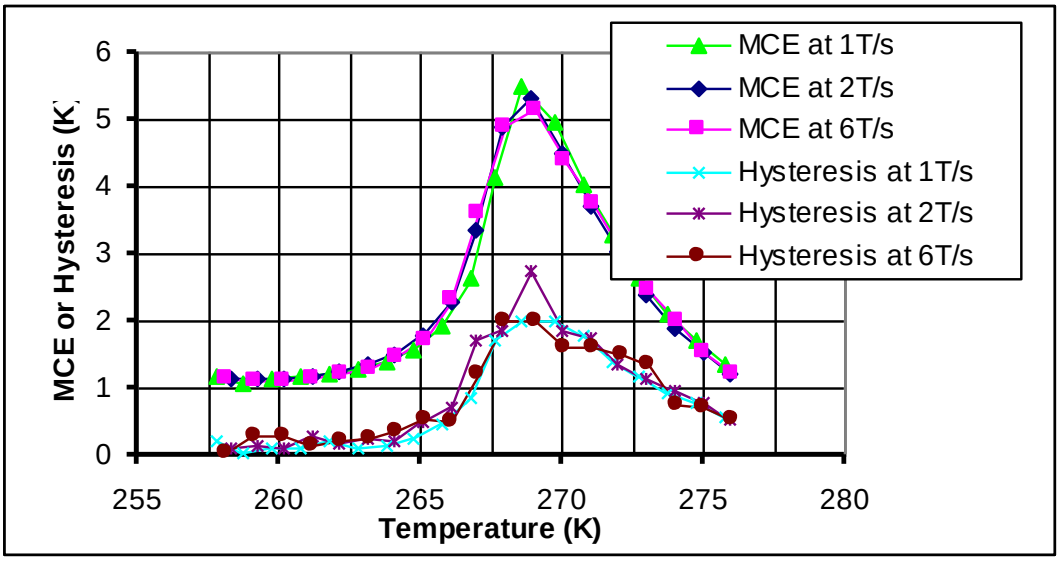

Figure 2.7. MCE and hysteresis of $Gd_5Si_2Ge_2$ at various sweeping rates measured during the heating mode.

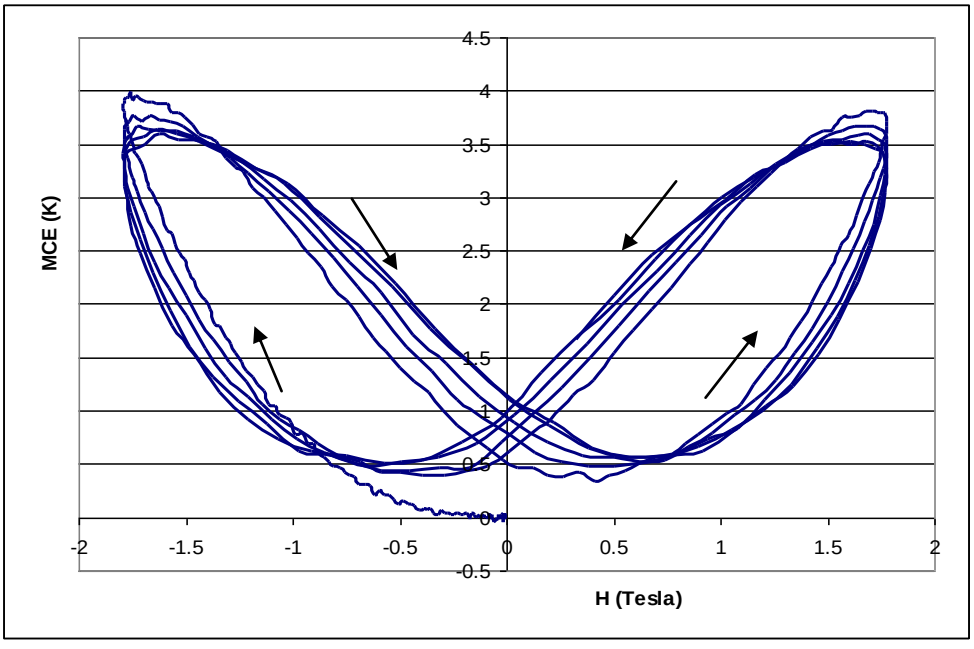

Figure 2.8. Multiple cycle test for $Gd_5Si_2Ge_2$ at 6 T/s measured during the heating mode.

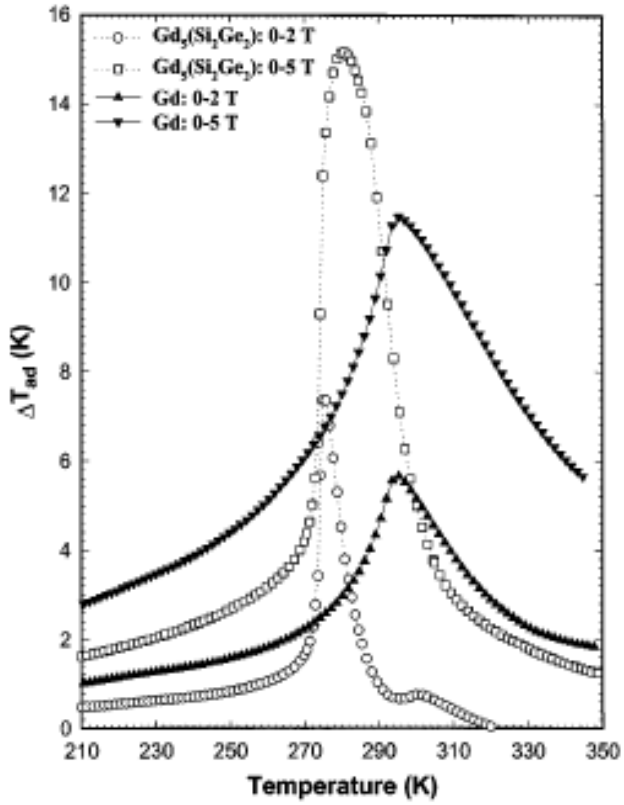

Figure 2.9. The magnetocaloric effect in $Gd_5(Si_2Ge_2)$ from 210 to 350 K in comparison with that of pure Gd for magnetic field change from 0 to 2T and 0 to 5T (Pecharsky et al. 1997 [3]).

$Gd_2Si_2Ge_2$ is fast enough to respond to an applied continuously changing field with a sweeping rate up to 6 T/s, and time dependence of the MCE is not evident in this material.

2.4 Results and Discussion for $Gd_5Si_{2.7}Ge_{1.3}$

The $Gd_5Si_{2.7}Ge_{1.3}$ is a second-order transition material with the Curie temperature of 315 K based on magnetization data. Figure 2.10 shows both MCE and hysteresis for both heating and cooling modes. In the heating mode, the initial sample temperature starts from the low point and progressively increases, while in the cooling regime, the sample.

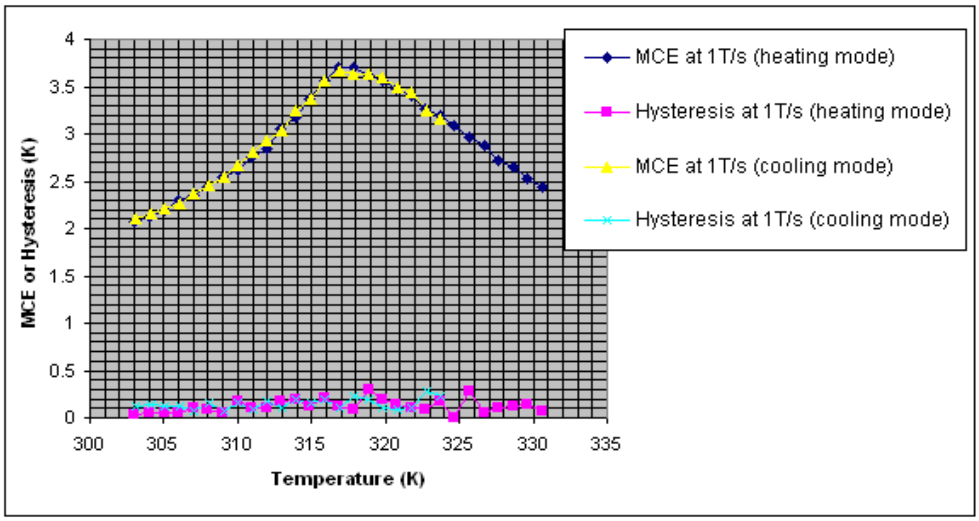

Figure 2.10. MCE and hysteresis of $Gd_5Si_{2.7}Ge_{1.3}$ at 1 T/s.

temperature starts from the high point and progressively decreases. The magnet-sweeping rate was 1 T/s. The curve of the heating process is the same as that of the cooling process. The maximum MCE (located at 317 to 318 K) is about 3.7 K at the maximum field of 1.78 Tesla. The thermal hysteresis is minimal, i.e., it is less than 0.3 K. As a comparison, gadolinium has an MCE of approximately 2.0 K at 317 K.

Figure 2.11 demonstrates a comparison for various sweep rates from 1 T/s to 6 T/s. The MCE curves at various sweep rates are almost the same, but the thermal hysteresis curves are a little different for different sweeping rates. Surprisingly, several data points for 2 T/s show very high hysteresis – from 1.2 to1.6 K, near the Curie temperature, and one data point for 2.5 T/s at 328 K displays a high hysteresis of 1.4 K. The hysteresis data for 4 T/s and 6 T/s do not show such high values, although they are a little higher than that for 1 T/s.

To see if the unexpected behavior in hysteresis at 2 T/s is repeatable, two more rounds of tests at 2 T/s were conducted, with the results shown in Figure 2.12. In the second

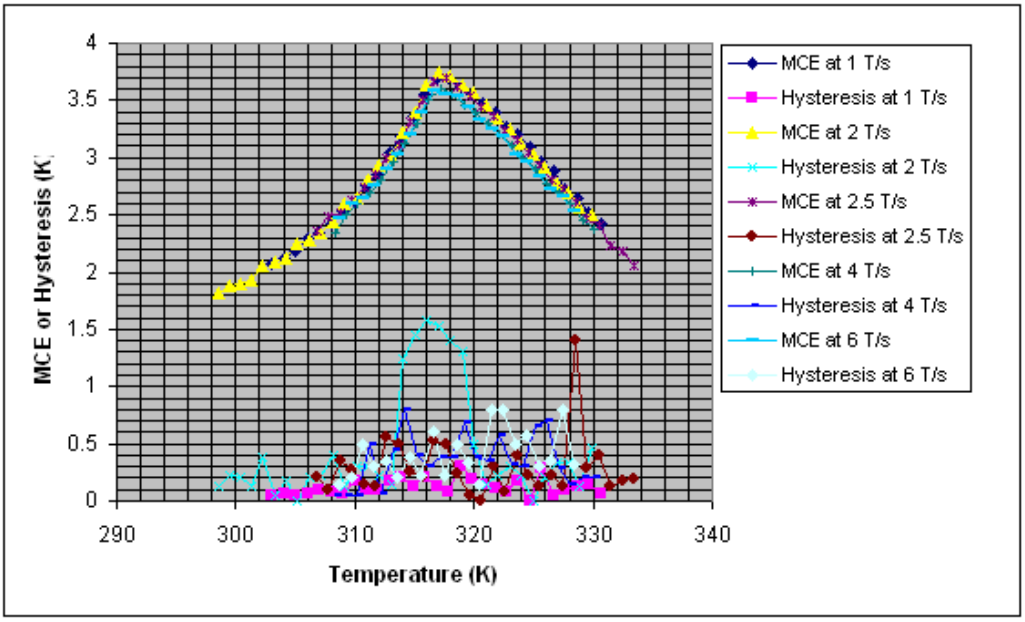

Figure 2.11. MCE and hysteresis of $Gd_5Si_{2.7}Ge_{1.3}$ at various sweeping rates.

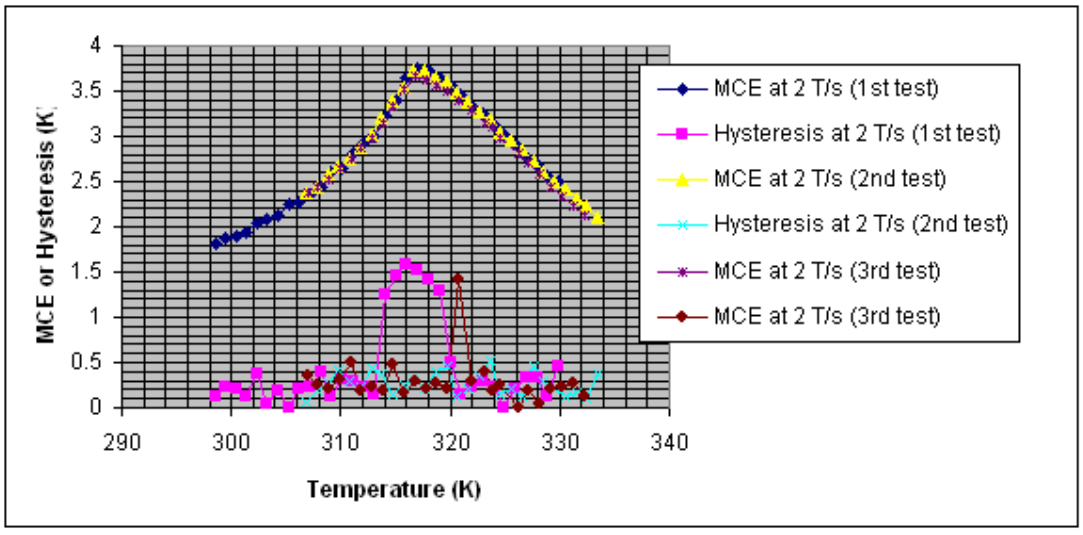

Figure 2.12. Repeated tests for 2 T/s.

test, no large hysteresis value was observed. But in the third test, one data point with high hysteresis (1.4 K) was observed. It seems that sporadic high hysteresis points could be triggered for the $Gd_5Si_{2.7}Ge_{1.3}$ material.

To further confirm the MMS machine was working correctly, the test at 1 T/s was repeated. Figure 2.13 shows that the second test gave the same results as the first.

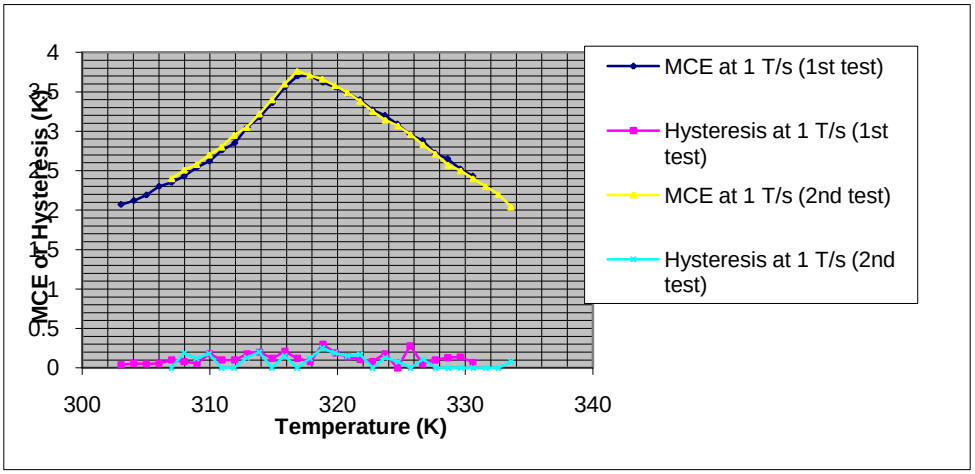

Figure 2.13. Repeated test for 1 T/s.

2.5 Findings

The absolute value of the directly measured MCE is close to that obtained from indirect measurement. MCE and hysteresis of $Gd_5Si_{2.7}Ge_{1.3}$ measured at various sweep rates showed insignificant differences in the heating mode and the cooling mode. $Gd_5Si_{2.7}Ge_{1.3}$ is shown to be a second-order material with the Curie temperature of 315 K based on magnetization data and direct measurements of the magnetocaloric effect.

2.6 References

[1] Y.A. Mudryk, Y. Lee, T. Vogt, K. A. Gschneidner, Jr., and V. K. Pecharsky *Phy. Rev*. B **71** (2005) 174104.

[2] A. O. Pecharsky, K. A. Gschneidner, Jr., and V. K. Pecharsky, J. Appl. Phys. **93** (s2003) 4722d.

[3] V. K. Pecharsky and K. A. Gschneidner, Jr., Phys. Rev. Lett. **78** (1997) 4494.

[4] K.A. Gschneidner Jr, V.K. Pecharsky, and A.O. Tsokol, *Rep. Prog. Phys*. **68** (2005) 1479-1539.

[5] V.K. Pecharsky and K.A. Gschneidner Jr, *Phy. Rev. Lett*. **78** (1997) 4494.

[6] A.O. Pecharsky, K.A. Gschneidner Jr, and V.K. Pecharsky, J. *Appl. Phys.* **93** (2003) 4722-4728.

[7] K.P. Khovaylo, V.V. Skokov , Y.S. Koshkid'ko, V.V. Koledov, V.G. Shavrov, V.D. Buchelnikov, S.V. Taskaev, H. Miki, T. Takagi, and A.N. Vasiliev, *Phy. Rev*. B **78** (2008) 060403.

[8] V.K. Pecharsky and K.A. Gschneidner Jr, *Adv. Mater.* (Weinheim) **13** (2001) 683-686.

[9] A. Giguere, M. Foldeaki, B.R. Gopal, R. Chahine, T.K. Bose, A. Frydman and J.A. Barclay, *Phys. Rev. Lett*. **83** (1999) 2262.

[10] Y.I. Spichkin, C.B. Zimm, and A.M. Tishin, Proc. *2nd Int. Conf. Magnetic Ref. at Room Temp*. Portoroz, Slovenia (2007) 135–143.

CHAPTER 3. MCE of MnFePAs Materials

Sesha Madireddi

A paper to be submitted to *The Journal of Magnetism and Magnetic Materials*

3.1 Introduction

$MnFe(P_{1-x}As_x)$ compounds have been extensively studied and are considered to be a promising magneto-caloric materials which undergoes an unusual first-order magneto-structural transition, [1]. It exhibits a GMCE [3, 4] potentially useful for room temperature magnetic refrigeration. MCE effects are accompanied by a crystal structure transformation, which is easily affected by the magnetic field and temperature.

In this study, the MMS from the AMT&C Corporation was used to measure the adiabatic temperature change of the samples provided by the Vander Waals-Zeeman Institute, University of Amsterdam. Materials measured in this work are listed in Table 1.

In the intermediate composition range ($0.15 < x < 0.66$), the compounds in the $MnFeP_{1-x}As_x$ system crystallize in the hexagonal Fe_2P-type of structure [4]. They have most interesting magnetic properties including a field-induced first-order magnetic transition. Polycrystalline samples of MnFePAs as listed in Table 3.1 were synthesized starting from the binary Fe_2P and $FeAs_2$ compounds, Mn chips, and P powder mixed in the appropriate proportions, by ball milling under a protective atmosphere. After this mechanical alloying process, one obtains an amorphous powder. To obtain the dense material of the crystalline phase, the powders are pressed into pellets and sealed in molybdenum tubes under an argon atmosphere. The solid state reaction was performed in a molybdenum crucible. First, the obtained mixture was sealed in the crucible in a 100- 200 mbar Ar atmosphere. Then, this

Table 3.1. MnFePAs compounds that were used for the direct measurements

S.No	Material Reference	Material Composition	Process variation
1	**Tc1_247K**	$MnFeP_{0.55}As_{0.45}$	Heat treatment protocols varied
2	**Tc2_261K**		
3	**Tc3_265K**		
4	**Tc4_272K**	$Mn_{1.1}Fe_{0.9}P_{0.54}As_{0.46}$	
5	**Tc5_281K**	$Mn_{1.1}Fe_{0.9}P_{0.5}As_{0.5}$	
6	**Tc6_286 K**	$Mn_{1.1}Fe_{0.9}P_{0.54}As_{0.46}$	Heat treatment protocols varied
7	**Tc7_290K**		
8	**Tc8_296K**	$Mn_{1.1}Fe_{0.9}P_{0.47}As_{0.53}$	
9	**Tc9_295K**	$MnFeP_{0.53}As_{0.47}$	Heat treatment protocols varied
10	**Tc10_300K**		
11	**Tc11_300K**		
12	**Tc12_306K**		
13	**Tc13_314K**	$MnFeP_{0.45}As_{0.55}$	Heat treatment protocols varied
14	**Tc14_320K**		

crucible was heated at 1273 K for 100 hours, followed by a homogenization process at 923 K for 120 hours. Finally, the crucible was slowly cooled down to ambient conditions. For the sample labels in column 2, “Tc” means Curie temperature, and “Tc#_320K” means Curie temperature 320K based on initial magnetization data. Each material sample has a different composition and Curie temperature.

Large magnetoelastic phenomena have been observed in the hexagonal crystal structures of the system, $MnFeP_{1-x}As_x$, which are accompanied by an antiferro-ferromagnetic long-range ordering transition. The antiferro-ferromagnetic and ferro-paramagnetic transformations have been shown to be markedly field dependent [5].

The temperature dependence of the magnetization near room temperature of $MnFeP_{0.45}As_{0.55}$ and Gd, was determined in an applied magnetic field of 1 T. The change in

magnetization in $MnFeP_{0.45}As_{0.55}$ at the ordering temperature, T_C, is much larger than that of Gd, despite the fact that the magnetic moment of Gd is much larger at low temperatures (248 J/T compared to 125 J/T). Variation of the P/As ratio between 3/2 and 1/2 makes it possible to tune T_C and the optimal operating temperature between 200 and 350 K (-70.8 C and 80.8 C) without losing the large MCE [6].

The magnetic isotherms of $MnFeP_{0.45}As_{0.55}$ in the vicinity of its ordering temperature were measured with increasing and decreasing fields. The magnetization measurements showed that there exists a field-induced magnetic-phase transition. In low fields, the phase transition from the PM to the FM state exhibits a step-like discontinuity in the magnetization, but in higher fields the transition becomes smoother. The hysteresis observed in these isotherms is closely connected with the discontinuous change in the lattice parameters (c/a) reported for this compound [7].

Research into the electronic structure and magnetic properties of $Gd_5(Si_2Ge_2)$ and $MnFe(P_{0.333}As_{0.66})$ system of alloys have reported that the magnetic-structural transformation in these systems corresponds to a first-order phase transition [8].

3.2 Results and Discussion for MnFeAsP

The thermal loss for MnFePAs materials was expected to be lower than Gadolinium because of the much lower thermal conductivity, but heat loss was still a problem. Before measurement, each MnFePAs sample was cooled to liquid nitrogen temperature, and several thermal cycles between the temperature 50 K below the Curie temperature and 50 K above the Curie temperature were performed. This was to eliminate the “virgin” effect of the material [10].

A typical test curve for a MnFePAs material is provided in Figure 3.1 showing the magnetic field curve (red) and adiabatic temperature difference ($\Delta T_{ad)}$ curve (blue) with time. The curve of field vs. temperature, which is more useful, is shown in Figure 3.2. Similar to that shown in Figure 3.1, this test was also half-cycle rotation. The arrow in Figure 3.2 shows the direction of the temperature change. The temperature curve of demagnetizing is above that of magnetizing due to hysteresis of the MnFePAs materials. The temperature change at the peak point is the maximum MCE. The gap between the temperature of the magnetizing process and that of the demagnetizing process is an indicator of hysteresis magnitude. For the test shown in Figure 3.2, MCE is 4 K and (maximum) hysteresis is 0.75 K.

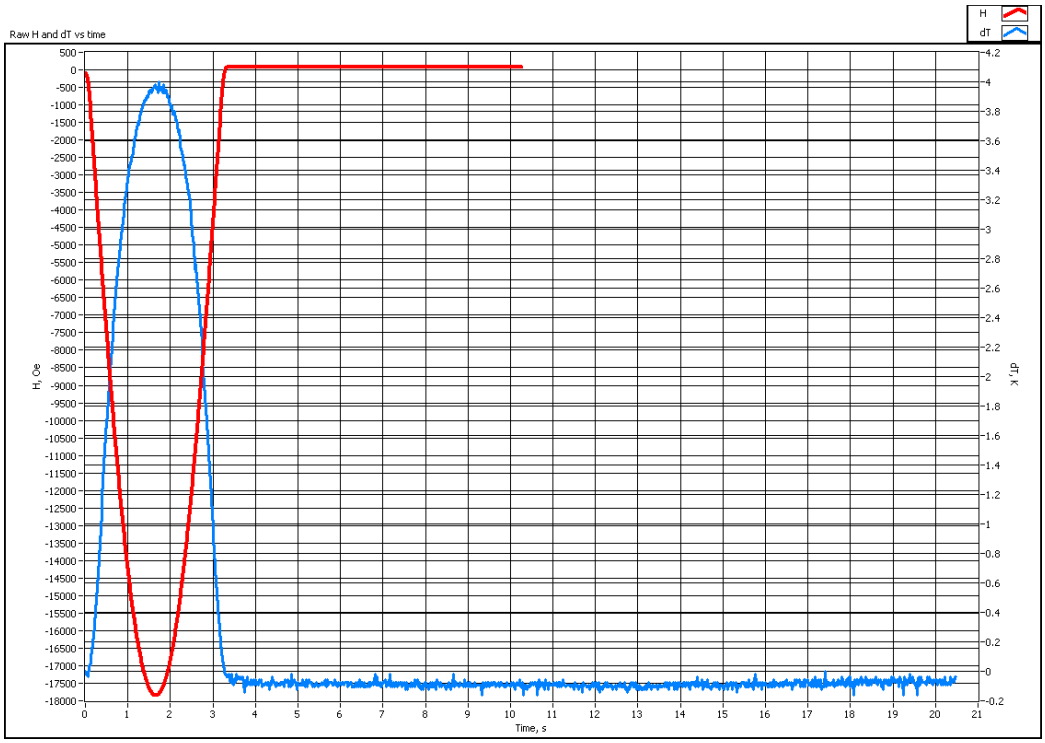

Figure 3.1. Temperature & field vs. time for a typical MnFePAs test at 1T/s.

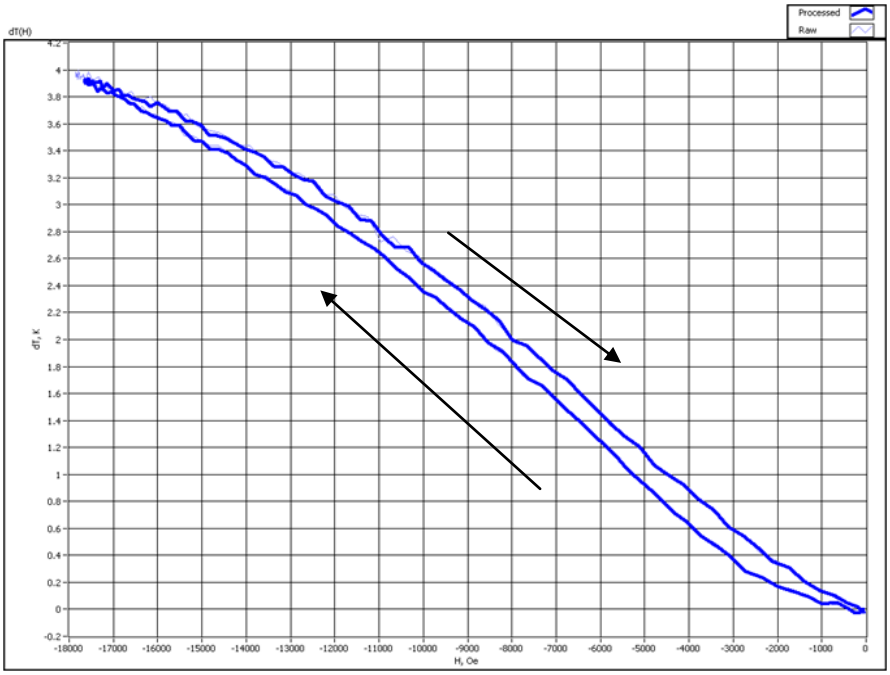

Figure 3.2. Adiabatic temperature change vs. field for a typical MnFePAs test at 1T/s.

The test data are summarized in Tables 3.2, 3.3, and 3.4. Two batches of MnFePAs materials were received from the University of Amsterdam. Both MCE (adiabatic temperature change) and maximum hysteresis at various field sweeping rates are given. The "Tc" in the table is based on the peak point in the curve of the temperature change in current study. All the materials were tested at 1 T/s sweeping rate, and some of them were also measured at other sweeping rates between 0.25 ~ 6 T/s to evaluate time dependence of the MCE and hysteresis. As stated before, for 0.5 T/s and 0.25 T/s, since the sweeping rate is slow and the tests cannot be treated as "adiabatic", the measured MCE and hysteresis were both undervalued. The data of 0.25 and 0.5 T/s are listed in Table 3.3 only for reference.

Table 3.2. Summary of test results for MnFePAs samples and 1.78 Tesla

S.No	Material Reference	Material Composition	Process variation	Tc	MCE	Max Hysteresis	Bandwidth
1	**Tc1_247K**	$MnFeP_{0.55}As_{0.45}$	Heat treatment is variant	254.5	2.78	1.08	5.4
2	**Tc2_261K**			261	3.2	1.05	4.75
3	**Tc3_265K**			268	3.4	0.95	5
4	**Tc4_272K**	$Mn_{1.1}Fe_{0.9}P_{0.54}As_{0.46}$		272.5	3.95	0.86	8.35
5	**Tc5_281K**	$Mn_{1.1}Fe_{0.9}P_{0.5}As_{0.5}$		282	3.21	0.65	8.2
6	**Tc6_286 K**	$Mn_{1.1}Fe_{0.9}P_{0.54}As_{0.46}$	Heat treatment is variant	287	4.09	1.15	5.65
7	**Tc7_290K**			288	4.35	1.02	4.8
8	**Tc8_296K**	$Mn_{1.1}Fe_{0.9}P_{0.47}As_{0.53}$		292	4.2	1.62	5.5
9	**Tc9_295K**	$MnFeP_{0.53}As_{0.47}$	Heat treatment is variant	292	5.4	1.3	4.2
10	**Tc10_300K**			297	3.3	0.7	6.75
11	**Tc11_300K**			298	4.42	1.2	7.4
12	**Tc12_306K**			304.5	4.8	0.98	7.4
13	**Tc13_314K**	$MnFeP_{0.45}As_{0.55}$	Heat treatment is variant	311	3.92	0.56	3
14	**Tc14_320K**			312	3.58	0.6	4.8

Table 3.3. MCE for MnFePAs samples at different sweep rates

S.No	MCM	Tc (K)	MCE (K)							
			0.25 T/s	0.5 T/s	1 T/s		2 T/s	3 T/s	4 T/s	6 T/s
					(Heating)	(Cooling)				
1	Tc1_247K	~ 254.5	2.73		2.78	2.85		2.7		2.7
2	Tc2_261K	~ 261			3.2	3.38				
3	Tc3_265K	~ 268	3.33		3.4	3.52		3.12		3.3
4	Tc4_272K	271 ~ 272.5	4.1	3.95	3.95	4.23				4.02
5	Tc5_281K	281 ~282			3.21	3.36				
6	Tc6_286 K	~ 287	4.15	4.14	4.09	4.4	3.88		3.8	3.87
7	Tc7_290K	~288	4.26	4.3	4.35		4.22		4.2	4.2
8	Tc8_296K	~ 292			4.2	4.33				
9	Tc9_295K	291 ~ 292			5.4	5.68				
10	Tc10_300K	296 ~ 297			3.3	3.32				3.2
11	Tc11_300K	297 ~ 298			4.42	4.6				
12	Tc12_306K	303.5 ~ 304.5	4.65		4.8	4.95				4.7
13	Tc13_314K	310 ~ 311			3.92	4.05				
14	Tc14_320K	311 ~ 312			3.58	4.06				
	Average		3.87	4.13	3.58	4.06				

Typical MCE or hysteresis vs. temperature curves are given in Figure 3.3 using "Tc6_286K" material at 1T/s (1.78 Tesla max field) as an example. Each material was tested in a temperature range of approximately 20 K (from 10 K below Curie temperature to 10 K above Curie temperature).

Table 3.4. Hysteresis of MnFePAs samples at different sweep rates

S.No	MCM	Tc (K)	Maximum Hysteresis (K)							
			0.25 T/s	0.5 T/s	1 T/s		2 T/s	3 T/s	4 T/s	6 T/s
					(Heating)	(Cooling)				
1	Tc1_247K	~ 254.5	0		1.08	0.57		1.5		1
2	Tc2_261K	~ 261			1.05	0.96				
3	Tc3_265K	~ 268	0		0.95	1.05		1.6		1
4	Tc4_272K	271 ~ 272.5	0.3	0.66	0.86	0.74				1.35
5	Tc5_281K	281 ~282			0.65	0.72				
6	Tc6_286 K	~ 287	0.4	1.06	1.15	1.3	2.3		1.2	1.3
7	Tc7_290K	~288	0.42	0.94	1.02		1.35		1.35	1.07
8	Tc8_296K	~ 292			1.62	1.2				
9	Tc9_295K	291 ~ 292			1.3	1.7				
10	Tc10_300K	296 ~ 297			0.7	0.86				1.4
11	Tc11_300K	297 ~ 298			1.2	1.05				
12	Tc12_306K	303.5 ~ 304.5	0		0.98	1.2				1.4
13	Tc13_314K	310 ~ 311			0.56	0.84				
14	Tc14_320K	311 ~ 312			0.6	0.9				
	Average				0.60	0.90				

Temperature bandwidth (defined here as the temperature span over which the materials exhibits MCE reaching at least 70 % of the maximum MCE) of MnFePAs samples were measured at only a1T/s sweep rate for both the heating mode and the cooling mode with results summarized in the Table 3.5.

One can see from Figure 3.3 that the result of the heating test is the same as the cooling test for the part above the Curie temperature, but the peak point of the cooling curve is 0.3 K higher than the heating curve, and the cooling curve is above the heating curve for temperatures lower than the Curie temperature. The peak point of the cooling curve shifts to the left (lower temperature) by 0.5 to 1.0 K compared to the heating curve. With decreasing temperature, the heating curve and cooling curve overlap again. In fact, this phenomenon was observed for all MnFePAs materials. From Table 3.3, on average, the cooling curve has peak MCE ~0.5 K higher than the heating curve.

Table 3.5. Temperature bandwidth of MnFePAs samples at 1T/s sweep rate

S.No	MCM	Tc (K)	Temperature Bandwidth of 70% MCE (K)	
			1 T/s	
			Heating	Cooling
1	Tc1_247K	~ 254.5	7.4	7.9
2	Tc2_261K	~ 261	8.2	8.2
3	Tc3_265K	~ 268	7.4	7.45
4	Tc4_272K	271 ~ 272.5	5.5	5.7
5	Tc5_281K	281 ~282	8.35	8.3
6	Tc6_286 K	~ 287	5	5.05
7	Tc7_290K	~288	4.8	
8	Tc8_296K	~ 292	4.75	5
9	Tc9_295K	291 ~ 292	3	3.55
10	Tc10_300K	296 ~ 297	6.75	6.8
11	Tc11_300K	297 ~ 298	4.8	4.87
12	Tc12_306K	303.5 ~ 304.5	4.2	4.25
13	Tc13_314K	310 ~ 311	5.65	5.85
14	Tc14_320K	311 ~ 312	5.4	5.45
	Average		5.40	5.45

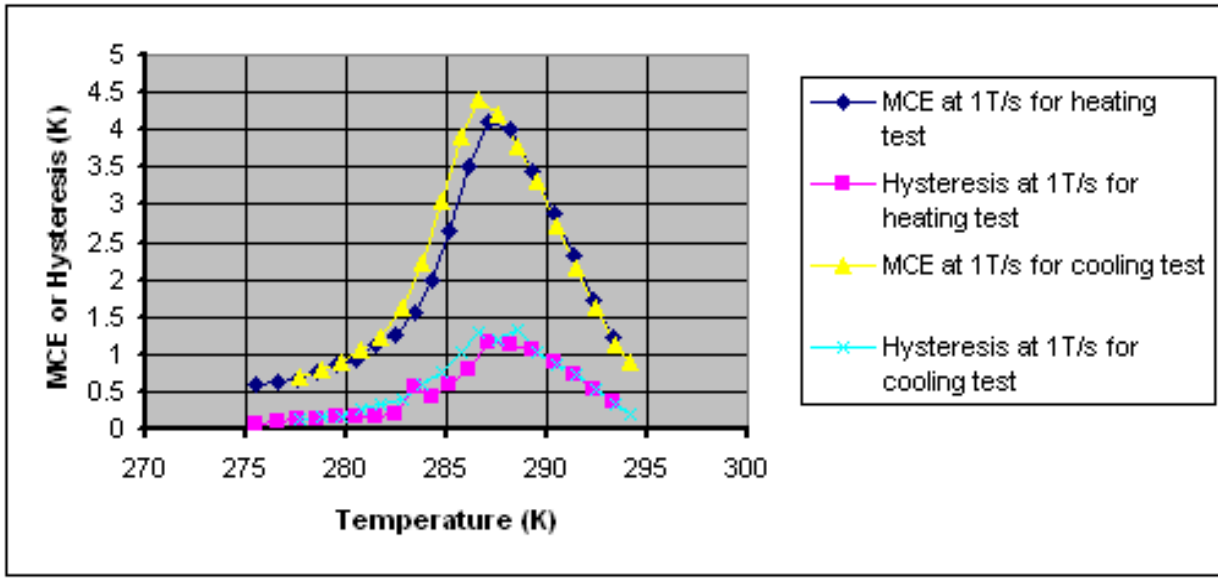

Figure 3.3. Data curves for "Tc6_286K" ($Mn_{1.1}Fe_{0.9}P_{0.54}As_{0.46}$) at 1T/s.

Only one sample ("Tc9_295K") has MCE (5.4 K) higher than the peak MCE of the baseline Gadolinium (5.0 K). The MCE of most other samples is between 3.0 and 4.5K. Maximum measured hysteresis is between 0.6 and 2.3 K with most between 1.0 and 1.6 K. The temperature bandwidth for 70% MCE is 3.0 to 8.4 K.

Figure 3.4 gives the direct measurements for the sample (Tc5_281 K) $Mn_{1.1}Fe_{0.9}P_{0.5}As_{0.5.}$ Figure 3.5 provides an MCE comparison of MnFePAs materials and Gadolinium at 1 T/s (1.78 Tesla max field). Note that each point on the MnFePAs curve represents a different material. A higher MCE is generally associated with higher hysteresis. MCE data are more repeatable and reliable than hysteresis data.

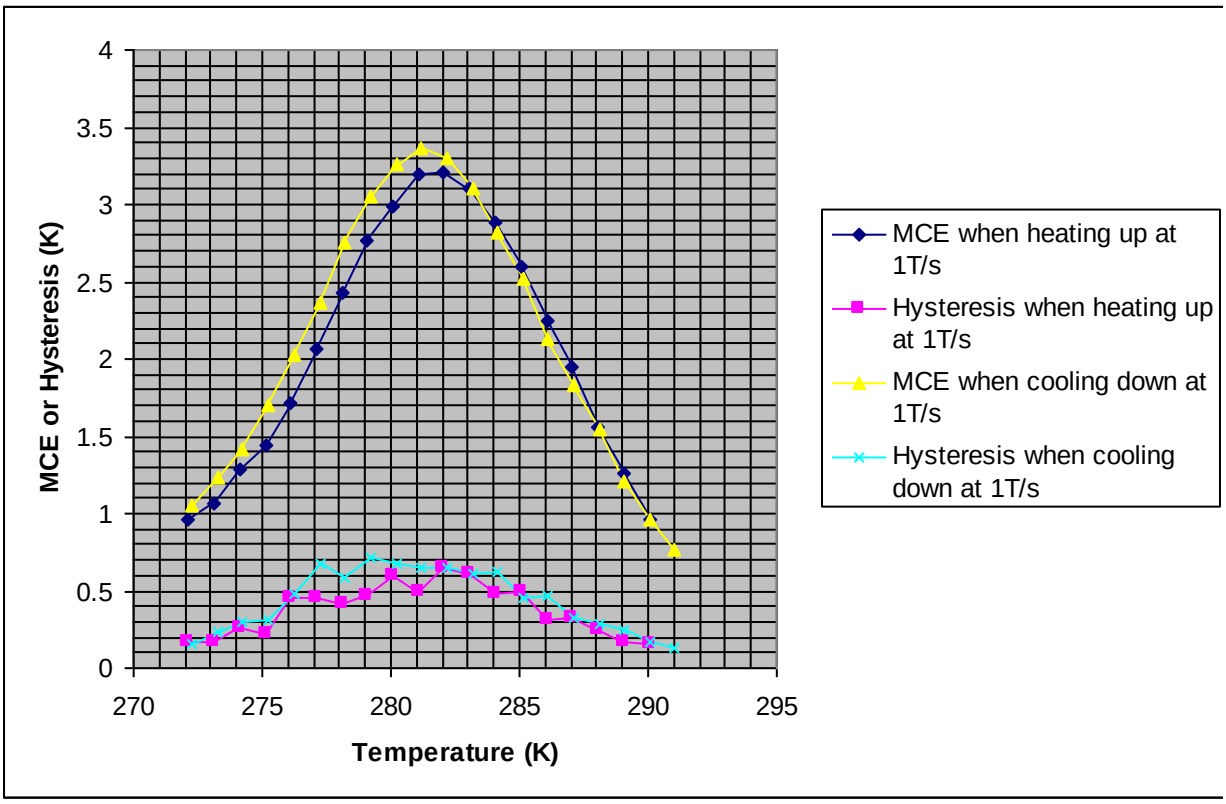

Figure 3.4. Data curves for "Tc5_281K" $Mn_{1.1}Fe_{0.9}P_{0.5}As_{0.5}$ at 1T/s.

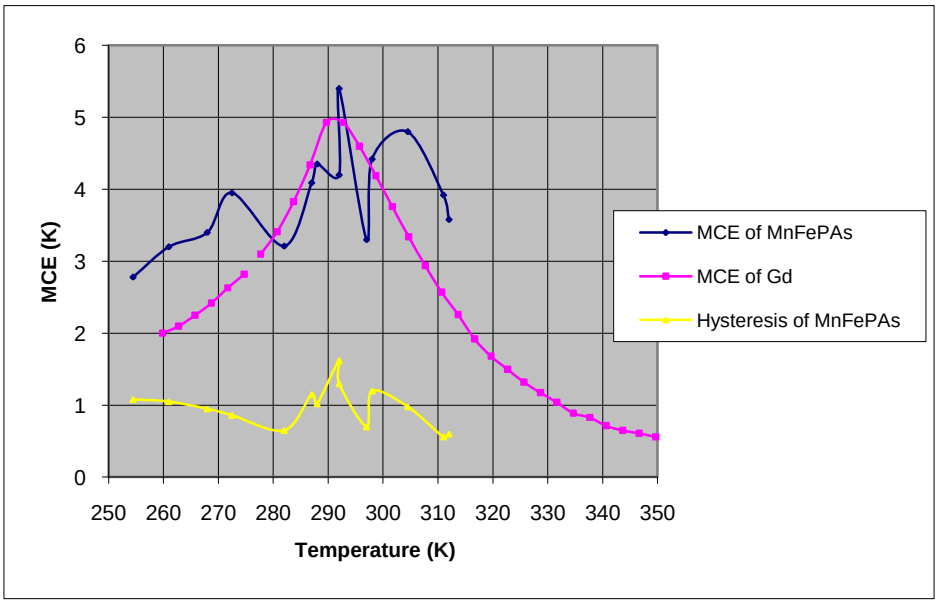

Figure 3.5. Comparison of MCEs of MnFePAs alloys and Gadolinium.

Comparing the data for various magnetic field change rates between 1 T/s and 6 T/s, one can see both MCE and hysteresis are influenced by the sweeping rate, but it seems that MCE/hysteresis is just a weak function of the sweeping rate. Table 3.4 gives a comparison of the average MCE and hysteresis of 1 T/s to that of other sweeping rates. For a fair comparison, only the 1 T/s data for the materials tested for other sweeping rates and compared to the 1 T/s data are used to calculate the average (for example, seven materials were tested for 6 T/s, as shown in Table 3.2; therefore, only the 1 T/s data of these seven materials were used to calculate the average of the 1 T/s tests), and the resulting comparison is given on the last line in Table 7.1 (see Chapter 7). Based on Table 3.6, all of the MCEs at 2 to 6 T/s are slightly higher than that at 1 T/s, and all of the hystereses at 2 to 6 T/s are modestly higher than that at 1 T/s. The relationship between MCE/hysteresis appears to be weak and non-linear.

Table 3.6. Comparison of the 1 T/s data with other sweep rate data

	MCE (K)							Maximum hysteresis (K)						
Sweeping rate (T/s)	**1**	**0.25***	**0.5***	**2**	**3**	**4**	**6**	**1**	**0.25***	**0.5***	**2**	**3**	**4**	**6**
1 T/s vs. 0.25 T/s	*3.9*	3.87						*1.01*	0.19					
1 T/s vs. 0.5 T/s	*4.13*		4.05					*1.01*		0.89				
1 T/s vs. 2 T/s	*4.22*			4.05				*1.09*			1.83			
1 T/s vs. 3 T/s	*3.09*				2.91			*1.02*				1.55		
1 T/s vs. 4 T/s	*4.22*					4		*1.09*					1.28	
1 T/s vs. 6 T/s	*3.81*						3.71	*0.96*						1.22

Note: MCE and hysteresis data for 0.25 T/s and 0.5 T/s are undervalued because the testing was under non-adiabatic condition.

Due to the high heat losses due non-adiabatic conditions for these tests, the 0.25 T/s and 0.5 T/s data cannot be used for evaluating the time dependence of MCE and hysteresis directly. However, it is possible to correct the error by estimating the heat loss of MnFePAs using Computational Fluid Dynamics simulation to compare Gadolinium and MnFePAs (with different thermal conductivity and specific heat). It is also worthy of note that one must be very careful in interpretation of the data of 3 T/s or higher, because eddy currents might exist in the sample holder, and multiple-period magnet rotation has to be conducted due to low acceleration of step motor rotation for 3 T/s or higher (thus the first and last cycle data must be excluded). Figure 3.6 shows typical multiple-period testing at 6 T/s. As one can see, even if the first and last periods are excluded, each of the remaining periods is slightly different from the others in both position and magnitude. This may be due to combination of minor heat loss to the environment, minor heat gain from eddy currents, and other. It is challenging to judge the MCE and maximum hysteresis for this kind of multiple-period test. Similar phenomena were observed for $Gd_5Si_2Ge_2$ at 6 T/s in Chapter 2, Figure 2.7.

Figure 3.7 shows a typical multiple-period test for adiabatic temperature change vs field at 6 T/s.

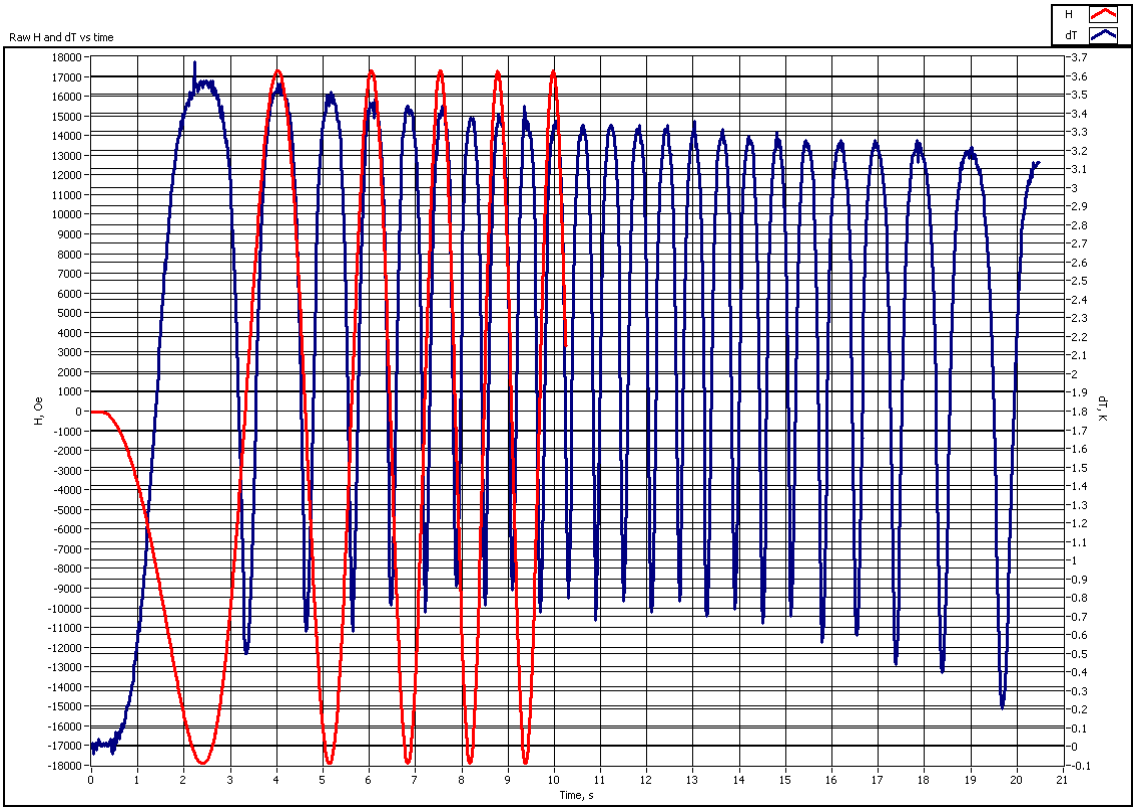

Figure 3.6. Temperature (blue) & field (red) vs. time during multiple cycling at 6 T/s.

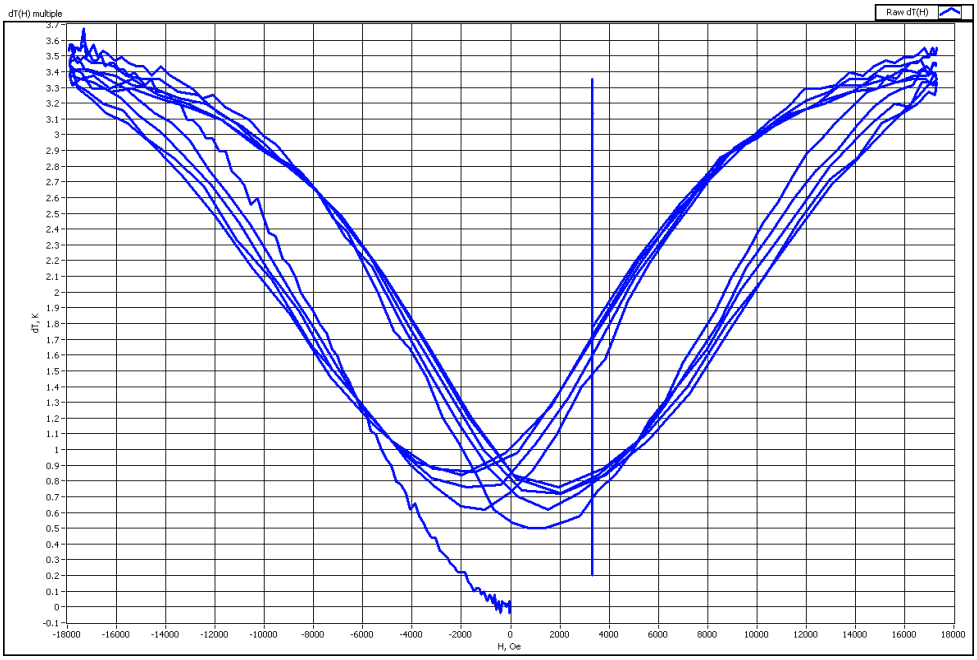

Figure 3.7. MCE curves for a typical 6 T/s multiple-period test.

3.3 Conclusions

The MMS has been used to directly measure MCE of MnFePAs. Only one MnFePAs sample has MCE (5.4K) higher than the baseline Gadolinium (5.0K), and most MnFePAs samples have MCE between 3.0 and 4.5K for the maximum field of 1.78 Tesla, and most have maximum hysteresis between 1.0 and 1.6 K. The MCE and hysteresis of MnFePAs is influenced by the field sweeping rate, but it appears that the relationship between the MCE/hysteresis and field change rate is weak and non-linear.

3.4 References

[1] R. Zach, M. Guillot, and R. Fruchart, J. Magn. Magn. Mater. **89** (1990) 221.

[2] V. K. Pecharsky and K. A. Gschneidner, Jr., Adv. Mater. **13** (2001) 683.

[3] O. Tegus, E. Bruc¨k, L. Zhang, Dagula, K. H. J. Buschow, and F. R. de Boer, Physica B **319** (2002) 174.

[4] K. A. Gschneidner, Jr. and V. K. Pecharsky, Phys. Rev. Lett. **78** (1997) 4494.

[5] Madeleine Bacmann , Jean-Louis Soubeyroux , Ray Barrett , Daniel Fruchart , Ryszard Zach , Stanislas Niziol , Robert Fruchart , J. Magn.Magn. Mater. **134** (1994) 59-67.

[6] O. Tegus, E. BruÈ ck, K. H. J. Buschow & F. R. de Boer, Nature . **415** (2002).

[7] O. Bacmann, L. Lundgren, in: K.H.J. Buschow (Ed.),Handbook of Magnetic Materials, Vol. 6, North-Holland, Amsterdam (1991) 181–287.

[8] G. D. Samolyuk and V. P. Antropov, J. Magn. Magn. Mater. **93** (2003) 6884.

[9] E. Br.uck, O. Tegus, X.W. Li, F.R. de Boer, K.H.J. Buschow, Physica B **327** (2002) 431.

[10] E. Bruck, O. Tegus, D.T. Cam Thanh, Nguyen T. Trung, K.H.J. Buschow, International Journal of refrigeration **31** (2008) 763–770.

CHAPTER 4. MCE of LaFeSiH

Sesha Madireddi

A paper to be submitted to *The Journal of Magnetism and Magnetic Materials*

4.1 Introduction

$La(Fe_{1-x}Si_x)_{13}$ and its hydrides have been considered to be promising materials for magnetic refrigeration due to their high magnetocaloric effect and relatively low hysteresis. It has been demonstrated [1] that in the concentration range $0.1 \leq x \leq 0.14$, the GMCE in $La(Fe_{1-x}Si_x)_{13}$ is associated with thermally induced first-order magnetic transition between the ferromagnetic (F) and the paramagnetic (P) phases at the Curie temperature T_c located around 200K. Additionally, the magnetic field induced first-order itinerant-electron metamagnetic (IEM) transition also occurs just above T_c in relatively low magnetic fields. In this concentration range and T_c around 200K, the typical isothermal entropy (ΔS_m) and adiabatic temperature change (ΔT_{ad}) for a 0- 2 Tesla field change is 20 J/kg-K and 6.5K, respectively. Hysteresis of $La(Fe_{1-x}Si_x)_{13}$ with x =0.1 from magnetization curves is 4 kOe, which is less than half of that observed in $Gd_5(Si_xGe_{4-x})$ materials. Outside of this concentration range, although the ordering temperature can be raised by replacing Fe with Si (higher x), the MCE is substantially reduced [2], and the ΔS_m curves show characteristics of second-order materials.

To raise the Curie temperature of $La(Fe_{1-x}Si_x)_{13}$ materials while maintaining high MCE performance in order to make it suitable for near room temperature refrigeration, two other major methods have been explored – Co substitution for Fe in various $La(Fe_{1-x}Si_x)_{13}$ based alloys to form $La(Fe_{13-x-y}Co_y)Si_x$ [3, 4], and addition of hydrogen to $La(Fe_{1-x}Si_x)_{13}$ to form

$La(Fe_{1-x}Si_x)_{13}H_y$ [1, 5, 6]. For the former method, Co additions significantly and linearly increase T_c from ~210 to ~330K, but ΔS_m is lowered by almost half. ΔT_{ad} measured by Huang et al. in 2007 and 2009 [7, 8] for $LaFe_{11.17}Co_{0.8}Si_{1.1}$ and $LaFe_{11}Co_{0.9}Si_{1.1}$ is only 2.3 and 1.5K, respectively, at 1.48 T. On the other hand, addition of hydrogen and the resultant $La(Fe_{1-x}Si_x)_{13}H_y$ materials are more promising, in general ΔS_m only slightly decreases while ΔT_{ad} exhibits an increase compared to parent materials of $La(Fe_{1-x}Si_x)_{13}$ [2]. The Curie temperature, $T_{c,}$ increases in a linear fashion with increasing hydrogen concentration (y).

Currently, most adiabatic temperature rise data are obtained from indirect measurements using magnetization and/or heat capacity data, but several direct measurements have been reported. Hu et al. [9] reported a direct ΔT_{ad} value at 183 K for $La(Fe_{11.7}Si_{1.3})$, while Fujieda et al. [1] made both indirect and direct ΔT_{ad} measurements on $La(Fe_{11.44}Si_{1.56})$ at 188 K. These data show the directly measured ΔT_{ad} for a 0-2 Tesla field range is 20- 30% lower than the indirect measurement. Fujieda et al. [1] also directly measured ΔT_{ad} for $La(Fe_{11.44}Si_{1.56})H_{1.6}$ and reported a measured value of only 4 K for a 0-2 Tesla field change at T_c =319K which is probably lower than the indirect value by about 2 to 3 K, based on indirect values for samples with a similar Fe:Si ratio and similar hydrogen doping levels, representing a discrepancy of 50-75%.

Sample $La(Fe_{1-x}Si_x)_{13}$ materials developed thus far are generally bulk alloys which need very long annealing time (one week or longer). IFW-Dresden and Neomax of Hitachi Metals have been exploring rapid solidification – both melt spinning and strip casting methods [10, 11]. The rapid solidification method of either melt spinning or strip casting takes a very short time for the annealing process (minutes to 1 hour) and has been used for mass production of Nd-Fe-B magnets in industry. In addition to the decisive advantage of drastically reduced

processing time, both Gutfleisch and Hirosawa reported significantly increased ΔS_m for the $La(Fe_{0.88}Si_{0.12})_{13}$ material from melt spinning or strip casting method. Gutfleisch et al. [10] attributed the large ΔS_m to the enhancement due to a more homogeneous element distribution. This topic is discussed further in the following section of test results and discussion.

This chapter reports experimental results for three $La(Fe_{1-x}Si_x)_{13}H_y$ materials prepared by Neomax using strip casting followed by hydrogen absorption. Direct measurement of adiabatic temperature rise, $\Delta T_{ad,}$ was performed under wide temperature range from 260 to 310 K and various magnetic field sweeping rates from 0.25 to 6 T/s. This is the first time the MCE is directly measured under different field rates and systematically evaluated for time dependence effect.

4.2 Material Preparation

Three LaFeSiH series materials, namely $La(Fe_{1-x}Si_x)_{13}H_y$ with x = 0.12 and y = 1.46, 1.18 and 1.06, respectively, were prepared by the Neomax of Hitachi Metals. The parent material of $La(Fe_{1-x}Si_x)_{13}$ was made using the strip casting process with a short period of annealing (1 hour), and the hydrides were obtained by direct hydrogenation of prepared materials. Because the resultant hydrides were very brittle (powders), these material samples were pressed into small rectangular pieces (see Figure 4.1) for the purpose of temperature rise measurement using thermocouples. Based on magnetization data from Neomax, the Curie temperature of the three materials is 26.9^{o}C, 14.5^{o}C, and 8.2^{o}C, respectively. Hirosawa et al. [11] has reported that the rapidly solidified $La(Fe_{1-x}Si_x)_{13}$ alloys based on the melt spinning or strip casting process can have isothermal entropy, ΔS_m, as high as 20 J/kg-K for a

Figure 4.1. Photo of the $La(Fe_{0.88}Si_{0.12})_{13}H_{1.46}$ sample.

field span between 0 and 1 Tesla. This ΔS_m value is very high compared to that for bulk material samples.

4.3 Results and Discussion for $La(Fe_{0.88}Si_{0.12})_{13}H_{1.46}$

Test facility and procedure are described in Chapter1. Figures 4.2 through 4.4 show the MCE (adiabatic temperature change, ΔT_{ad}) and hysteresis under different magnetic sweep rates. Again, these MCE data are based on a maximum magnetic field of 1.78 Tesla. The maximum MCE of these materials is only 2.5 K at 1.78 T or 1.4 K/T, which is less than half of ΔT_d for bulk materials, but close to 1.8 K/T from Neomax indirect measurement for the same materials using magnetization and heat capacity data (personal communication with Dr. Yoshiharu Uno, Neomax, Japan, Hitachi Metals). IFWs directly measured ΔT_{ad} for $La(Fe_{0.89}Si_{0.11})_{13}H_{1.6}$ using melt spinning fabrication [12] are also 1.8 K/T. The low ΔT_{ad} is strange because the ΔS_m of the same materials is significantly higher than those of the bulk materials. One possible reason for the low ΔT_{ad} is that the test samples were formed by mechanically pressing powders into solid rectangular pieces for which the temperature measured using the thermocouple may tend to be lower due to suppressed heat exchange between neighboring particles. The issue of low ΔT_{ad} for rapid solidification $La(Fe_{1-x}Si_x)_{13}$ or its hydrides is worthy of further investigation.

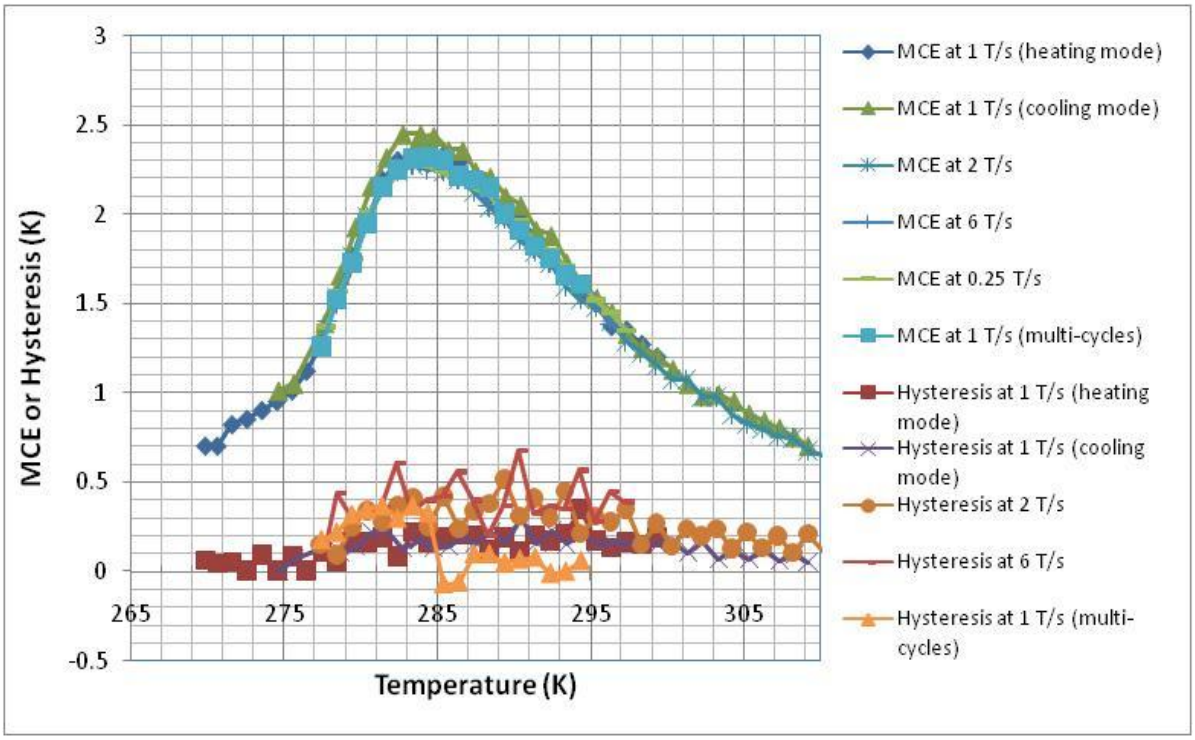

Figure 4.2. MCE or hysteresis of $La(Fe_{0.88}Si_{0.12})_{13}H_{1.46}$ at various sweep rates.

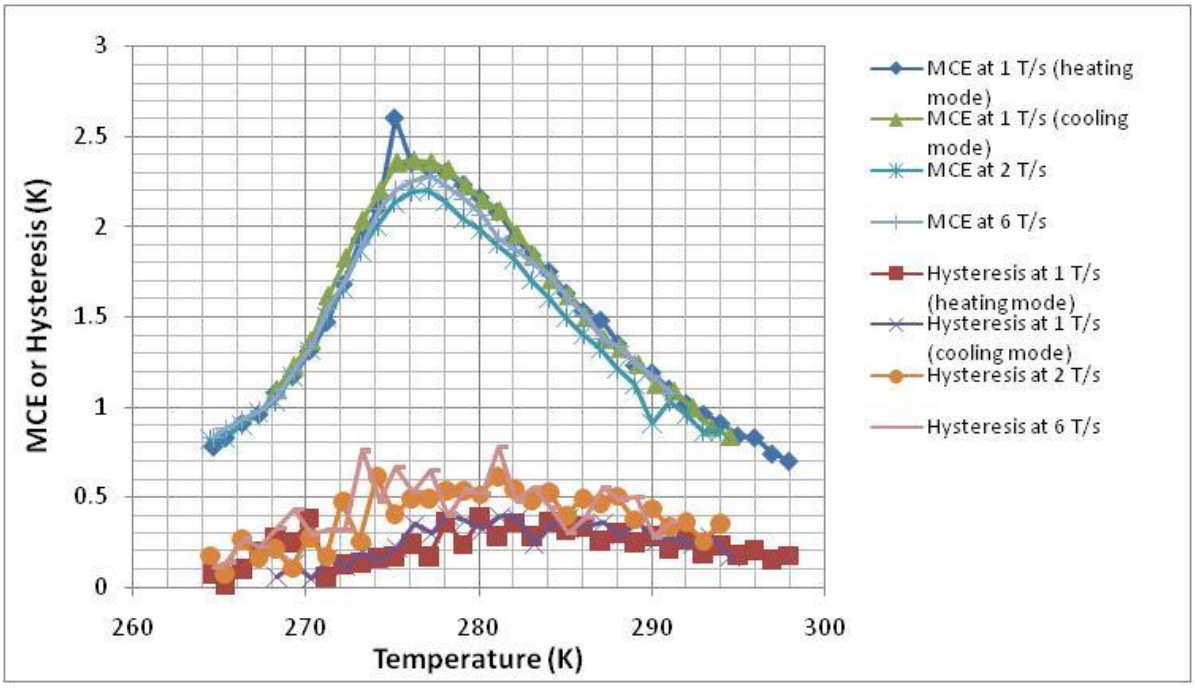

Figure 4.3. MCE or hysteresis of $La(Fe_{0.88}Si_{0.12})_{13}H_{1.18}$ at various sweep rates.

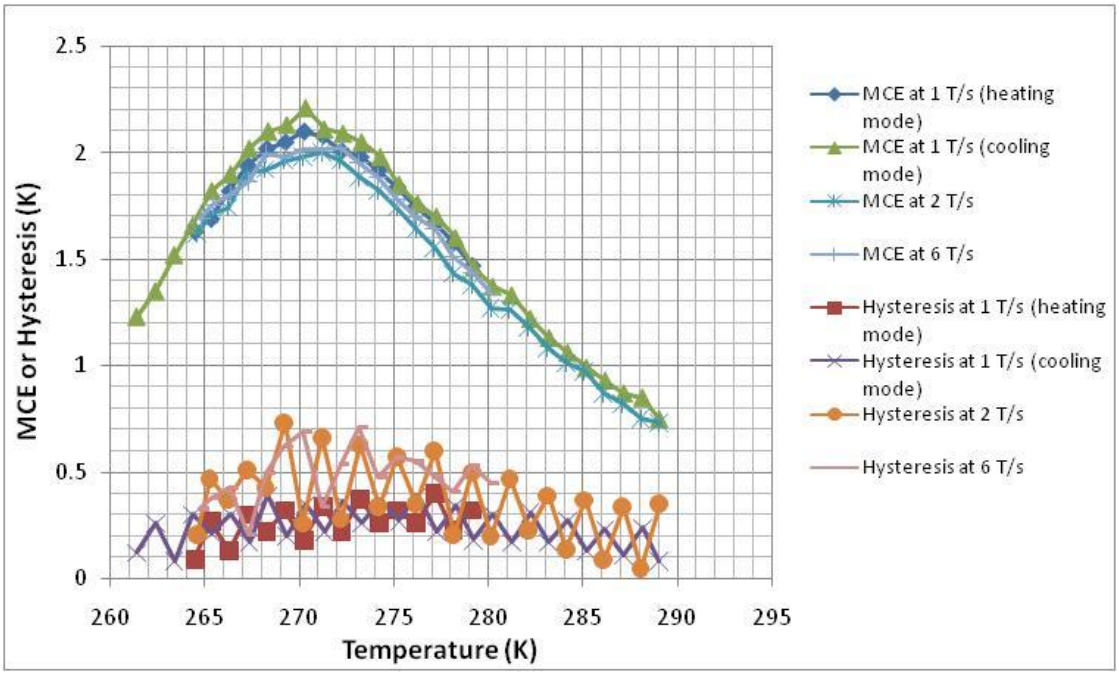

Figure 4.4. MCE or hysteresis of $La(Fe_{0.88}Si_{0.12})_{13}H_{1.06}$ at various sweep rates.

Thermal hysteresis measured in this work is low (about 0.5K maximum). Figure 4.5 presents the adiabatic temperature change (ΔT_{ad}) vs. magnetic field for $La(Fe_{0.88}Si_{0.12})_{13}H_{1.46}$ near its ordering temperature. One can see that the gap between the magnetizing curve and demagnetizing curve (or hysteresis) is small, the ΔT_{ad} increases almost linearly with magnetic field starting from 0 at 0 T to 2.4 K at 1.78T, and that overall characteristics are more like a second-order material.

Unlike most other first-order materials like $Gd_5Si_2Ge_2$ and MnFePAs, the MCE data of the $La(Fe_{1-x}Si_x)_{13}H_y$ materials tested in this work do not show measurable differences between the heating mode and the cooling mode. It seems there is no significant difference in MCE performance and characteristics for different magnetic field change rates from 0.25 T/s to 6 T/s. This is consistent with observations for other materials investigated in this study.

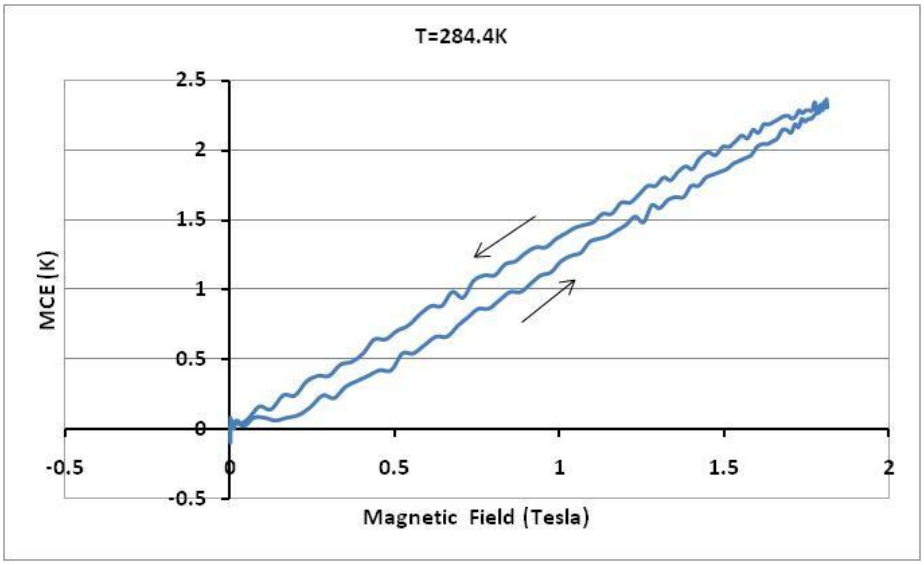

Figure 4.5. Adiabatic temperature change (ΔT_{ad}) vs. magnetic field for $La(Fe_{0.88}Si_{0.12})_{13}H_{1.46}$.

The actual ordering temperature (or temperature at which the adiabatic temperature change peaks) is shifted to the left lower temperatures compared to that from the magnetization measurement. Based on the MCE vs. operating temperature curves, the temperature of the peak MCE is 284 K, 277 K, and 271 K for sample $La(Fe_{0.88}Si_{0.12})_{13}H_{1.46}$, $La(Fe_{0.88}Si_{0.12})_{13}H_{1.18}$, and $La(Fe_{0.88}Si_{0.12})_{13}H_{1.06}$, respectively. The sequence of the ordering temperatures is consistent with hydrogen concentration.

4.4 Conclusions

Three LaFeSiH series materials, namely $La(Fe_{1-x}Si_x)_{13}H_y$ with x = 0.12 and y = 1.46, 1.18 and 1.06, respectively, were prepared using the rapid solidification method followed by direct hydrogenation, and their adiabatic temperature change (ΔT_{ad}) was directly measured using the MMS device under a wide range of operating temperature and magnetic sweeping rate from 0.25 to 6 T/s. The maximum ΔT_{ad} is only 2.5 K at 1.78 T, equal to 1.4 K/T, which

are much lower than those of indirect or direct measurements for bulk alloy samples, but close to those reported for other rapidly solidified samples. This phenomenon of low ΔT_{ad} for rapid solidification material samples is worthy of further investigation. The characteristics of the ΔT_{ad} curves are similar for different magnetic field sweeping rates from 0.25 to 6 T/s, and no time dependence of MCE is observed. In general, the thermal hysteresis of the LaFeSiH materials is low – only 0.5 K maximum.

4.5 References

[1] Fujieda S, Hasegawa Y, Fujita A and Fukamichi K, 2004, *J. Magn. Mater*. **272-276**, 2365.

[2] Gschneidner Jr. KA, Pecharsky VK and Tsokol AO, 2005, Recent development in magnetoclaoric materials, *Rep. Prog. Phys.* **68**, 1479.

[3] Hu F X, Qian X L, Sun J R, Wang G J, Zhang X X, Cheng Z H and Shen B G, 2002, *J. Appl.Phys*. **93**, 5503.

[4] Liu X B and Altounian Z, 2003, *J. Magn. Mater*. **264**, 209.

[5] Chen Y F, Wang F, Shen B G, Hu H X, Sun J R, Wang G J and Cheng Z H, 2003, J. *Phys. Condens. Matter* **15**, 161.

[6] Fujieda S, Fujita A, Fukamichi K, Yamazaki Y and Iijima Y, 2001, *Appl. Phys. Lett*. **79**, 653.

[7] Huang J H, Song L, Jin P Y, Yan H W, Wang Y, Tegus O and Zhang J X, 2003, Research on the Magnetocaloric effect of $LaFe_{11.17-x}Co_{0.78}Si_{1.05}B_x$, *Thermag II Proceedings*: 155.

[8] Balli M, Fruchart D, Sari O, Gignoux D, Huang J H and Egolf P W, 2009, Direct measurement of the Magnetocaloric effect in $La(Fe_{13-x-y}Co_y)Si_x$ compounds near room temperature, *Thermag III Proceedings*: 75.

[9] Hu F X, Shen B G, Sun J R, Wang G J and Cheng Z H, 2002, *Appl. Phys. Lett*. **80**, 826.

[10] Gutfleisch O, Yan A and Muller K H, 2005, large Magnetocaloric effect in melt-spun $LaFe_{13-x}Si_x$, *J. Appl. Phys*. **97**, 10M305.

[11] Hirosawa S, Hiroyuki T and Bekki K, 2006, Rapidly solidified $La(Fe_{1-x}Si_x)_{13}$ alloys and their Magnetocaloric properties, *IEEE Trans. on Mag*.42-10.

[12] J. Lyubina, O. Gultfleisch, M.D. Kuz'Min, M. Richter, Proc. 3rd IIF-IIR Inter. Conf. Magn. Refrig. (editor-in-chief P. Egolf), Des Moines, USA, May 2009, P.49.

CHAPTER 5. MCE of $Ni_{55.2}M_{18.6}Ga_{26.2}$

Sesha Madireddi

A paper to be submitted to *The Journal of Magnetism and Magnetic Materials*

5.1 Introduction

Ni_2MnGa-based Heusler alloys are mostly known as magnetic shape-memory alloys [1]. The structural (cubic-tetragonal or cubic-orthorhombic) transition in these alloys produces extremely large lattice strains (up to ~6 %) [2, 3]. Due to a coupling between magnetism and structure in these compounds [4, 5], the large linear strains can be activated by applied magnetic field [3] which opens many opportunities for practical application of these materials.

The MCE in $Ni_{2+x}Mn_{1-x}Ga$ compounds have been closely examined recently due to high Curie temperature (exceeding room temperature) and a large magnetic entropy change associated with a first-order magnetostructural transition [2–6]. The components used in a preparation of the materials are relatively inexpensive and non-toxic so this new potential class of magnetic refrigerants quickly attracted the attention of magnetocaloric community. Unfortunately, despite huge magnetic entropy change (ΔS_M),[8.9] the adiabatic temperature change ($\Delta T_{ad.}$) is quite small (2.2 K for ΔH = 0-5 Tesla field change or 1.5 K for ΔH = 0-2 Tesla)[9] limiting their practical use. Direct magnetocaloric measurements showed that the actual temperature change during the transition with a field sweep rate of 2 T/s was even lower: 1.2 K for ΔH = 0-1.85 Tesla in the cooling protocol and only 0.8 K for same magnetic field change during heating [13]. Nevertheless, there is great interest in the properties of the

$Ni_{2+x}Mn_{1-x}Ga$ phases because the number of materials, which show high ΔS_M at room temperature is limited, while the demand for them is large.

This work provides unique information about these materials by reporting the heat capacity data in applied magnetic fields of 0, 1, and 2 Tesla using a relatively large (~1 g) bulk piece of each material. The magnetocaloric properties of exactly the same alloy are determined by both direct and indirect (magnetization, heat capacity) methods. The well-studied $Ni_{2.19}Mn_{0.81}Ga$ composition ($Ni_{55.2}Mn_{18.6}Ga_{26.2}$) was chosen for the investigation because the temperatures of both magnetic (T_C) and structural (T_m) transitions coincide in this compound,[6,13] and it has high magnetic entropy change.[8,9]

5.2 Experimental Procedure

Nearly 15 g of $Ni_{55.2}Mn_{18.6}Ga_{26.2}$ material were arc melted from pure metals. Beforehand, the commercial grade manganese was cleaned in weak nitric acid and arc melted. This procedure provides additional cleaning of the Mn metal and minimizes its weight loss during sample preparation. The arc-melted button was then sealed in a quartz tube backfilled with He gas, and heat treated at 850 °C for 1 week. The resulting sample has good mechanical integrity. A small amount of powder necessary for x-ray powder diffraction was obtained by hand grinding in a mortar and an x-ray powder diffraction pattern was collected at ambient conditions on a Philips PANalytical X-ray powder diffractometer. The resulting pattern shows broad Bragg peaks but, apparently, the high temperature cubic phase is already distorted at room temperature, meaning that the martensite-austenite transformation occurs at higher temperature than the temperature of the x-ray powder diffraction measurement (~295 K). No impurity phases were observed.

The magnetic measurements were performed using an MPMS XL-7 SQUID magnetometer, manufactured by Quantum Design, Inc., which operates in a temperature interval of 1.7 – 400 K and in magnetic fields up to 7 T. The accuracy of magnetic measurements was better than 1%. The heat capacity in magnetic fields up to 10 T was measured between ~2 and 350 K in a semiadiabatic heat pulse calorimeter, which has been described elsewhere [15]. The direct magnetocaloric measurements were performed as described above.

5.3 Results and Discussion for $Ni_{55.2}M_{18.6}Ga_{26.2}$

5.3.1 Magnetization

Magnetization measurements were performed in 0.1 Tesla and 2 Tesla applied magnetic fields as a function of temperature from 2 to 360 K in zfc heating (ZFC) and field cooling (FC) modes (see Figure 5.1). The field-cooled warming (FCW) data were collected in 0.1 Tesla field as well. The extremely sharp magnetic ordering transition occurs at T_C = 320 K for heating and at 315 K for cooling. No other magnetic transition has been observed. The transition temperature agrees well with Zhou et al.[8], but is somewhat lower than that reported by Vasil'ev et al.[3], which is not surprising considering the high compositional sensitivity of T_C [3, 14]. The transition temperature increases with increasing field and at 2 Tesla the T_C is 325 K for heating and 317 K for cooling. Both 0.1 Tesla and 2 Tesla data indicate single paramagnetic (PM) to ferromagnetic (FM) transition on cooling, and the fact that the transition shifts to higher temperature in higher magnetic fields suggest its first-order nature and the existing magnetostructural coupling. However, it is easy to see (Figure 5.1)

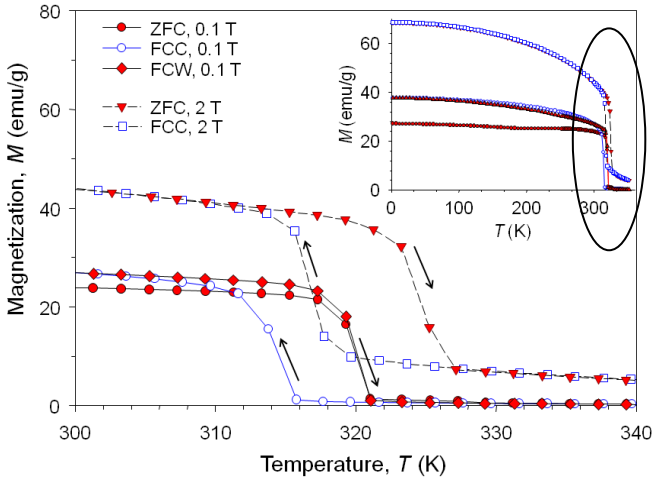

Figure5.1. The magnetization of the $Ni_{2.19}Mn_{0.81}Ga$ alloy as a function of temperature measured at 0.1 and 2 T applied magnetic fields in the temperature range from 300 K to 340 K. The inset shows the full temperatures range, from 2 to 360 K.

that the field dependence of the transition temperature is different for heating and cooling protocols, effectively increasing hysteresis in high magnetic fields. A similar phenomenon was observed in the $Ni_{2.18}Mn_{0.82}Ga$ alloy [6], but the increase of the transition temperature with applied field was higher for cooling than for heating. Again, an extremely high sensitivity to the chemical composition observed in $Ni_{2+x}Mn_{1-x}Ga$ alloys [14] explains why alloys with close composition none-the-less show different Curie temperatures and different dT_C/dH dependencies.

The sharp PM to FM transition indicates a potential for the high magnetic entropy change, however, it also suggests strong superheating and a highly metastable state of the compound in this part of the phase diagram. The extremely large volume change [5] with a corresponding strong relief of the accumulated stress by the crystal lattice at the transition point [4], combined with a complicated interplay of structural and magnetic lattices [13] create great potential for a severe non-equilibrium conditions in $Ni_{2.19}Mn_{0.81}Ga$ and related alloys.

Magnetization isotherms, *M(H)*, were collected around the transition in three different modes. First, *M(H)* curves were collected in a 5 K interval from 290 to 340 K and the temperature of each subsequent measurement was increased after a previous isotherm ended. A second set of isotherms was collected using the procedure described by Zhou et al. [8]: the sample was heated up to 340 K [above the $T_C(T_m)$ temperature], zero-field cooled to 260 K, and heated up to the desired temperature before each *M(H)* measurement (Figure 5.2). The third set of data was recorded similarly to the second, but the temperature interval between curves was set to 2.5 K instead of 5 K. These data sets were used to calculate magnetic entropy change (ΔS_M) during the transition by employing a Maxwell relation.

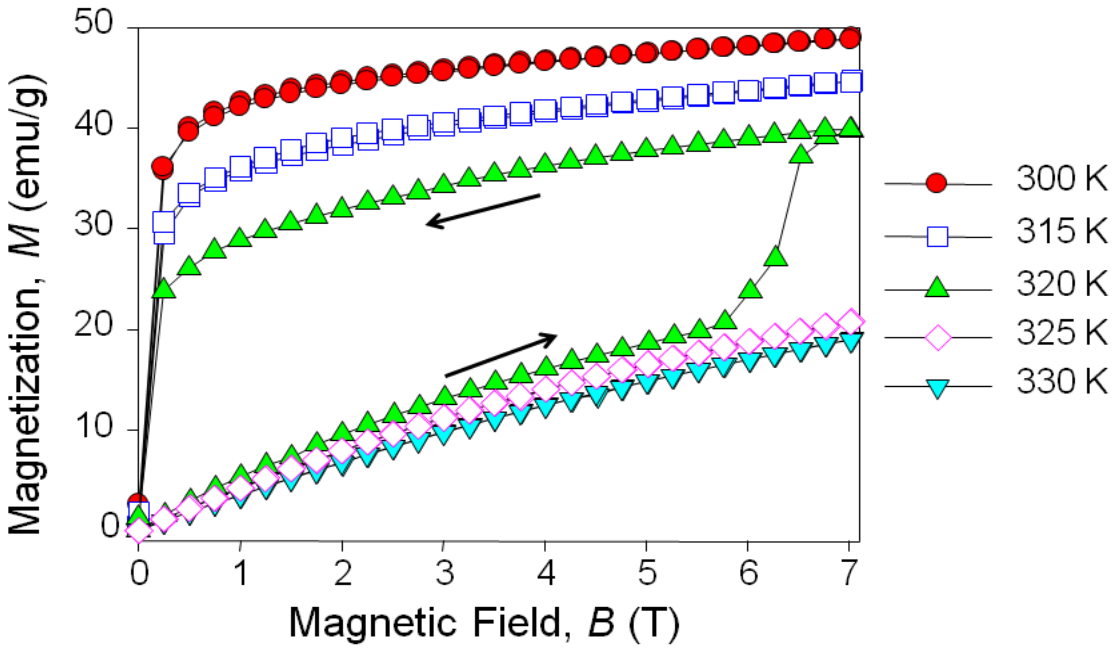

Figure 5.2. The magnetization of the $Ni_{2.19}Mn_{0.81}Ga$ alloy as a function of magnetic field measured at several temperatures around the transition. The results are shown for five temperatures only for clarity.

5.3.2 Heat capacity

The heat capacity was measured using a semi-adiabatic calorimeter from 2 to 350 K in applied magnetic fields of 0, 1, and 2 Tesla (Figure 5.3). The sharp first-order type of the transition has been observed at 323 K, about 3 K higher than the T_c from M(T) measurements. The peak at 2 Tesla, however, agrees well with *M(T)* data. The field dependence of the transition temperature is weak (~ 1 K/T). Surprisingly, instead of a single peak expected from the magnetization data, a double peak feature was actually observed. The second, smaller peak occurs at ~3 K higher than the main peak and moves with the main peak towards high temperatures with the application of the magnetic field. The possibility of sample inhomogeneity cannot be completely ruled out since the material is very sensitive to the chemical composition, the heat capacity sample (~1.0 g) is much larger than the magnetization sample (~15 mg), and the transition temperatures are only a few degrees different. However, the inhomogeneity normally results in a broad single peak while, in this case, there are two distinct transitions. Alternatively, the presence of the second peak moving up with field suggests that an additional structural transition may exist slightly above the T_C, i.e., the structural transition is not completed in one step due to large strain [4]. Such an effect has been observed in other studies of $Ni_{2+x}Mn_{1-x}Ga$ alloys, i.e., in linear thermal expansion measurements[12]. Intriguingly, this second peak appears to be coupled with the magnetic sublattice (it moves with field also), but it does not influence either magnetic data or the direct magnetocaloric measurement results, despite the latter having been obtained from the same physical sample. However, if it is an “aftershock” of the main transition, it should move with the main transition, without being coupled with the magnetic sublattice.

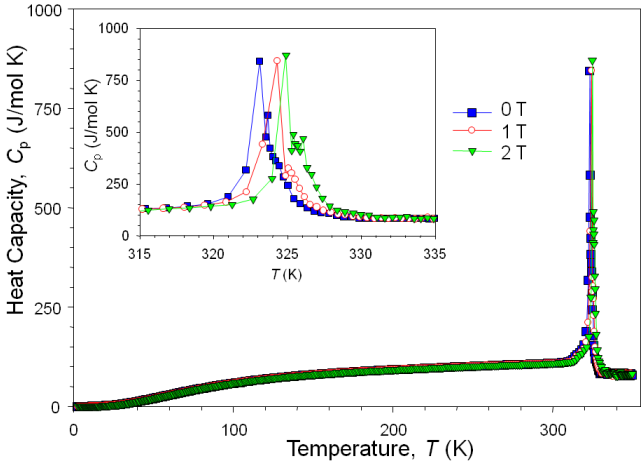

Figure 5.3. The heat capacity of the $Ni_{2.19}Mn_{0.81}Ga$ alloy as a function of temperature measured at 0, 1, and 2 Tesla applied magnetic fields. The inset magnifies the heat capacity in the temperature range between 315 K and 335 K.

5.3.3 Magnetocaloric effect from indirect methods

The magnetic entropy change determined from *M(H)* curves is shown in Figure 5.4. The values of ΔS_M correspond to giant magnetocaloric effect, and they are independent of whether the sample was zero-field cooled or heated in field. However, the calculated magnetic entropy change values when the *M(H)* curves are collected with a 2.5 K step (Figure 5.4a) are much higher than those computed from the M(H) data measured with a 5 K step (Figure 5.4b). Even though this difference is not realistic, this is not surprising because in very sharp transitions such as these, a large magnetization change can be obtained with a very small temperature step – just enough to cross the phase boundary line. This, again, indicates the highly metastable nature of the transition, since ideally, ΔS_M should not depend on how it is calculated. However, because the numerical integration of Maxwell's equation is normally used for the ΔS_M calculation, the smaller temperature steps may result in a so-called

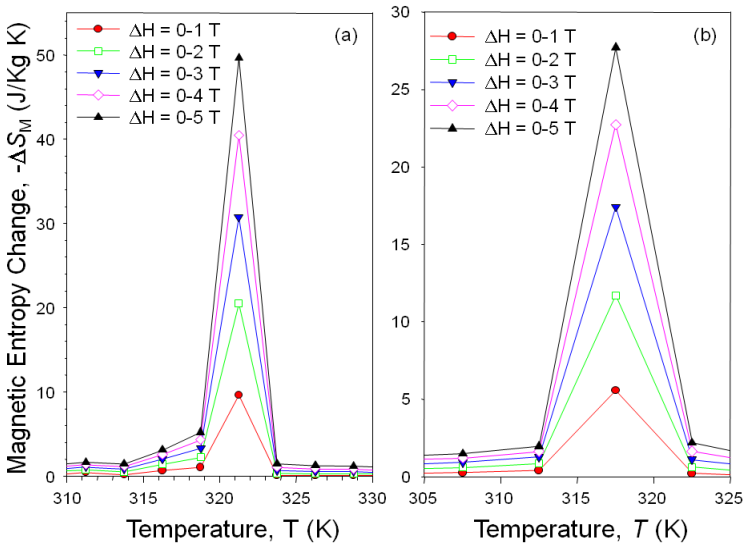

Figure 5.4. The magnetic entropy change ($Ni_{2.19}Mn_{0.81}Ga$) calculated using Maxwell relation from the *M*(H) data: (a) 2.5 K step between *M(H)* curves; (b) 5 K step between *M(H)* curves.

colossal magnetocaloric effect, while using larger temperature steps decreases the calculated effect. Unfortunately, in both cases, obtained numbers are not reliable, and are presented here only as an example illustrating the limits of the application of Maxwell's equations for magnetic entropy change calculations in first-order materials.

The magnetocaloric properties of an $Ni_{2.19}Mn_{0.81}Ga$ sample calculated from the heat capacity data are shown in Figure 5.5. The $\Delta T_{ad.}$ results agree very well with those calculated from the DSC experiment [9], while ΔS_M values are lower. The results confirm that the high magnetic entropy change values in this material are accompanied by a relatively low adiabatic temperature change. Taking into account the accumulation of experimental errors in the entropy, *S(T)*, integration, which makes the $\Delta T_{ad.}$ values for the 0 to 2 Tesla field change look a bit overestimated (Figure 5. 5b), it is clear that the $\Delta T_{ad.}$ values from this measurement basically agree with those obtained by direct measurement (see below), and, thus, should be intrinsic.

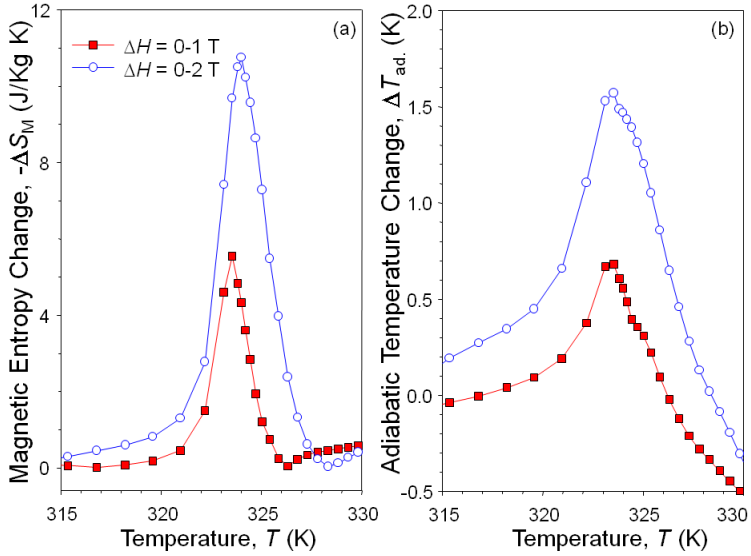

Figure 5.5. The magnetocaloric properties of the $Ni_{2.19}Mn_{0.81}Ga$ calculated from the heat capacity data: (a) magnetic entropy change; (b) adiabatic temperature change.

5.3.4 Direct magnetocaloric effect measurements

The magnetocaloric effect observed in direct measurements using two sweep rates of 1 T/s and 2 T/s is shown in Figure 5.6. The obtained values essentially agree with the values calculated from heat capacity data and with the results reported by Khovailo et al [13]. The MCE is larger during the cooling than during the heating, the effect claimed to be related to the latent heat release during exothermic austenite-martensite transformation [13] but, in fact, it is more likely related to the extent of hysteresis and fine details of the phase diagram in the magnetic field – temperature coordinates (also see Chapter 2). The temperature of the maximum MCE at the sweep rate of 1 T/s corresponds to the temperature of the heat capacity peak. While the maximum value of MCE does not depend on the magnetic field sweep rate (Figure 5.6), in agreement with Ref.13, the temperature of its maximum is about 1 K lower in the 2T/s data, which may be related to the complex kinetics of the transition, as shown by the heat capacity data (Figure 5.3).

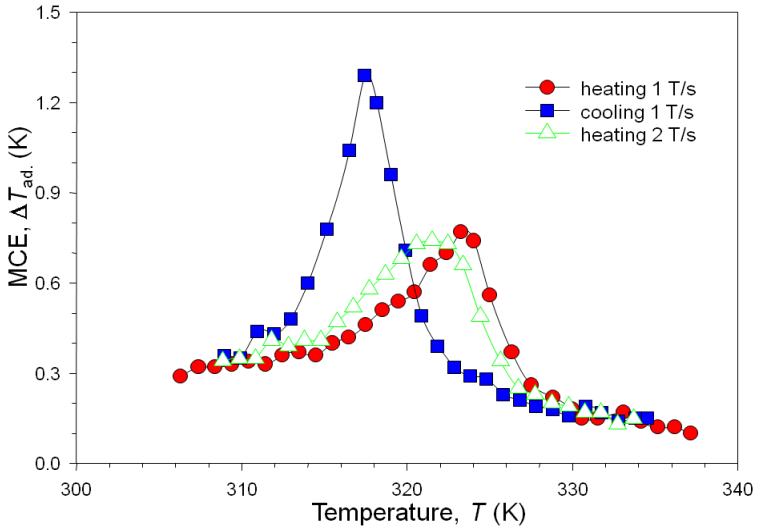

Figure 5.6. The magnetocaloric effect observed in the $Ni_{2.19}Mn_{0.81}Ga$ alloy by direct magnetocaloric measurements.

5.4 Conclusions

The heat capacity measurements of the $Ni_{2.19}Mn_{0.81}Ga$ shape-memory alloy showed a double feature peak at the temperature of the coupled martensite-ferromagnetic transformation. The origin of this feature could be related to a multi-step transition observed by other methods such as linear thermal expansion studies. However, the possibility of sample inhomogeneity enhanced by the strong compositional dependence of T_C in $Ni_{2+x}Mn_{1-x}Ga$ alloys should be considered as well, because some compositional gradient is almost inevitable in a large enough alloy.

The weak d*T*c/d*H* dependence observed in the heat capacity data is directly related to a relatively low adiabatic temperature change observed in these alloys, limiting their use in magnetocaloric applications.

The use of Maxwell's equations for the analyses of *M*(H) data cannot produce reliable estimation of MCE in these materials. At the same time, the $\Delta T_{ad.}$ calculated from heat capacity data shows reasonable agreement with the result of the direct magnetocaloric

measurements of the same sample, and the latter are in very good agreement with literature. These results provide an additional confirmation that heat capacity measurements in applied magnetic fields, and especially, a direct measurement of a magnetocaloric effect, can be used for the quantitative estimation of the magnetocaloric effect in strongly first-order transition systems like $Ni_{2+x}Mn_{1-x}Ga$.

5.5 References

[1] K. A. Gschneidner, Jr. and V. K. Pecharsky, Annu. Rev. Mater. Sci. **30**, 387 (2000).

[2] M. Richard, J. Feuchtwanger, D. Schlagel, T. Lograsso, S. M. Allen, and R. C. O'Handley, Scr. Mater. **54**, 1797 (2006).

[3] A. Sozinov, A. A. Likhachev, N. Lanska, and K. Ullakko, Appl. Phys. Lett. **80**, 1746 (2002).

[4] V. K. Pecharsky and K. A. Gschneidner, Jr., in *Magnetism and Structure in Functional Materials*, edited by A. Planes, L. Manosa, and A. Saxena, Springer Series in Materials Science (Springer-Verlag, Heidelberg, 2005), **79**, Ch. 11, p. 199.

[5] A. N. Vasil'ev, A. D. Bozhko, V. V. Khovailo, I. E. Dikshtein, V. G. Shavrov, V. D. Buchelnikov, M. Matsumoto, S. Suzuki, T. Takagi, and J. Tani, Phys. Rev. B **59**, 1113 (1999).

[6] V. V. Khovailo, T. Takagi, J. Tani, R. Z. Levitin, A. A. Cherechukin, M. Matsumoto, and R. Note, Phys. Rev. B **65**, 092410 (2002).

[7] F. Albertini, F. Canepa, S. Cirafici, E. A. Franceschi, M. Napoletano, A. Paoluzi, L. Paretti, and M. Solzi, J. Magn. Magn. Mater. **272-276**, 2111 (2004).

[8] X. Zhou, W. Li, H. P. Kunkel, and G. Williams, J. Phys.: Condens. Matter **16**, L39 (2004).

[9] M. Pasquale, C. P. Sasso, L. H. Lewis, L. Giudici, T. Lograsso, and D. Schlagel, Phys. Rev. B **72**, 094435 (2005).

[10] C. P. Sasso, M. Pasquale, L. Giudici, S. Besseghini, E. Villa, L. H. Lewis, T. A. Lograsso, and D. L. Schlagel, J. Appl. Phys. **99**, 08K905 (2006).

[11] J. Marcos, L. Mañosa, A. Planes, F. Casanova, X. Battle, and A. Labarta, Phys. Rev. B **68,** 094401 (2003).

[12] M. Khan, S. Stadler, J. Craig, J. Mitchell, and N. Ali, IEEE Trans. Mag. **42**, 3108 (2006).

[13] V. V. Khovaylo, K. P. Skokov, Yu. S. Koshkid'ko, V. V. Koledov, V. G. Shavrov, V. D. Buchelnikov, S. V. Taskaev, H. Miki, T. Takagi, and A. N. Vasiliev, Phys. Rev. B **78**, 060403R (2008).

[14] V. V. Khovaylo, V. D. Buchelnikov, R. Kainuma, V. V. Koledov, M. Oshtuka, V. G. Shavrov, T. Takagi, S. V. Taskaev, and A. N. Vasiliev, Phys. Rev. B **72**, 224408 (2005).

[15] V. K. Pecharsky, J. O. Moorman, and K. A. Gschneidner, Jr., Rev. Sci. Instrum. **68**, 4196 (1997).

[16] S. Madireddi, M. Zhang, V. K. Pecharsky, and K. A. Gschneidner, Jr., Proc. 3rd IIF-IIR Inter. Conf. Magn. Refrig. (editor-in-chief P. Egolf), Des Moines, USA, May 2009, P.185.

CHAPTER 6. MCE of Dy, Tb, $DyCo_2$, $(Hf_{0.83}Ta_{0.17})Fe_{1.98}$, $GdAl_2$ and Nd_2Fe_{17}, Materials

Sesha Madireddi

A paper to be submitted to *The Journal of Applied Physics*

6.1 Introduction

All of the intermetallic compounds described in this Chapter were prepared by arc-melting. The lanthanide metals were 99.5% pure and were prepared by the Materials Preparation Center of the Ames Laboratory, Iowa State University, while Al and Fe were purchased from commercial sources claiming >99.5% purity. Since $GdAl_2$ melts congruently, it was examined in the arc-melted condition. Nd_2Fe_{17}, however, melts incongruently and, thus, it was annealed at 1000^{o}C for two weeks to insure chemical homogeneity. This was confirmed by x-ray powder diffraction methods, which showed it to be single phase material within the limits of detection of this technique, i.e., the sample could have about 5% of a second phase present in it.

The experimental details of the direct measurements to determine the MCE have been explained in the Chapter 1.

6.2 Dysprosium

Terbium and Dysprosium order antiferromagnetically with a helical spin structure at T_N (Tb ~ 229 K, Dy ~ 178 K) which transform at lower temperatures to ferromagnetic order at T_c (Tb ~ 221 K, Dy ~ 85 K) [1].

Dysprosium metal exhibits two magnetic transitions [2]: a paramagnetic to antiferromagnetic (Neel) transition at $T_N \simeq 180$ K upon cooling, and a first-order antiferromagnetic to ferromagnetic transition at $T_c \simeq 90$ K upon cooling. The indirect measurements of the MCE effect are shown in Figure 6.1a and 6.1b for a very high purity Dy metal sample. The sharp rise in ΔT_{ad} at the first-order transition at ~ 90 K is quite evident in Figure 6.1. This is typical of first-order transitions.

6.3 Results and Discussion for Dy

As a rare earth metal, Dy has some interesting magnetocaloric phenomena. It has two magnetic phase change temperatures, T_N = 180 K for the second-order transition and T_c = 90 K for the first-order transition [2]. Since it is difficult for the MMS device to maintain stable 90 K or lower operating temperature, only the MCE at temperature around 180 K was measured, and the results are presented in Figure 6.2 to Figure 6.5. Figure 6.2 gives curves of MCE or hysteresis vs. temperature under various field sweep rates from 1 T/s to 6 T/s. It must be noted that Dy has a very unique behavior - for temperatures below 180 K, it shows negative MCE (maximum adiabatic temperature change is about – 0.9 K), but for temperatures above 180 K, the MCE becomes positive (maximum adiabatic temperature change is close to 1.8 K), and there is a huge jump near the 180 K transition temperature. Such oscillatory phenomenon has been reported by Gschneidner et al. [2] for Dy using indirect measurements as shown in Figure 6.1.

Figures 6.3 to 6.5 show the adiabatic temperature change vs. field change process for operating temperature of 175 K, 179 K, and 180 K, respectively and field change rate of 1 T/s. When the operating temperature (175 K) is below the transition temperature (~180 K),

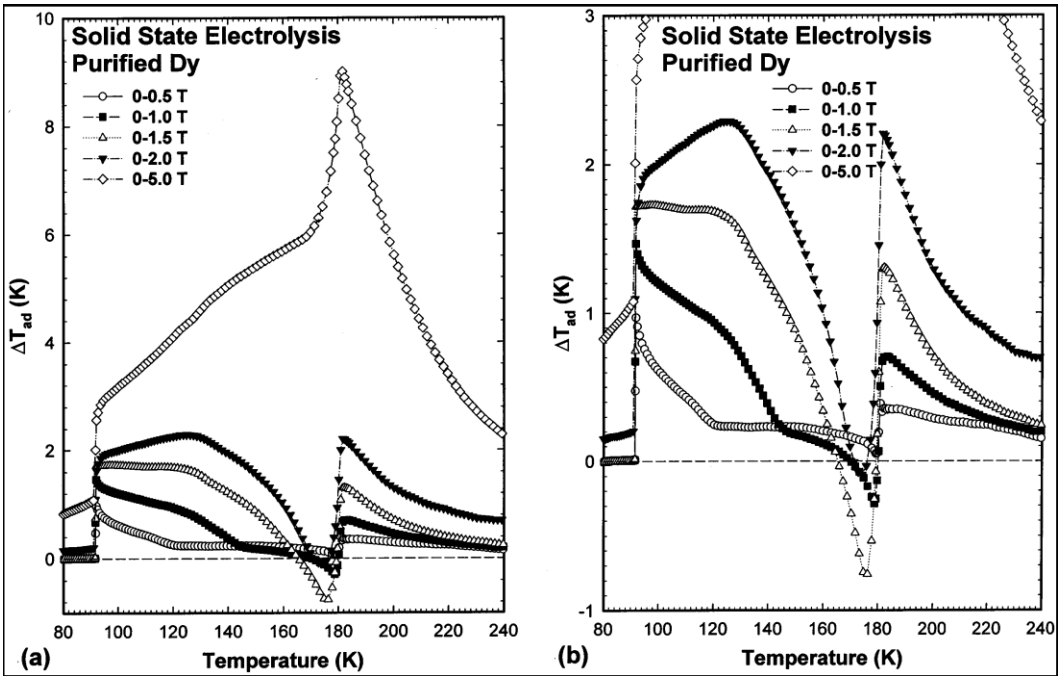

Figure 6.1. The adiabatic temperature change for solid state electrolysis purified Dy for field changes of 0–0.5, 0–1.0, 0–1.5, 0–2.0 and 0–5.0 Tesla: full ΔT_{ad} range (a) and an enlargement of the low values of ΔT_{ad} (b).Gschneidner, et.al.[2].

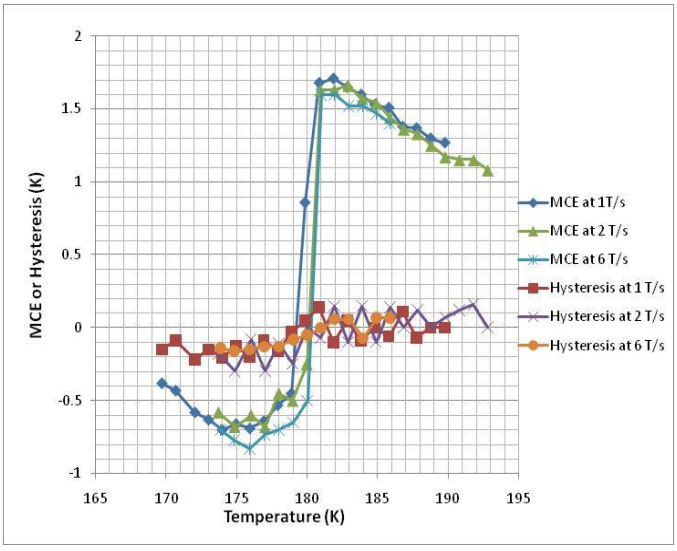

Figure 6.2. MCE and hysteresis data curves for Dy at under various field sweep rates.

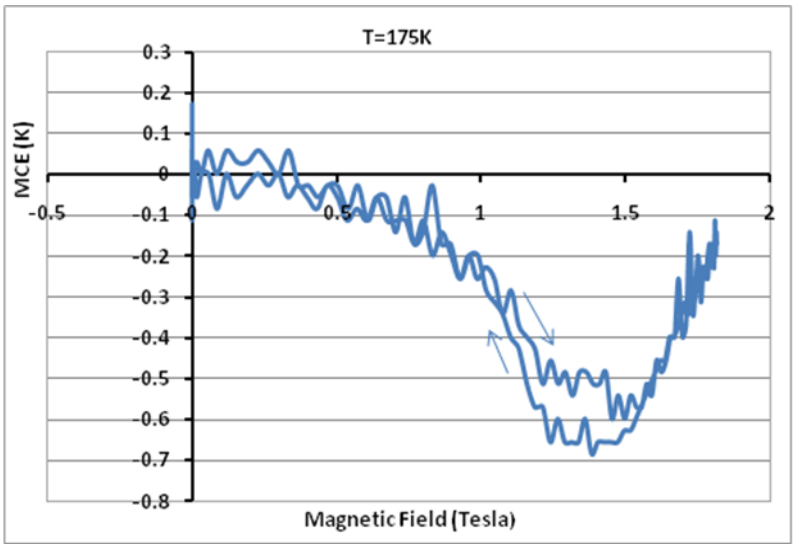

Figure 6.3. MCE curves for Dy at Temperature 175 K, 1T/s.

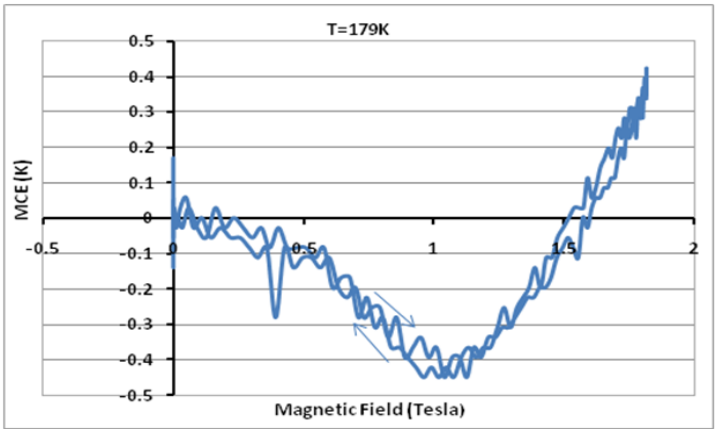

Figure 6.4. MCE curves for Dy at Temperature 179 K, 1T/s.

the MCE is negative with magnetic field increasing from zero and reaches a peak value of -0.6K when magnetic field reaches to 1.4 Tesla, and then drops back to - 0.1 K with field reaching 1.8 Tesla. When the magnetic field decreases from 1.8 Tesla to 0, the MCE almost repeats the magnetizing process – it reaches – 0.7 K at 1.4 Tesla and then increases to 0 K at 0 Tesla (Figure 6.3). When the operating temperature (179K) is near the transition temperature, the MCE is negative at the beginning of the magnetizing process and reaches

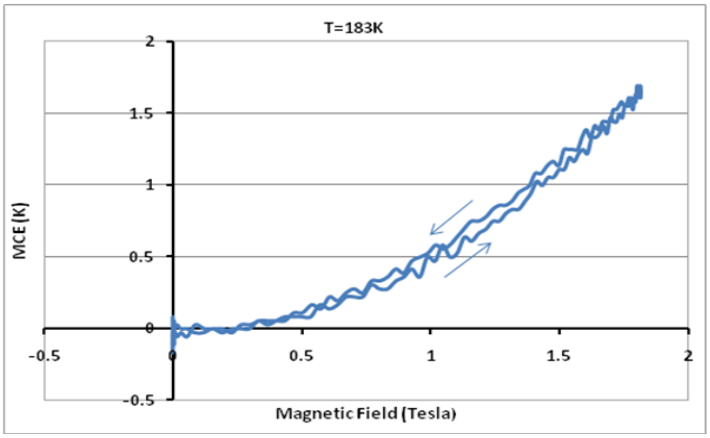

Figure 6.5. Adiabatic temperature change vs. field for a typical Dy at Temperature 183 K, 1T/s.

the peak value of -0.45K at 1.1 Tesla, and then starts to increase with magnetic field going up, reaching zero at about 1.5 Tesla, becomes positive from there on, and increases to 0.4K at 1.8 Tesla (Figure 6.4).

When the operating temperature is above the transition temperature (i.e., 183 K), the MCE is always positive (Figure 6.5).

One may notice that as the temperature is increased, the negative MCE peak occurs at low fields and the sign of the MCE is reversed at high fields.

The arrows in Figures 6.3 to 6.5 show the direction for magnetizing/demagnetizing process. As shown in Figure 6.2, there is little or no difference in the different field change rates up to 6 T/s, and as expected, the thermal hysteresis of the Dy as a second-order material is minimal (within ± 0.2 K).

6.4 Results and Discussion for Tb

It is known that at certain temperature intervals, Tb and Dy have helicoidal antiferromagnetic (HAFM) spin structure, in which the magnetic moments within one and

the same basal plane of their hexagonal closely packed (hcp) crystal structure order ferromagnetically and are rotated by some angle with respect to those in the neighboring basal plane (Tb and Dy have hcp crystal structure) [5–8].

Magnetic phase diagrams of Dy and Tb single crystals were constructed on the basis of magnetization vs. field measurements, in particular, by Nikitin et al. [10] and Bykhover et al. [9].

Y. I. Spichkin reported that the magnetocaloric effect in Tb, Dy, Er and $Tb_{0.5}Dy_{0.5}$ at the first-order transition is mainly related to the change of the exchange energy taking place at the transition. In addition, Figure 6.6 shows that the adiabatic temperature change in Tb is minimal and it has a first-order transition at ~220 K [4]. Based on specific heat

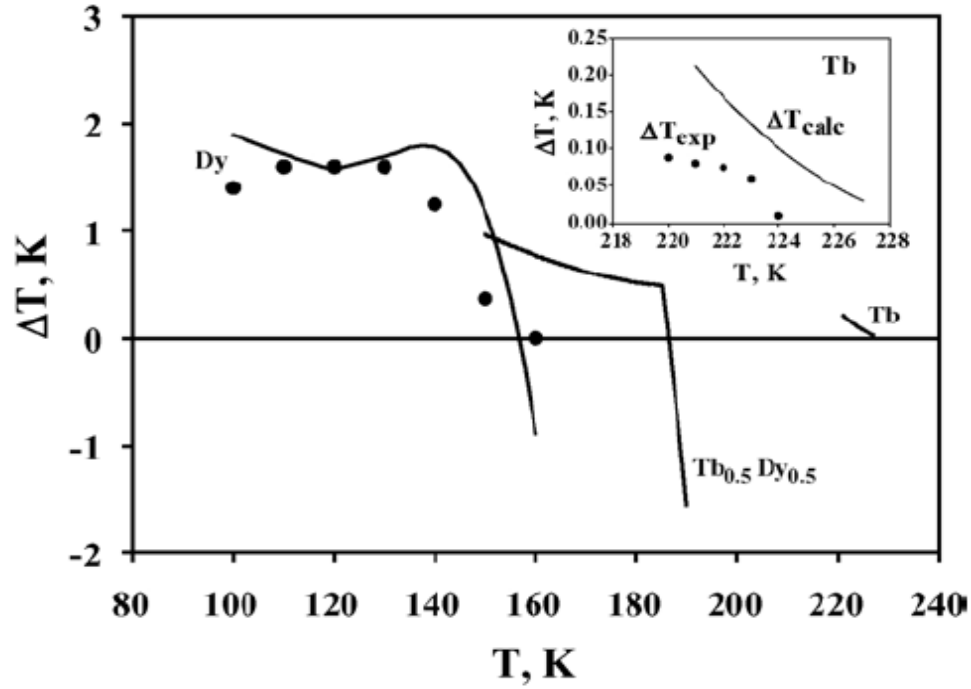

Figure 6.6. The temperature dependences of the magnetocaloric effect (adiabatic temperature change) at the first-order transition in Tb, Dy and $Tb_{0.5}Dy_{0.5}$ (inset shows $\Delta T(T)$ for Tb). Experimental values of _*T* measured for Tb(_*H*= 0.35 kOe) and Dy (ΔH= 20 kOe) single crystals are shown by black circles [4].

measurements T.J. McKenna has reported that Tb has a first-order transition at ~220 K [3]. The first-order transition is weak and sometimes it is not seen, especially in Tb samples of low purity.

Figure 6.7 shows the curves of MCE vs. operating temperature for the terbium metal (Tb). Tb is one of the best materials tested so far. Its maximum adiabatic temperature change is 5.1 K at 1.78 Tesla, even higher than that of elemental gadolinium. The ordering temperature is around 231K. As a second-order material, Tb has a wide working temperature and minimal thermal hysteresis. No difference exists between the heating and cooling process. Figure 6.8 presents the adiabatic temperature change (ΔT_{ad}) vs. magnetic field near its ordering temperature. The ΔT_{ad} increases almost linearly with magnetic field from 0 to 0.5 Tesla, and the linear relationship still holds after 0.5 Tesla, but its slope is slightly lower.

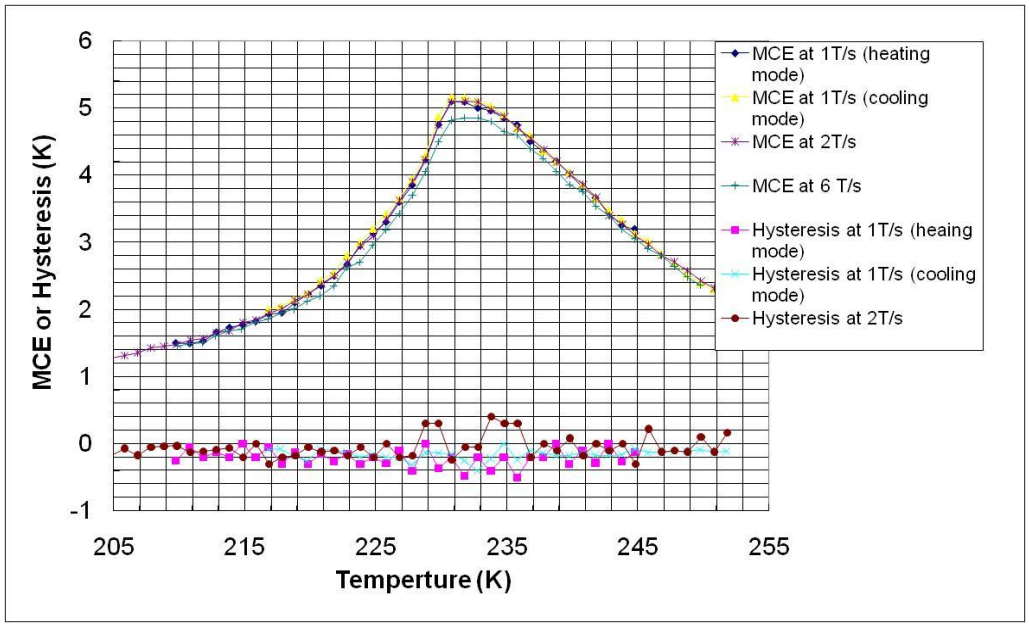

Figure 6.7. MCE and Hysteresis data curves for Tb at under various field sweeping rates.

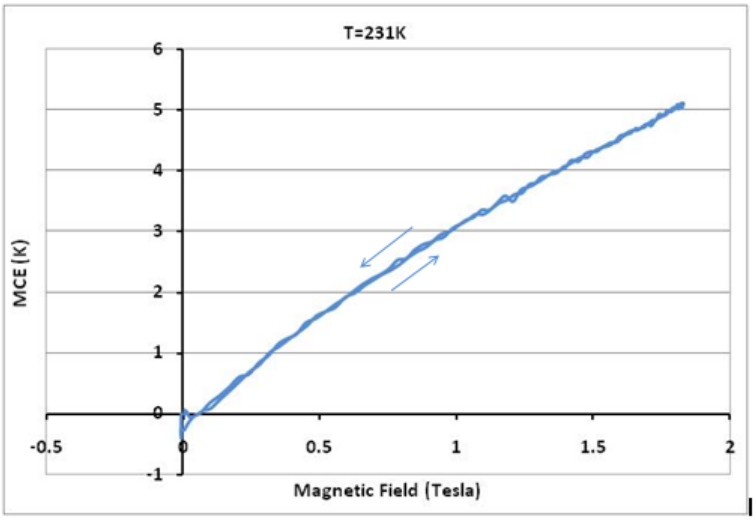

Figure 6.8. Adiabatic temperature change vs. field for Tb at 231 K with the magnetic field sweep rate of 1T/s.

6.5 Results and Discussion for $GdAl_2$

The magnetocaloric properties of $GdAl_2$ and Nd_2Fe_{17} have been determined by Dan'kov [11]. S. Yu. Dan'kov reported that the magnetocaloric effect in terms of the adiabatic temperature, ΔT_{ad}, as obtained from direct measurements in a pulsed field and from heat capacity measurements for magnetic field changes of 0 to 2 Tesla and 0 to 5 Tesla as shown in Figure 6.9. These results are in good agreement with the values calculated from heat capacity data. The required for the sample temperature to reach its maximum value due to magnetocaloric effect in a slow rising magnetic (2 T) equals approximately 3s, which is 0.7 T/s.

Figure 6.10 shows the MCE or hysteresis vs. operating temperature at different magnetic field sweeping rates for the $GdAl_2$ materials. The ordering temperature is around 167 K, and the maximum adiabatic temperature change (MCE) is about 1.82 K for a 1.78

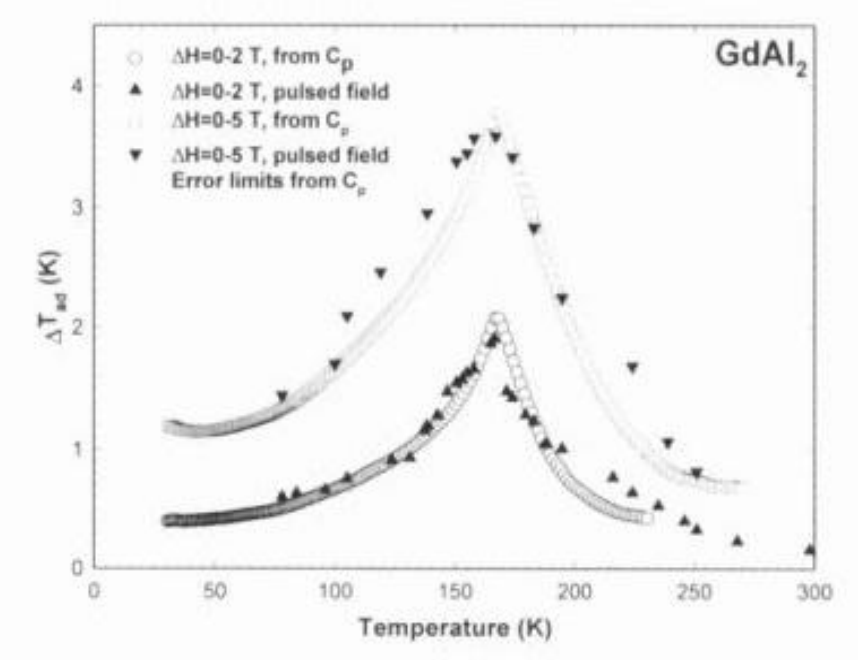

Figure 6.9. The adiabatic temperature rise for $GdAl_2$ for field changes of 0–0–2.0 and 0–5.0 Tesla as a function of temperature as determined from indirect measurements (S. Yu. Dan'Kov et al. [11]).

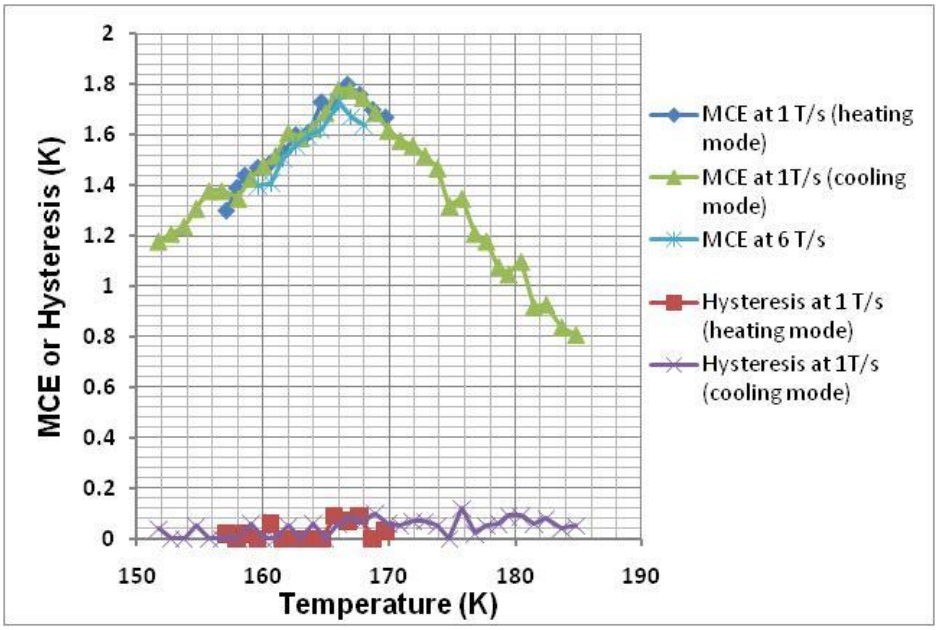

Figure 6.10. MCE and hysteresis data curves for $GdAl_2$ at under various field sweeping rates.

Tesla field. One can see from this figure that the hysteresis is almost zero, there is no difference between the results for 1 T/s and 6 T/s, and also no difference heating mode and cooling mode. These are all characteristics of a second order material. In addition, the useful operating temperature range is wide; for example, the temperature bandwidth for 70% of the peak MCE is 14 K. This is a good characteristic for magnetic refrigeration application. These results are good agreement with measurements by S. Yu. Dan'Kov et al. [11].

6.6 Results and Discussion for Nd_2F_{17}

The magnetic behavior of Nd_2Fe_{17} has been studied by a number of investigations, for example see Ref. 12. This phase is reported to order ferromagnetically between 329 to 335 K, and does not exhibit any other magnetic ordering phenomenon below the Curie temperature, which occurs many times in compounds with both a 3*d* and a 4*f* component.[11]

S. Yu. Dan'kov reported that the Nd_2Fe_{17} intermetallic compound has a magnetic ordering temperature slightly above room temperature, which makes it attractive for near room temperature magnetocaloric applications (the high temperature heat rejection side of a magnetic refrigerator or cooler, or the low temperature side of a heat pump) [11].

Similarly, when the direct ΔT_{ad} (from both semi-static and pulse field measurements) are compared to those obtained from heat capacity measurements, one sees excellent agreement (see Figure 6.11).

Figure 6.12 shows that Nd_2F_{17} has low MCE – only 0.95 K near the Curie temperature of 330 K at 1.78 Tesla. These results are in good agreement with S. Yu. Dan'Kov, .et al.[11] measurements. In the case of Nd_2Fe_{17}, at 332 K, a small amount of hysteresis is present for the heating mode, however, it is absent during the cooling mode, see Figure 6.12.

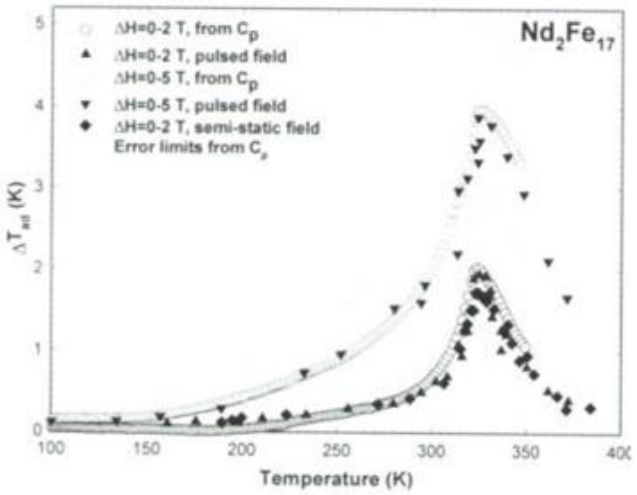

Figure6.11. The adiabatic temperature rise for Nd_2Fe_{17} for magnetic field increase from 0 to 2 Tesla and 0 to 5 Tesla as a function of temperature as determined from heat capacity and direct (pulse field) measurements. [11]

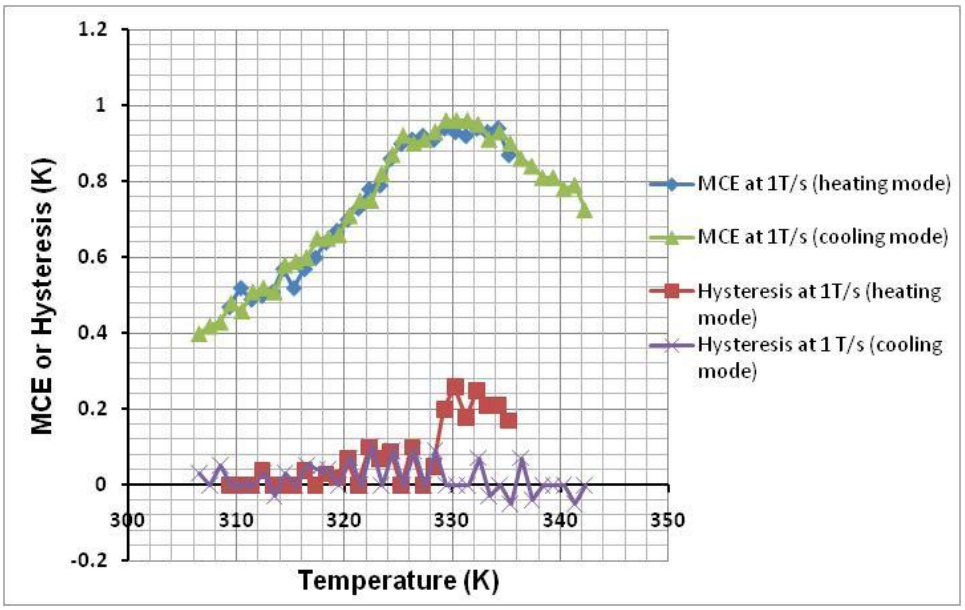

Figure 6.12. MCE and Hysteresis data curves for Nd_2Fe_{17} at under various field sweeping rates.

6.7 Results and Discussion for $Hf_{(1-x)}Ta_xFe_{1.99}$

Recently, the focus of intensive research for several 3*d*-based intermetallic compounds suitable for magnetic refrigeration , $(Hf_{0.83}Ta_{0.17})Fe_{2+x}$, and FeRh, have been investigated with respect to their magnetocaloric properties [13].

A magnetic transition between ferromagnetic (F) and antiferromagnetic (AF) states has been of considerable interest in the field of itinerant-electron magnetism [14].

The occurrence of a first-order ferromagnetic → antiferromagnetic (FM→AFM) transition with increasing temperature, *T,* in the pseudobinary $Hf_{(1-x)}Ta_xFe_2$ systems having tantalum concentrations in the $0.1<x<0.3$ interval were observed by Nishihara and Yamaguchi [15]. A reversed (AFM→FM), but otherwise similar first-order transition takes place as *T* increases near room temperature in Fe–Rh alloys, which have been suggested as candidate working materials for magnetic refrigeration [16]. In both systems, the FM↔AFM transition is evidently sensitive to preparation conditions as well as composition. Annealed $Hf_{(1-x)}Ta_xFe_{1.99}$ materials were investigated, while as-cast $Hf_{0.8}Ta_{0.2}Fe_{1.97}$ was employed in a recent study of thermal and transport properties by Wada, Shimamura, and Shiga, who observed a sharper transition in as-cast, as compared with annealed, samples. [17]

The sensitivity of the structural and magnetic properties to departures from stoichiometry were explored by focusing on a series of samples with fixed Hf:Ta concentration ratio. Reported for several alloys were the determination of a magnetocaloric property, the isothermal field-induced entropy change ΔS. Herbst et al. [18] reported the indirect MCE (magnetization) for low magnetic fields (0.9 Tesla) in the three $(Hf_{0.83}Ta_{0.17})Fe_{2-x}$ alloys, where $x = 0.09$, 0, and -0.09. All three materials order antiferromagnetically near room temperature and have a relatively low MCE (-5.6, -16, and -11 mJ/cm^3 K, respectively), which shows nearly conventional behavior [18]

6.7.1 Sample preparation

Ingots having nominal compositions specified by $(Hf_{0.83}Ta_{0.17})Fe_{(1.98)}$ were prepared by induction melting the elemental constituents in BN crucibles under argon. The purity of the iron and tantalum employed was 99.7%, with 0.27% Zr as the major impurity.

Phase purity and structure were established by x-ray powder diffraction (XRD) measurements as shown Figure 6.13.

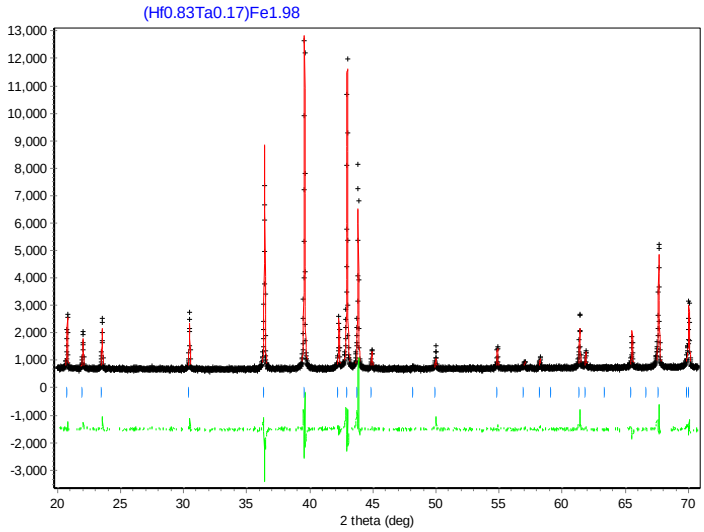

Figure 6.13. X-ray powder diffraction (XRD) measurements for $(Hf_{0.83}Ta_{0.17})Fe_{(1.98).}$ The pattern corresponds to a single phase material with the cubic Laves phase structure.

6.7.2 Magnetization

Magnetization was measured in a 2 T magnetic field on heating from 10 to 300 K (Fig. 6.14). The sample undergoes a sharp transformation from the FM into PM state, comparable with some other first-order materials that show transition around room temperature, i.e., $Gd_5Si_2Ge_2$ [19]. This indicates a potential for the high magnetic entropy

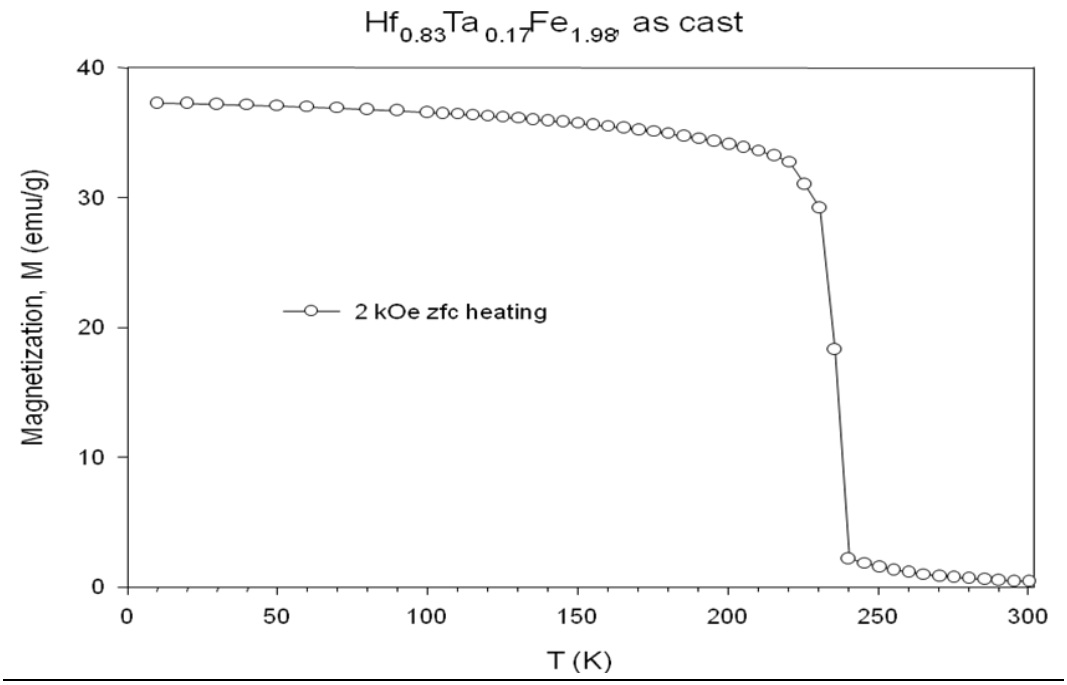

Figure 6.14. Magnetization data for $(Hf_{0.83}Ta_{0.17})Fe_{(1.98)}$ measured in a 2kOe magnetic field during heating after the sample was cooled in zero magnetic field.

change, however, it also suggests strong superheating and possibility of highly metastable state of the compound in this part of the phase diagram.

6.7.3 Results and discussion for $(Hf_{0.83}Ta_{0.17})Fe_{1.98}$

The Curie temperature is 236.7 K, and the sample is a first-order material with magnetostructural transition. The maximum MCE at 1.78 Tesla of the $(Hf_{0.83}Ta_{0.17})Fe_{1.98}$ is about 3.5 K (Fig. 3.14). It shows a difference between the heating mode and the cooling mode similar to that for $Gd_5Si_2Ge_2$ and MnFePAs materials described in Chapter 2 and Chapter 3. Similar to $Gd_5Si_2Ge_2$, although the thermal hysteresis is high in the middle of the magnetizing or demagnetizing process, it is low at the end of magnetizing or demagnetizing.

As shown in Figure 6.15, the Curie temperature in the critical field is as high as 1 Tesla, as shown in Figure 6.16 for the MCE curve at operating temperature = 240.6 K. Closer to the Curie temperature, the critical field is lower (only about 0.5 Tesla), but when magnetic field exceed 1.4 Tesla, the MCE does not increase much with the field. This behavior can be seen in Figure 6.17 for MCE at temperature = 236.7 K. Furthermore, for temperatures close to *Tc* (e.g. T= 236.7 K), the MCE tends to saturate with field.

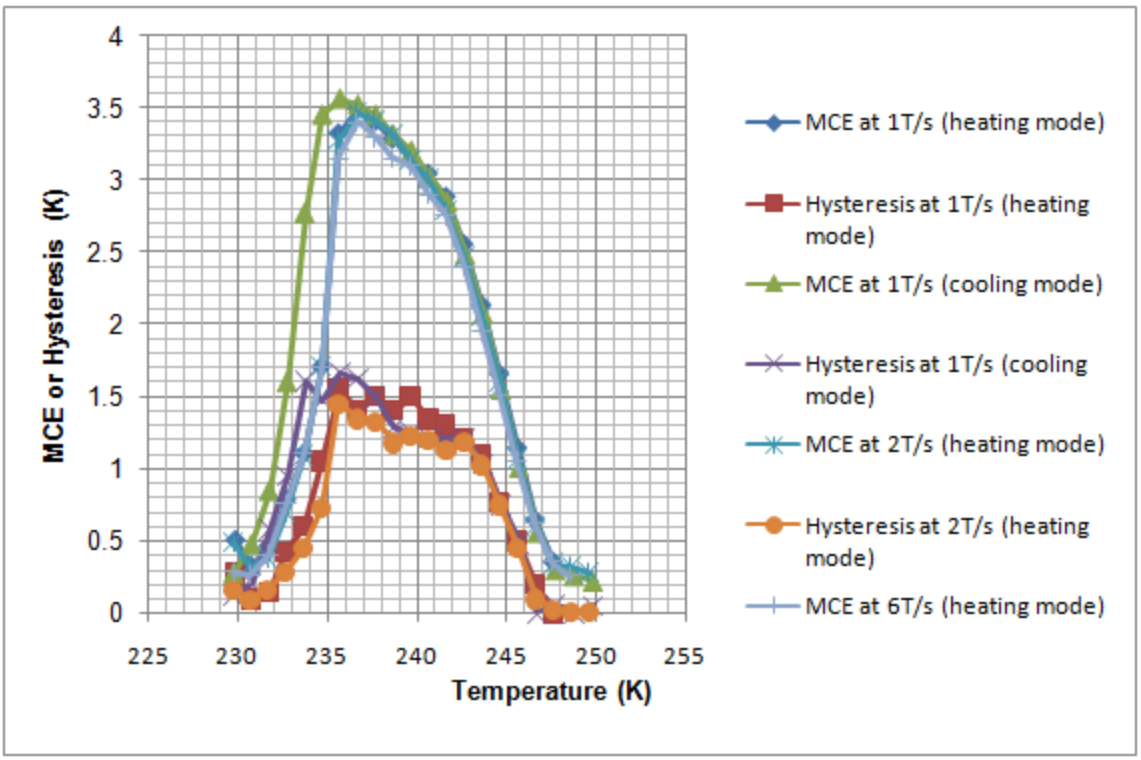

Figure 6.15. MCE and hysteresis data curves for $(Hf_{0.83}Ta_{0.17})Fe_{1.98}$ measured with various field sweeping rates.

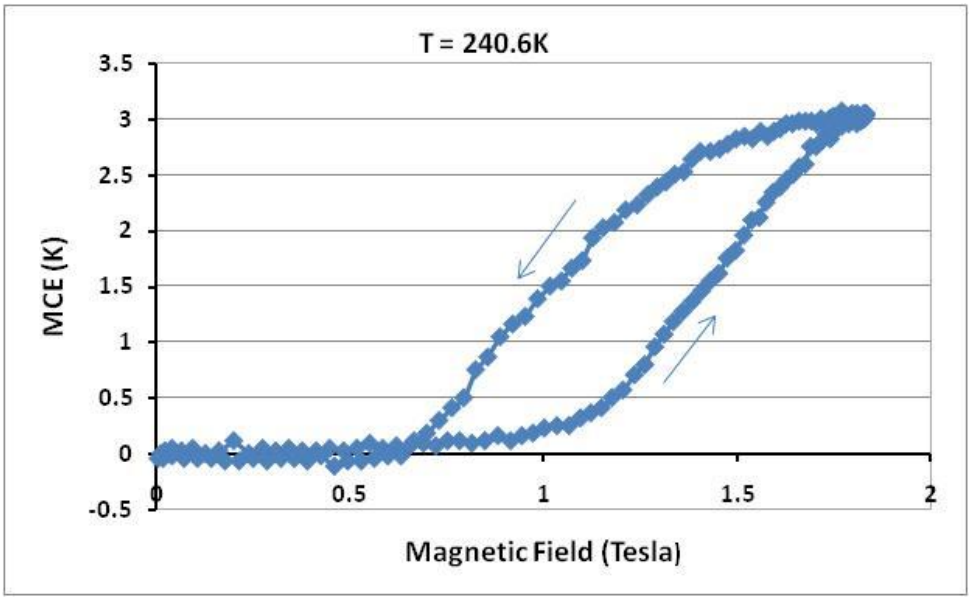

Figure 6.16. Adiabatic temperature change vs. field for $(Hf_{0.83}Ta_{0.17})Fe_{1.98}$ measured at 240.6 K with the magnetic field sweep rate of 1T/s.

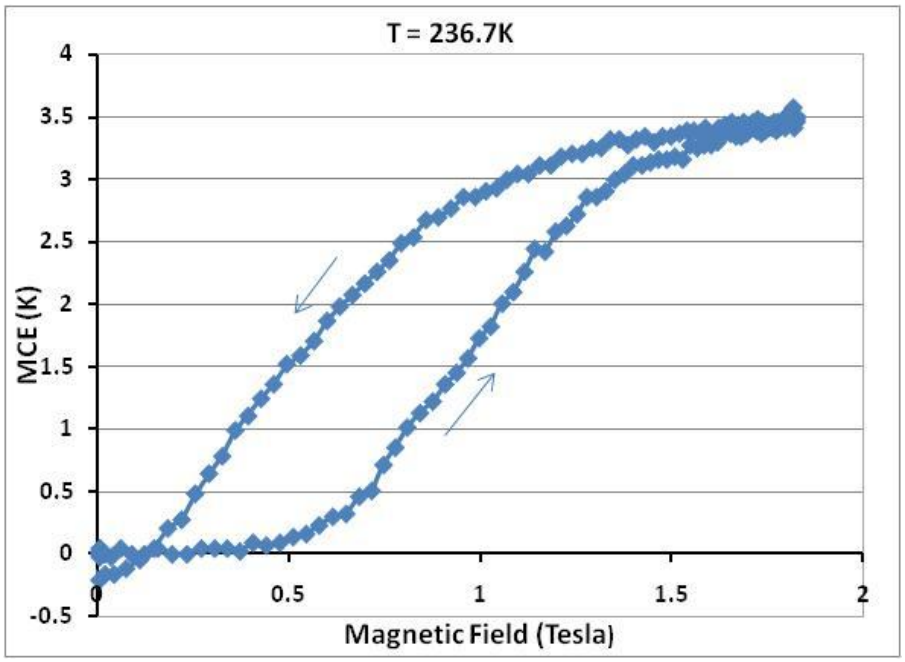

Figure 6.17. Adiabatic temperature change vs. field for $(Hf_{0.83}Ta_{0.17})Fe_{1.98}$ measured at 236.7 K with the magnetic field sweep rate of 1T/s.

6.8 Results and Discussion for $DyCo_2$

The well-known members of RCo_2 family, $DyCo_2$, $HoCo_2$, and $ErCo_2$ exhibit first-order itinerant electron metamagnetic phase transformations [20]. The first-order nature of the phase transition in $DyCo_2$ is confirmed by the behavior of heat capacity (Figure 6.18) and by the lattice distortion accompanied by the discontinuities of unit-cell dimensions and phase volume observed at the phase transition temperature (Figure 6.19) in zero magnetic fields. Nevertheless, regardless of this, no obvious thermal (not shown) or magnetic hysteresis can be detected in this material. The MCE in $DyCo_2$ (Figure 6.20) is substantial, and it also exhibits a behavior typically expected for first-order phase transformation materials [21].

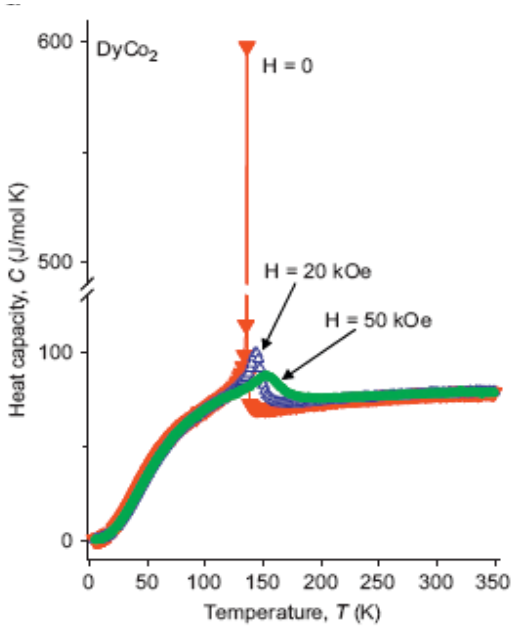

Figure 6.18. The heat capacity in the vicinity of the first-order phase transformation of polycrystalline $DyCo_2$ [3]

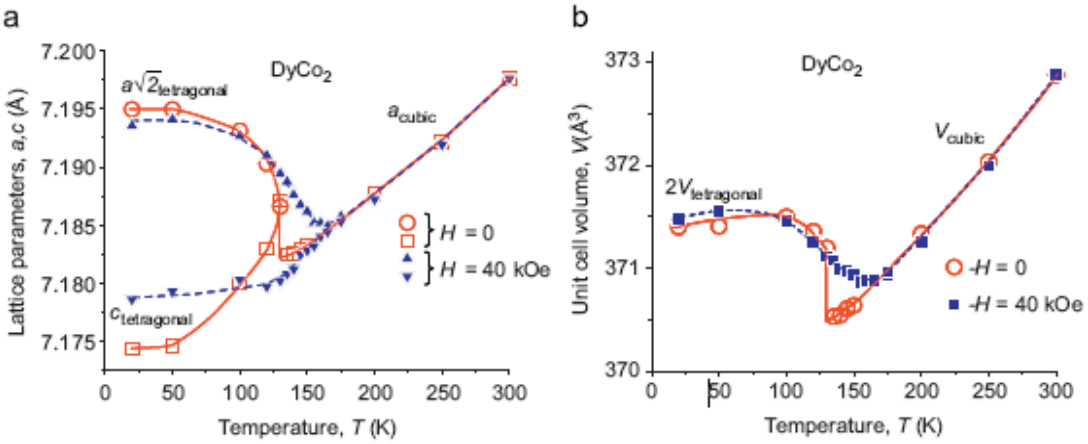

Figure 6.19. Unit-cell dimensions (a) and phase volume (b) of $DyCo_2$ as functions of temperature determined from X-ray powder diffraction data collected in 0kOe (open symbols) and 40kOe magnetic (filled symbols) fields [22].

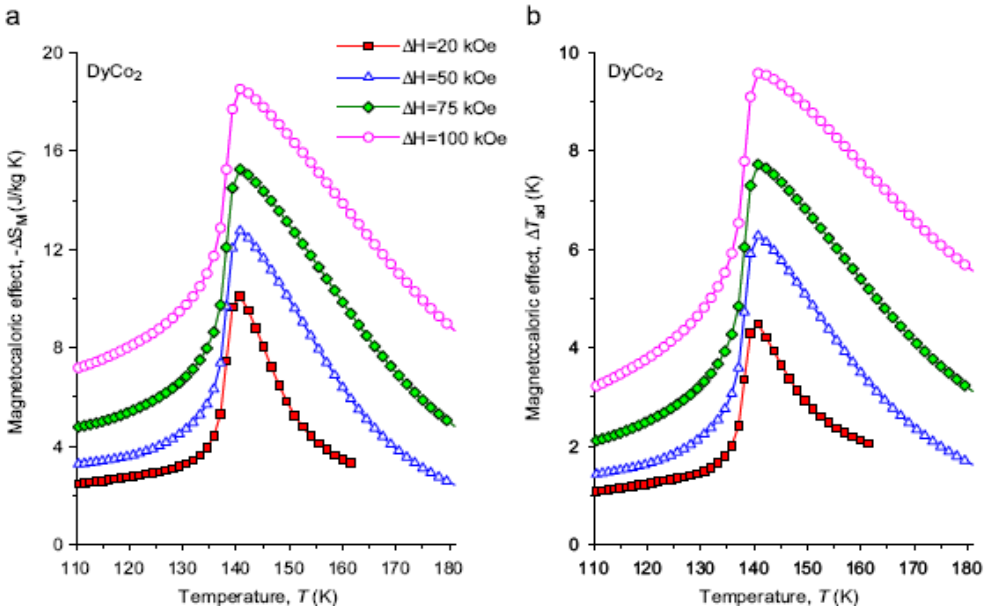

Figure 6.20. The magnetocaloric effect of $DyCo_2$ [ΔS_M left panel (a) and ΔT_{ad} right panel (b) calculated from heat capacity data measured as function of temperature in magnetic fields 0,20,50,75, and 100kOe [22].

$DyCo_2$ is a first-order transition material with the Curie temperature around 142 K. Figure 6.21 shows the MCE and hysteresis at different temperatures and varying magnetic field sweeping rates. The measured maximum MCE is 3.0K (at 1.78 Tesla) near the operating temperature of 139. Similar to LaFeSiH materials, there is no difference between the heating mode and the cooling mode. The thermal hysteresis is relatively low compared to most of other first-order materials.

No significant difference exists in MCE behavior under various magnetic change rates from 1 T/s to 6 T/s.

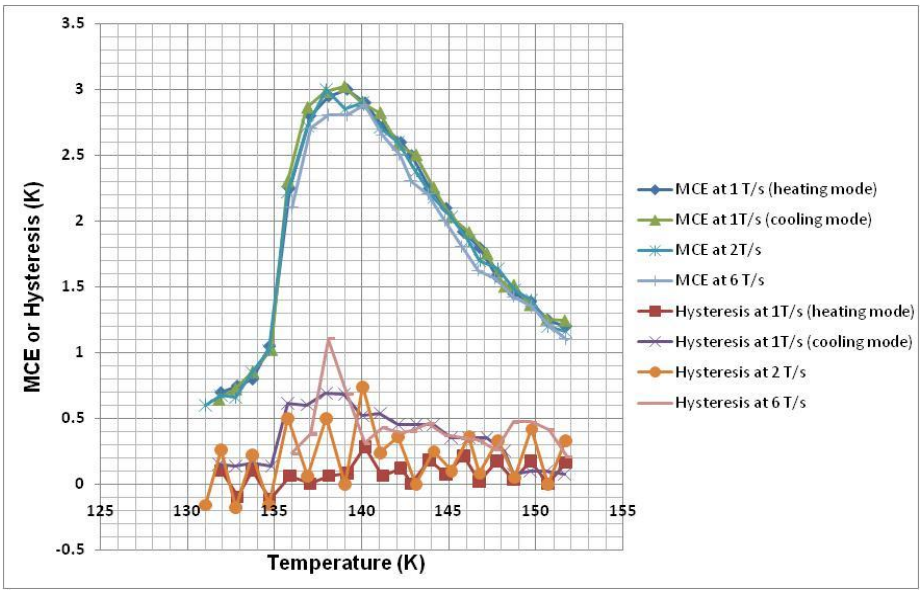

Figure 6.21. MCE and hysteresis data curves for $DyCo_2$ at under various field sweeping rates.

6.9 Conclusions

Several Magnetocaloric materials, including Dy, Tb, $GdAl_2$, Nd_2Fe_{17}, $(Hf_{0.83}Ta_{0.17})Fe_{1.98}$ and $DyCo_2$, have been directly measured for their adiabatic change under different magnetic sweep rates up to 6 Tesla/s.

As a rare earth metal, Dy has some interesting magnetocaloric phenomena. It is noted that Dy has a very unique behavior – for temperatures below 180 K, it shows negative MCE (maximum adiabatic temperature change is about – 0.9 K) at 175 K which is below the transition temperature (~180 K). When the operating temperature (179K) is near the transition temperature, the MCE is negative at the beginning of the magnetizing process and becomes positive with increasing magnetic field, and increases to 0.4K at 1.8 Tesla. When the operating temperature is above the transition temperature (i.e., 183 K), the MCE is always positive. There is no difference among different field change rates up to 6 T/s, and as expected, the thermal hysteresis of the Dy as a second-order material is minimal (within ± 0.2 K).

Tb is one of the best materials that has been tested to date. Its maximum adiabatic temperature change is 5.1 K at 1.78 Tesla, even higher than that of elemental gadolinium. The ordering temperature is around 231K. As a second-order material, Tb has a wide working temperature and minimal thermal hysteresis. No difference exists between the heating and cooling process. The ΔT_{ad} increases almost linearly with magnetic field from 0 to 0.5 Tesla, and the linear relationship still holds after 0.5 Tesla, but its slope is slightly lower. The first-order transition is weak.

$GdAl_2$ exhibits second order characteristics. The ordering temperature is around 167 K, and the maximum adiabatic temperature change (MCE) is about 1.82 K for a 1.78 Tesla

field. The hysteresis is almost zero, there is no difference between the results for 1 T/s and 6 T/s, and also no difference heating mode and cooling mode. These are all characteristics of a second order material. In addition, the useful operating temperature band is wide – for example, the temperature bandwidth for 70% of the peak MCE is 14 K. This is a good characteristic for magnetic refrigeration application.

Nd_2Fe_{17} intermetallic compound has a magnetic ordering temperature slightly above room temperature, which makes it attractive for near room temperature magnetocaloric applications. Nd_2F_{17} has low MCE – only 0.95 K near the Curie temperature of 330 K at 1.78 Tesla. In the case of Nd_2Fe_{17}, at 332 K, the hysteresis is present during the heating mode, however, it is absent during the cooling mode.

The $(Hf_{0.83}\ Ta_{\ 0.17})Fe_{1.98}$ material has ΔT_{ad} = 3.5K near 237K operating temperature, but it is a first order magnetostructural transition material with thermal hysteresis of 1.5K. The maximum MCE at 1.78 Tesla of the $(Hf_{0.83}Ta_{0.17})Fe_{1.98}$ is about 3.5 K. It shows a difference between the heating mode and the cooling mode similar to that for $Gd_5Si_2Ge_2$ and MnFePAs. Similar to $Gd_5Si_2Ge_2$, although the thermal hysteresis is high in the middle of the magnetizing or demagnetizing process, it is low at the end of magnetizing or demagnetizing. Closer to the Curie temperature, the critical field is lower (only about 0.5 Tesla), but when magnetic field exceed 1.4 Tesla, the MCE does not increase much with the field. The MCE tends to saturate with field.

The first-order nature of the phase transition in $DyCo_2$ is confirmed by the behavior of heat capacity and by lattice distortion accompanied by the discontinuities of unit-cell dimensions and phase volume observed at the phase transition temperature in zero magnetic fields. Yet, regardless of this, no obvious thermal or magnetic hysteresis can be detected in

this material. The MCE in $DyCo_2$ is substantial, and it also exhibits a behavior typically expected for first-order phase transformation materials. $DyCo_2$ has ΔT_{ad} = 3K near the ordering temperature of 139K with a thermal hysteresis of only 0.5K. This is good considering its low ordering temperature. It may be good for low temperature refrigeration applications .

6.10 References

[1]. R.J. Elliott, *Magnetic Properties of Rare Earth Metals.* Plenum, London (1972).

[2] K. A. Gschneidner, Jr. and V. K. Pecharsky, Mater. Sci. Engin. A, **287**, 2000, Pages 301-310.

[3] T.J. McKenna, S.J. Campbell,* D.H. Chaplin and G.V.H. Wilson, Solid State Comm. , **40**, 177-181.

[4] Y.I. Spichkin, A.M. Tishin */ Journal of Alloys and Compounds* **403**, (2005) 38-44.

[5] K.N.R. Taylor, M.I. Darby, Physics of Rare Earth Solids, Chapman and Hall Ltd., London, 1972.

[6] J. Jensen, A.R. Mackintosh, Rare Earth Magnetism: Structure and Excitations, Clarendon Press, Oxford, 1991.

[7] W. Koehler, I. Cable, H. Child, M. Wilkinson, E. Wollan, Phys. Rev.**158**, (1967) 450.

[8] M. Wilkinson, W. Koehler, E. Wollan, J. Cable, J. Appl. Phys. **32**, (1961) 48.

[9] S.E. Bykhover, S.A. Nikitin, Y.I. Spichkin, A.M. Tishin, Z.S. Umkhaeva, Sov. Phys. JETP **70**, (1990) 1121.

[10] S.A. Nikitin, A.M. Tishin, P.I. Leontiev, J. Magn. Magn. Mater. **92**, (1991) 405.

[11] S. Yu. Dan'Kov, V. V. Ivtchenko, A.M. Tishin, K. A. Gschneidner, Jr., and V. K. Pecharsky, Adv. Cryog. Engin. , **46A**, 397-404.

[12] F. Weitzer, K. Heibl and P Rogl, J Appl. Phys. **65**, (1989) 4963.

[13] K. A. Gschneidner, Jr. and V. K. Pecharsky. Annu. Rev. Mater. Sci. (2000). **30**, 387–429.

[14] J.S.Kouvel and C.C. hartelius, J.Appl.Phys.Suppl.**33**, (1962) 1343.

[15]Y. Nishihara and Y. Yamaguchi, J. Phys. Soc. Jpn. **51**, (1982) 1333.

[16] M. P. Annaorazov, K. A. Asatryan, G. Myalikgulyev, S. A. Nikitin, A. M. Tishin, and A. L. Tyurin, Cryogenics **32**, (1992) 867.

[17] H.Wada, N.Shimamura, M.Shiga , Phys. Rev. B **48**, (1993) 10221.

[18] Herbst JF, Fuerst CD, McMichael RD.1996. *J. Appl. Phys.* **79**, 5998-6000

[19] V. K. Pecharsky and K. A. Gschneidner, Jr., in *Magnetism and Structure in Functional Materials*, edited by A. Planes, L. Manosa, and A. Saxena, Springer Series in Materials Science (Springer-Verlag, Heidelberg, 2005), **79**, Ch. 11, p. 199.

[20] N.H. Duc, T. Goto, in: K.A. Gschneidner Jr., L.R. Eyring (Eds.), Handbook on the Physics and Chemsitry of Rare Earths, vol. 26, Elsevier, Amsterdam, 1999, p. 177 (Ch. 171).

[21] V.K. Pecharsky, K.A. Gschneidner Jr., A.O. Pecharsky, A.M. Tishin, Phys. Rev. B **64**, (2001) 144406.

[22] V.K. Pecharsky, K.A.GschneidnerJr., Ya.Mudryk, DurgaPaudyal, Magn. Magn. Mater. **321**, (2009) 3541–3547

CHAPTER 7. GENERAL CONCLUSIONS

A MMS test facility was developed to investigate the MCE characteristics of a number of both second order and first order phase transition materials under different operating conditions. The absolute value of the directly measured MCE of $Gd_2Si_2Ge_2$ is close to that obtained from indirect measurement. Significant differences in the heating mode and the cooling mode were observed. The kinetic response of the magneto-structural change in $Gd_2Si_2Ge_2$ is fast enough to respond to an applied continuously changing field with a sweeping rate up to 6 T/s, and time dependence of the MCE is not evident in this material.

MCE and hysteresis of $Gd_5Si_{2.7}Ge_{1.3}$ measured at various sweeping rates showed insignificant differences in the heating mode and the cooling mode. The absolute value of the directly measured MCE is close to that obtained from indirect measurement. $Gd_5Si_{2.7}Ge_{1.3}$ is shown to be a second-order material with the Curie temperature of 315 K based on magnetization data and direct measurements of MCE.

The MMS has been used to directly measure MCE of MnFePAs. Only one MnFePAs sample has MCE (5.4K) higher than the baseline Gadolinium (5.0K), and most MnFePAs samples have MCE between 3.0 and 4.5K for the maximum field of 1.78 Tesla, and most have maximum hysteresis between 1.0 and 1.6 K. The MCE and hysteresis of MnFePAs is influenced by the field sweeping rate, but the relationship between the MCE and hysteresis, and field change rate is weak and non-linear.

Three LaFeSiH series materials, namely $La(Fe_{1-x}Si_x)_{13}H_y$ with x = 0.12 and y = 1.46, 1.18 and 1.06, respectively, were prepared using the rapid solidification method, and their adiabatic temperature changes (ΔT_{ad}) were directly measured using the MMS device under a

wide range of operating temperature and magnetic sweeping rate from 0.25 to 6 T/s. The maximum ΔT_{ad} is only 2.5 K at 1.78 T, equal to 1.4 K/T, which is much lower than that of indirect or direct measurement for bulk alloy samples, but close to that for other rapidly solidified samples. This phenomenon of low ΔT_{ad} for rapid solidification material samples is worthy of further investigation. The characteristics of the ΔT_{ad} curves are very similar for different magnetic field sweeping rates from 0.25 to 6 T/s, and no time dependence of MCE is observed. In general, the thermal hysteresis of the LaFeSiH materials is low – only 0.5 K maximum.

The heat capacity measurements of the $Ni_{2.19}Mn_{0.81}Ga$ shape-memory alloy showed a double feature peak at the temperature of the coupled martensite-ferromagnetic transformation. The origin of this feature could be related to the multi-step transition observed by other methods such as linear thermal expansion studies. However, the possibility of sample inhomogeneity enhanced by the strong compositional dependence of T_C in $Ni_{2+x}Mn_{1-x}Ga$ alloys should be considered as well, because some compositional gradient is almost inevitable in a large sample. The weak d*T*c/d*H* dependence observed in the heat capacity data is directly related to a relatively low adiabatic temperature change observed in these alloys, limiting their use in magnetocaloric applications. The use of Maxwell's equations for the analyses of *M*(H) data cannot produce reliable estimation of MCE in these materials. At the same time, the ΔT_{ad} calculated from heat capacity data show reasonable agreement with the result of the direct magnetocaloric measurements of the same sample, and the latter are in good agreement with the literature. These results provide an additional confirmation that heat capacity measurements in applied magnetic fields, and especially, a

direct measurement of a magnetocaloric effect, can be used for the quantitative estimation of the magnetocaloric effect in non-equilibrium first-order transition systems like $Ni_{2+x}Mn_{1-x}Ga$.

Several magnetocaloric materials, including Dy, Tb, $GdAl_2$, Nd_2Fe_{17}, $(Hf_{0.83}Ta_{0.17})Fe_{1.98}$ and $DyCo_2$, have been directly measured for their adiabatic change under different magnetic sweeping rates up to 6 Tesla/s.

As a rare earth metal, Dy has some interesting magnetocaloric phenomena. It is noted that Dy has a unique behavior – for temperatures below 180 K, it shows a negative MCE, the maximum adiabatic temperature change is about – 0.9 K at 175 K. When the operating temperature (179K) is near the transition temperature, the MCE is negative at the beginning of the magnetizing process and becomes positive with increasing field, and increases to 0.4K at 1.8 Tesla. When the operating temperature is above the transition temperature (i.e., 183 K), the MCE is always positive. There is no difference among different field change rates up to 6 T/s, and as expected, the thermal hysteresis of the Dy as a second-order material is minimal (within ± 0.2 K).

Tb is one of the best materials tested thus far. Its maximum adiabatic temperature change is 5.1 K at 1.78 Tesla, even higher than that of elemental gadolinium. The ordering temperature is around 231K. As a second-order material, Tb has a wide working temperature and minimal thermal hysteresis. No difference exists between the heating and cooling process. The ΔT_{ad} increases almost linearly with magnetic field from 0 to 0.5 Tesla, and the linear relationship still holds above 0.5 Tesla, but its slope is slightly lower. The first-order transition is weak.

$GdAl_2$ exhibited second order characteristics. The ordering temperature is around 167 K, and the maximum adiabatic temperature change (MCE) is about 1.82 K in a 1.78 Tesla field. The

hysteresis is almost zero, there is no difference between the results for 1 T/s and 6 T/s, and also no difference heating mode and cooling mode. These are all characteristics of a second order magnetic transition material. In addition, the useful operating temperature band is wide; for example, the temperature bandwidth for 70% of the peak MCE is 14 K. This is a good characteristic for magnetic refrigeration application.

Nd_2Fe_{17} intermetallic compound has a magnetic ordering temperature slightly above room temperature, which makes it attractive for near room temperature magnetocaloric applications. Nd_2F_{17} has low MCE – only 0.95 K near the Curie temperature of 330 K at 1.78 Tesla. In the case of Nd_2Fe_{17}, at 332 K, the hysteresis is present for the heating mode, however, it is absent during the cooling mode.

The $(Hf_{0.83}\ Ta_{\ 0.17})Fe_{1.98}$ material has ΔT_{ad} = 3.5K near 237K operating temperature, but it is a first-order magnetic material with magnetostructural transition. It exhibits a thermal hysteresis of 1.5K, at the Curie temperature, 236.7 K. It shows a difference between the heating mode and the cooling mode similar to that for the $Gd_5Si_2Ge_2$ and MnFePAs materials. Similar to $Gd_5Si_2Ge_2$, although the thermal hysteresis is high in the middle of the magnetizing or demagnetizing process, it is low at the end of magnetizing or demagnetizing process. Closer to the Curie temperature, the critical field is low (only about 0.5 Tesla), but when magnetic field exceed 1.4 Tesla, the MCE does not increase much with the field, i.e., the MCE tends to saturate with field.

The first-order nature of the phase transition in $DyCo_2$ was confirmed by the behavior of heat capacity and by lattice distortion accompanied by the discontinuities of unit-cell dimensions and phase volume observed at the phase transition temperature in zero magnetic fields. Nevertheless, regardless of this, no obvious thermal or magnetic hysteresis can be

detected in this material. The MCE in $DyCo_2$ is substantial, and it also exhibits a behavior typically expected for first-order phase transformation materials. $DyCo_2$ has ΔT_{ad} = 3K near 139K ordering material with thermal hysteresis only 0.5K. This is good considering its low work temperature, and potential use for low refrigeration temperature applications.

In general, time dependence of MCE has not been observed for these materials. This is consistent with the observation for other materials tested in this study (see Table 7.1).

Table 7.1. Summary of direct measurements for samples and 1.78 Tesla at 1 T/s

No	Material Reference	Material Composition	Process variation	Tc	MCE	Max Hysteresis	Bandwidth K	Transition
				K	K	K	70%	
1	AMES_GD	Gd		289.7	4.93	0	25	Second-order
2	AMES_$Gd_5Si_{2.7}Ge_{1.3}$	$Gd_5Si_{2.7}Ge_{1.3}$		317	3.7	0.1	18	Second-order
3	AMES_$Gd_5Si_2Ge_2$	$Gd_5Si_2Ge_2$		268	5.8	2.9	5	First-order
4	Tc1_247K	$MnFeP_{0.55}As_{0.45}$	Heat treatment protocols varied	254.5	2.78	1.08	5.4	First-order
5	Tc2_261K			261	3.2	1.05	4.75	First-order
6	Tc3_265K			268	3.4	0.95	5	First-order
7	Tc4_272K	$Mn_{1.1}Fe_9P_{0.54}As_{0.46}$		272.5	3.95	0.86	8.35	First-order
8	Tc5_281K	$Mn_{1.1}Fe_9P_{0.5}As_{0.5}$		282	3.21	0.65	8.2	First-order
9	Tc6_286 K	$Mn_{1.1}Fe_9P_{0.54}As_{0.46}$	Heat treatment protocols varied	287	4.09	1.15	5.65	First-order
10	Tc7_290K			288	4.35	1.02	4.8	First-order
11	Tc8_296K	$Mn_{1.1}Fe_9P_{0.47}As_{0.53}$		292	4.2	1.62	5.5	First-order
12	Tc9_295K	$MnFeP_{0.53}As_{0.47}$	Heat treatment protocols varied	292	5.4	1.3	4.2	First-order
13	Tc10_300K			297	3.3	0.7	6.75	First-order
14	Tc11_300K			298	4.42	1.2	7.4	First-order
15	Tc12_306K			304.5	4.8	0.98	7.4	First-order
16	Tc13_314K	$MnFeP_{0.45}As_{0.55}$	Heat treatment protocols varied	311	3.92	0.56	3	First-order
17	Tc14_320K			312	3.58	0.6	4.8	First-order
18	NEOMAX_1	$La(Fe_{0.88}Si_{0.12})_{13}H_{1.46}$		284	2.5	0.18	13	
19	NEOMAX_2	$La(Fe_{0.88}Si_{0.12})_{13}H_{1.18}$		277	2.37	0.17	10	
20	NEOMAX_3	$La(Fe_{0.88}Si_{0.12})_{13}H_{1.06}$		271	2.21	0.35	12	
21	AMES_$Ni_{2.19}Mn_{0.81}Ga$	$Ni_{2.19}Mn_{0.81}Ga$		317	1.3	0.72	4	First-order
22	AMES_Dy	Dy		*182	1.71	-0.1	10	Second-order
23	AMES_Tb	Tb		231	5.16	-0.15	14.7	Second-order
24	AMES_$GdAl_2$	$GdAl_2$		167	1.8	0.07	22.8	Second-order
25	AMES_Nd_2Fe_{17}	Nd_2Fe_{17}		330	0.96	0	23.5	Second-order
26	AMES_$(Hf_{0.83}Ta_{0.17})Fe_{1.98}$	$(Hf_{0.83}Ta_{0.17})Fe_{1.98}$		336.7	3.52	1.62	7.5	First-order
27	AMES_$DyCo_2$	$DyCo_2$		139	3	0.08	8	First-order

T_N = 180 K for the second-order transition, T_C = 90 K was not measured due to the MMS incapability .

Dy has two magnetic phase change temperatures, T_N = 180 K for the second-order transition and T_c = 90 K for the first-order transition [2].

Future Work

The following future work is suggested to build and expand upon the results of this thesis in order to obtain better understanding of the giant magnetocaloric effect and its suitability for near room temperature magnetic refrigeration:

1. Test additional materials with promising MCE performance using the MMS device, such as MnCoGe type, and others.
2. Further theoretical analysis for the phenomena observed in this study, including that in dynamic performance and difference between the cooling and heating modes. In either case, magnetocaloric performance of every material should be correlated with the phase diagram of the corresponding system in temperature-magnetic field coordinates.
3. Test a real active magnetic regenerating refrigerator (AMRR) with the MCM materials measured in this study, to confirm their performance for a wide range of operating parameters including magnetic field sweeping speed. This work is in progress.
4. Explore optimized AMR cycle design to make full use of the characteristics of the first order materials studied in this project, with the goal to increase the unit cooling capacity and energy efficiency. For example, explore ways to make use of the MCE difference between cooling and heating process.

ACKNOWLEDGMENTS

I would like to express my sincere gratitude to all the people who became involved with this research. I am especially thankful to my co-major professors, Viltalij K. Pecharsky and K. A. Gschneidner, Jr., for the exciting and productive time I spent at Ames Laboratory.

I am thankful to Prof. Ekkes Bruck University of Amsterdam, and Dr. Yoshiharu Uno, Neomax, Japan, who provided the sampled material for testing.

This research was made possible due to the able assistance of Dr. Yaroslav S. Mudryk in the lab, and my colleague, Ming Zhang, who collaborated with me in the direct measurement experiments at the Ingersoll-Rand Research Lab.

I would also like to thank my committee members for their many constructive discussions. Finally, I am grateful to all the graduate students and postdocs in the Ames Laboratory group for their help in the experiments and discussions.

The Ames Laboratory is supported by the Office of Basic Energy Sciences of the Office of Science of the U.S. Department of Energy under contract No. DE-AC02-07CH11358 with Iowa State University of Science and Technology.